IJEIR

International Journal of Engineering & Innovative Research

International Journal of Engineering and Innovative Research (IJEIR)

CONTENTS   **PAGE**

Research Articles

Research Article

Investigation of SnO2 and Ti-Doped SnO2 Thin Films for Morphological, Structural and Electrical Characterization

Authors: Ahmet Buğrahan BAYRAM (iD) Tuğba ÇORLU (iD)

International Journal of Engineering and Innovative Research

http://dergipark.gov.tr/ijeir

Investigation of SnO₂ and Ti-Doped SnO₂ Thin Films for Morphological, Structural and Electrical Characterization

Ahmet Buğrahan BAYRAM[1]*,** , Tuğba ÇORLU [2]

[1] Isparta University of Applied Sciences, Institute of Graduate Education, Department of Energy Systems Engineering, Isparta, Turkey.
[2] Innovative Technologies Application and Research Center, Suleyman Demirel University, Isparta, Turkey.

*Corresponding Author: d1940640016@isparta.edu.tr
**One of the authors, Ahmet Buğrahan BAYRAM, is a scholarship holder of YOK 100-2000.

ABSTRACT: In this work, SnO₂ and Ti-doped SnO₂ thin films were produced by successive ionic absorption and reaction methods on platin interdigital contacts. The thin films produced were not annealed. Structural properties of amorphous thin films were investigated using X-ray Diffraction (XRD), morphological properties using Scanning Electron Microscopy (SEM), optical and electrical properties of Ultraviolet-visible Spectrophotometer (UV-VIS) and Keithley 2400 instruments. From the XRD results, it was determined that the thin films were an amorphous structure. Surface analysis by SEM shows that all films are coated and smooth. The current-voltage measurements show that thin films are ohmic. Lnρ results also show that the lowest resistance value for SnO₂ thin films is after 320 °C temperature and after 360 °C temperature for Ti-doped SnO₂ thin films.

Keywords: Successive ionic layer adsorption and reaction (SILAR), Tin dioxide (SnO₂), Characterization

1. INTRODUCTION

There have been extensive studies on their use in semiconductor technology for transparent conductive oxides (TCOs). There are many TCOs such as zinc oxide, indium oxide, tin oxide, etc [1], [2]. Tin oxide thin films are widely used as, photoconductors, transparent conductors, catalysts, gas sensors and solar cells due to their numerous electrical and optical properties such as high electrical conductivity and transparency[3][4][5][6]. The most commonly observed phases of tin oxide are tin dioxide (SnO₂) and tin monoxide (SnO). In recent years, SnO₂ thin films have become a promising material because they exhibit many properties such as n-type conductors, long life, a band gap in the range of 3.0- 4.0 eV, low cost, good reproducibility and ease of fabrication [7]. SnO₂ thin films are materials with higher mechanical and chemical stability compared to other transparent conductive oxides[8]. SnO₂ thin films are materials with low resistivity and high optical transparency in the visible region. From the studies, it is found that the SnO₂ thin films can be further improved by doping with suitable materials such as Co, F, Zn, Cd and Fe [9][10][11][3][12][13]. Many methods such as successive ionic layer adsorption and reaction (SILAR), sputtering, chemical vapor deposition and ultrasonic spray pyrolysis are used to produce SnO₂ thin films [14][15][16]. The SILAR method is a low-cost, flexible, and easy-to-manufacture method. Although there are many studies on titanium-doped

tin oxide thin film in the web of science database like sol-gel [17], and ultrasonic spray technique [18], the SILAR method was not used in any of these studies.

The growth method affects the structural, optical and electrical properties of the films produced. Liu et. al. have studied the characteristics of nano Ti-doped SnO_2 powders prepared by sol–gel method [17]. Khelifi et. al. have investigated influence of Ti doping on SnO_2 thin films properties prepared by ultrasonic spray technique [18].

The main purpose of this study is to use the SILAR method and examine its effects compared to the commonly used methods for Ti-doped SnO_2 thin films. Along with the innovative production method in this field of study, it will show structural, optical and electrical changes on its difference from the traditional production method.

We prepared pure SnO_2 and Ti-doped SnO_2 thin films as a new approach using the SILAR deposition method. Then, structural properties of thin films were investigated by X-ray Diffraction (XRD), morphological properties using Scanning Electron Microscopy (SEM), for optical and electrical properties using ultraviolet-visible spectrophotometer (UV-VIS) and Keithley 2400 instruments.

2. Materials and Methods

SnO_2 and titanium-doped SnO_2 thin films were grown on platinum IDT substrates using the SILAR method. First, platinum contacts are grown on glass substrates with a thickness of 100 nanometers by thermal evaporation. Then, the grown platinum contacts were annealed at 300 °C for 15 minutes in a nitrogen environment. After the annealing process, the SnO_2 material was successfully grown by the SILAR method on the substrates. The SILAR method consists of four basic steps. These;

1) Immersion of the substrate in the prepared solution for a certain period of time and the accumulation of the ions in the solution on the substrate (adsorption).

2) Immersion in water at a certain temperature for a specified time in order to remove weakly bonded molecules that accumulate on the substrate and are not desired to grow from the surface.

3) Drying at room temperature for a specified time in order to increase the adhesion of the material desired to be enlarged to the surface.

4) Rinsing the substrate in pure water at room temperature for the specified time in order to completely purify the material from pollution atoms.

The growth process parameters were used in the same order that we used in our previous studies[19]. The same process is used for Ti-doped SnO_2 thin film. One SILAR cycle was given in Figure 1. Both thin-film productions were scaled up by completing the 40 SILAR cycles.
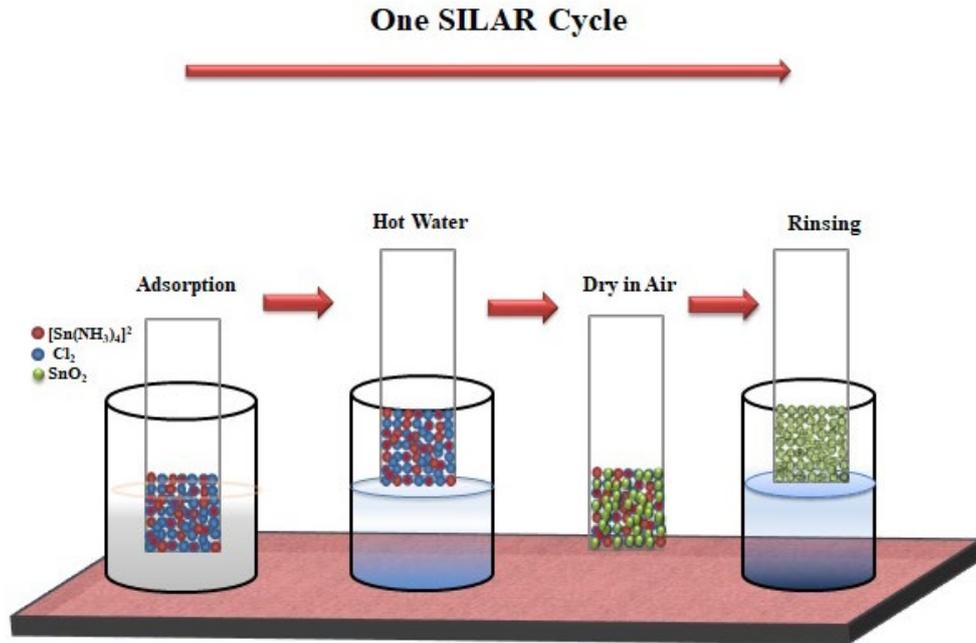
Figure 1. One SILAR cycle

3. Results and Discussions

3.1. XRD Results

The XRD patterns of SnO_2 and Ti-doped SnO_2 thin films grown by SILAR method, are shown in Figure 2. It is seen that undopped SnO_2 thin film has in semi-crystal structure. Addition of titanium, the XRD pattern of $SnTiO_2$ changed the SnO_2 structure and a transition from semi-crystalline to the crystalline structure was observed. The peaks belonging to the TiO_2 anatase phase confirmed 00-021-1272 PDF card occurred the different Bragg's peaks positioned at 2θ $\sim25.8°$, $37.8°$ and $48.05°$ corresponds to crystal planes as (101), (004) and (200). $SnTiO_2$ thin film has also in good agreement with 01-078-1063 positioned at $2\theta\sim26.83°$ and $29.74°$ corresponds to (112) and (113) crystal planes.
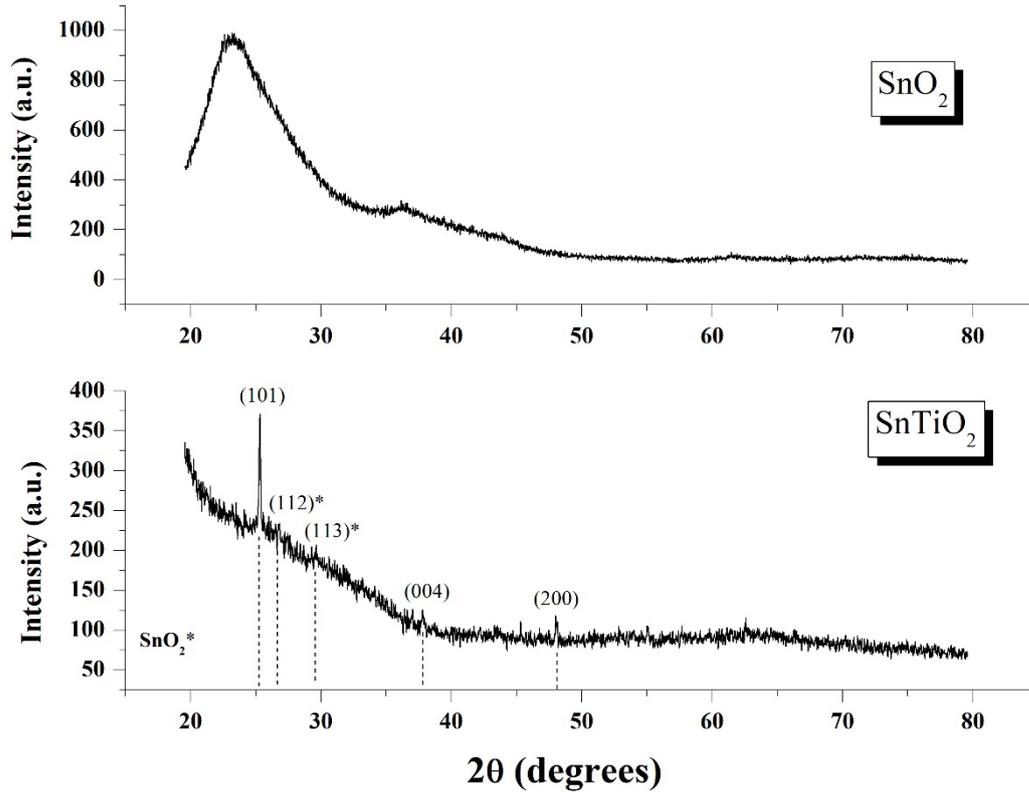
Figure 2. XRD patterns of SnO_2 and Ti-doped SnO_2 films

3.2. SEM Results

It is known that the surface properties affect the electro-optical properties of thin films. For example, it is a desired feature in gas sensor applications to ensure that the target gas adheres to the sensor surface. The surface properties of thin films are very important [2]. Figure 3 show SEM images of SnO_2 and Ti-doped SnO_2 thin films for 5 000x magnitude and 50 000x magnitude. It is seen that the un-doped films have a smooth surface morphology, but the smoothness of the thin film decrease with the titanium additive. Even if the decrease in homogeneity and smoothness has a negative effect in some applications, it is thought to be beneficial in optoelectronic applications as the surface area expands [3], [4].
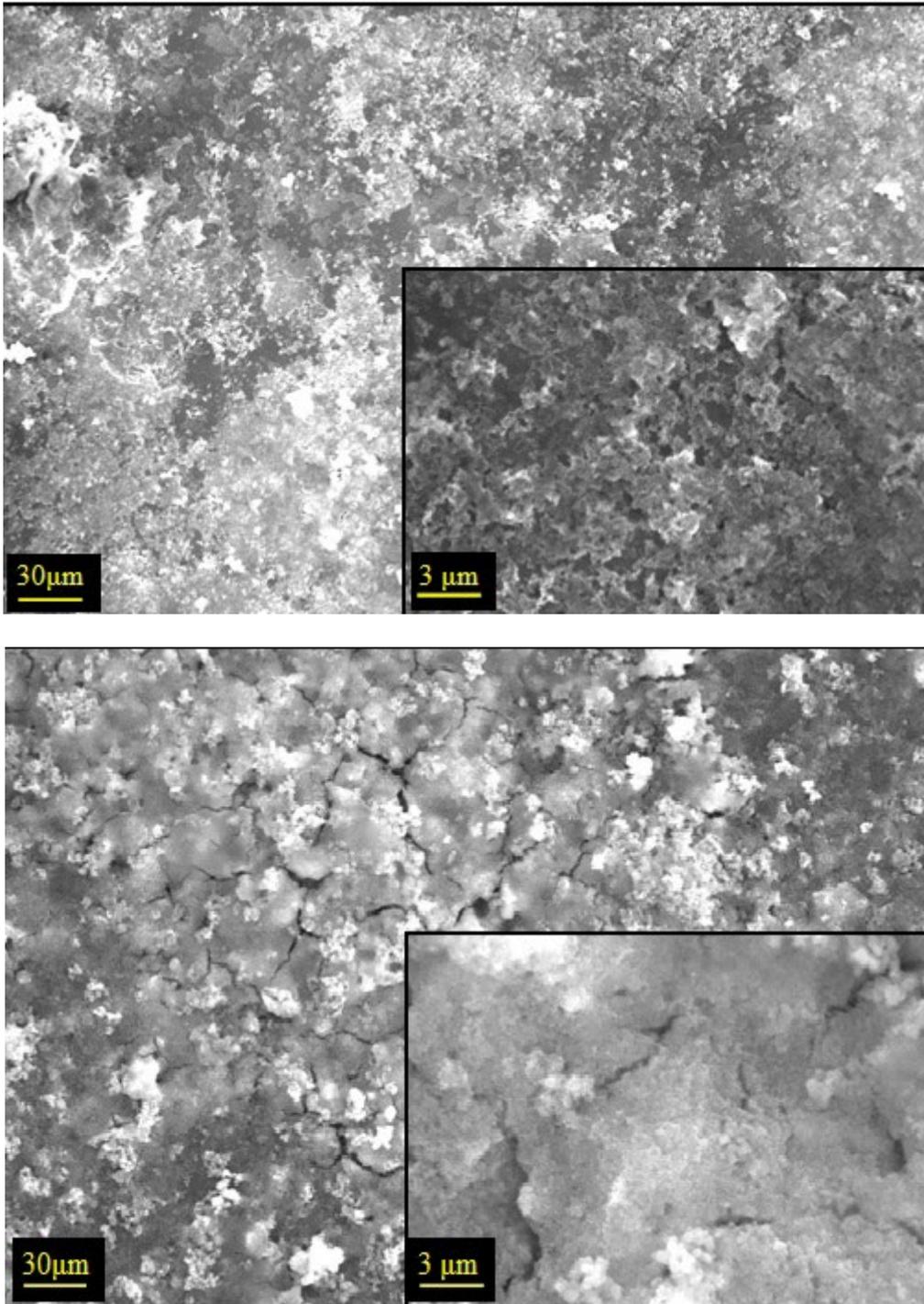
Figure 3. SEM images of SnO_2 and Ti-doped SnO_2 thin films

The EDS image of SnO_2 and Ti-doped SnO_2 thin films and the graphs showing the composition of the elements are shown in figures 4. The peaks of Sn and O belonging to the SnO_2 can be clearly observed in the spectrum, which shows a purity phase of SnO_2. Also, Ti can be clearly seen in the second spectrum. It is known that the other noticed idle peaks, such as Si and Na come from the glass substrate. The percentage values of the elements measured in thin films are given in Table 1.
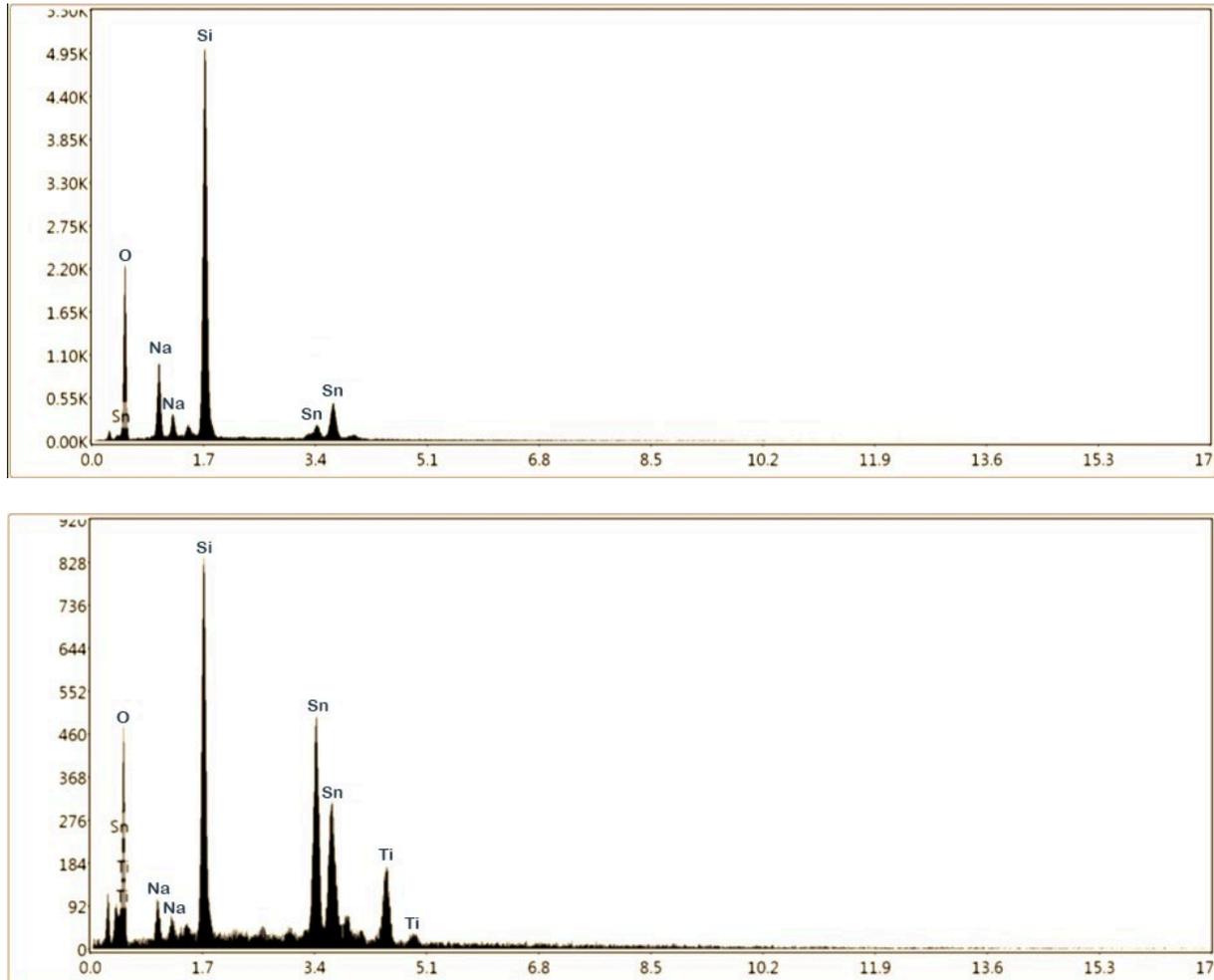
Figure 4. EDS plots of SnO$_2$ and Ti-doped SnO$_2$ thin films.

Table 1. Elements and their percentages in SnO$_2$ and SnTiO$_2$ thin films.

Elements (%)	SnO$_2$ Thin Film	SnTiO$_2$ thin film
O	76.09	35.82
Sn	23.91	50.62
Ti	0	13.56

3.3. UV-Visible Results

Band gap values of thin films were calculated using the data obtained as a result of UV-Visible measurements.

$$(\alpha h\nu)^n = A(h\nu - E_g)$$

where α is the absorption coefficient, $h\nu$ is the incident energy of the photon, A is constant, E_g is the band gap energy and n is the value defined by the indirect and direct band gap. Since SnO$_2$ has a direct band gap in band gap calculations, the n value is used 2[20]. UV-Visible measurements UV-visible absorption spectroscopy and band gap of SnO$_2$ and Ti doped SnO$_2$ thin films are shown in figures 5. The calculated optical band gap of undoped and Ti-doped thin films are 3.92 eV and 3.81 eV, respectively. The band gap decreases with Ti doping. The results were found to be compatible with the literature[18].
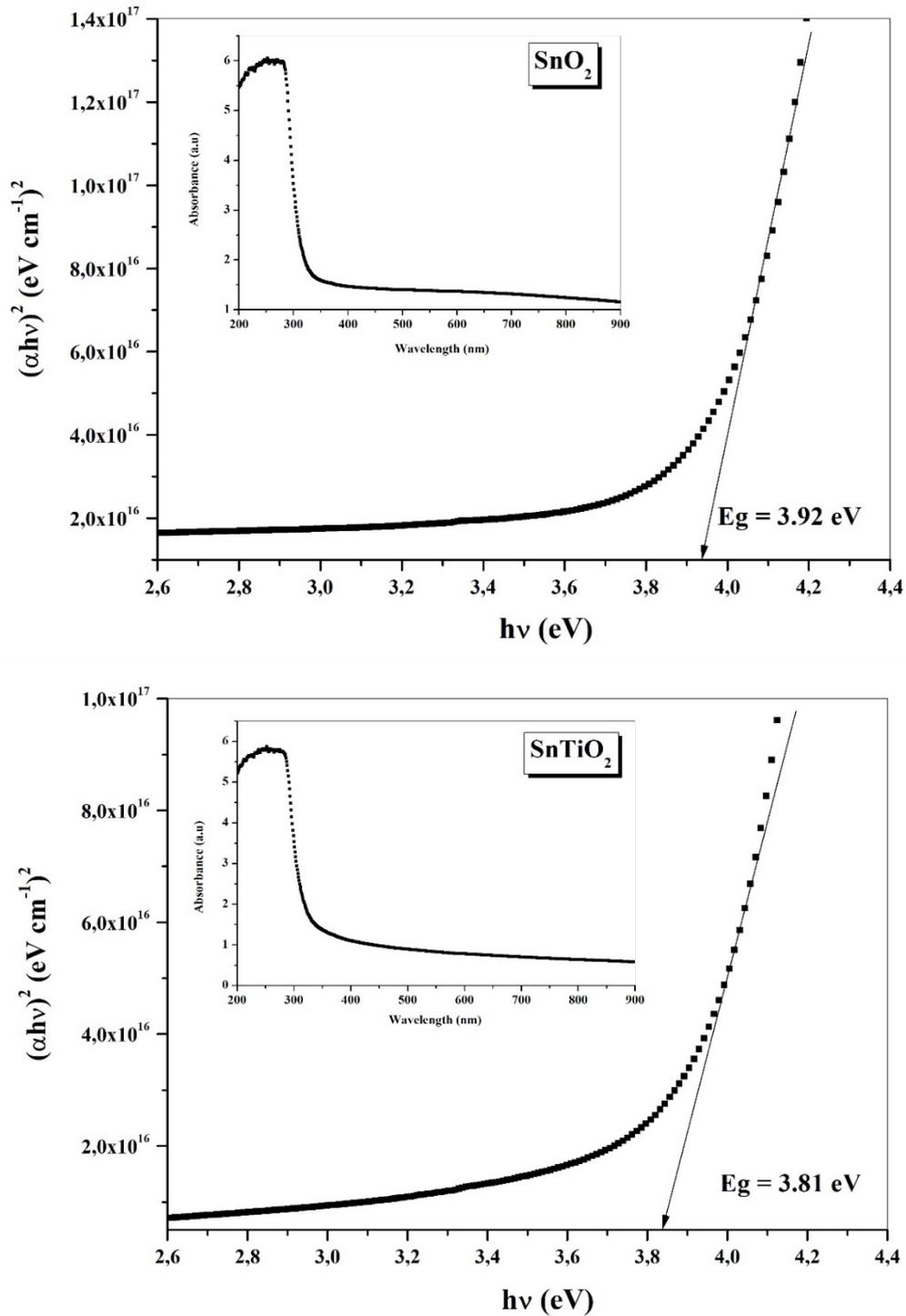
Figure 5. Tauc's plot of optical bandgap for SnO_2, Ti doped SnO_2

Urbach energy plots were given in Figure 6. Band tail energy or Urbach energy characterizes the degree of absorption edge contamination due to crystal lattice irregularity. In short, it is a measure of energy disorder at the band edge. The Urbach Tail values can be calculated with using formula 2 [21].

The equation for Urbach energy is given by,

$$\alpha = \alpha_0 e^{(E/E_u)} \tag{2}$$

where, α_0 is constant, E is the photon energy, α is the absorption coefficient, and E_u is the Urbach energy. The Urbach energy were obtained by plotting $\ln \alpha$ vs. hν. SnO$_2$ thin film Urbach energy value calculated to 0.43 eV and Ti-doped SnO$_2$ calculated value is found to be 0.44 eV. This values are almost close. However, the calculated values were found to be compatible with the literature [22][23].
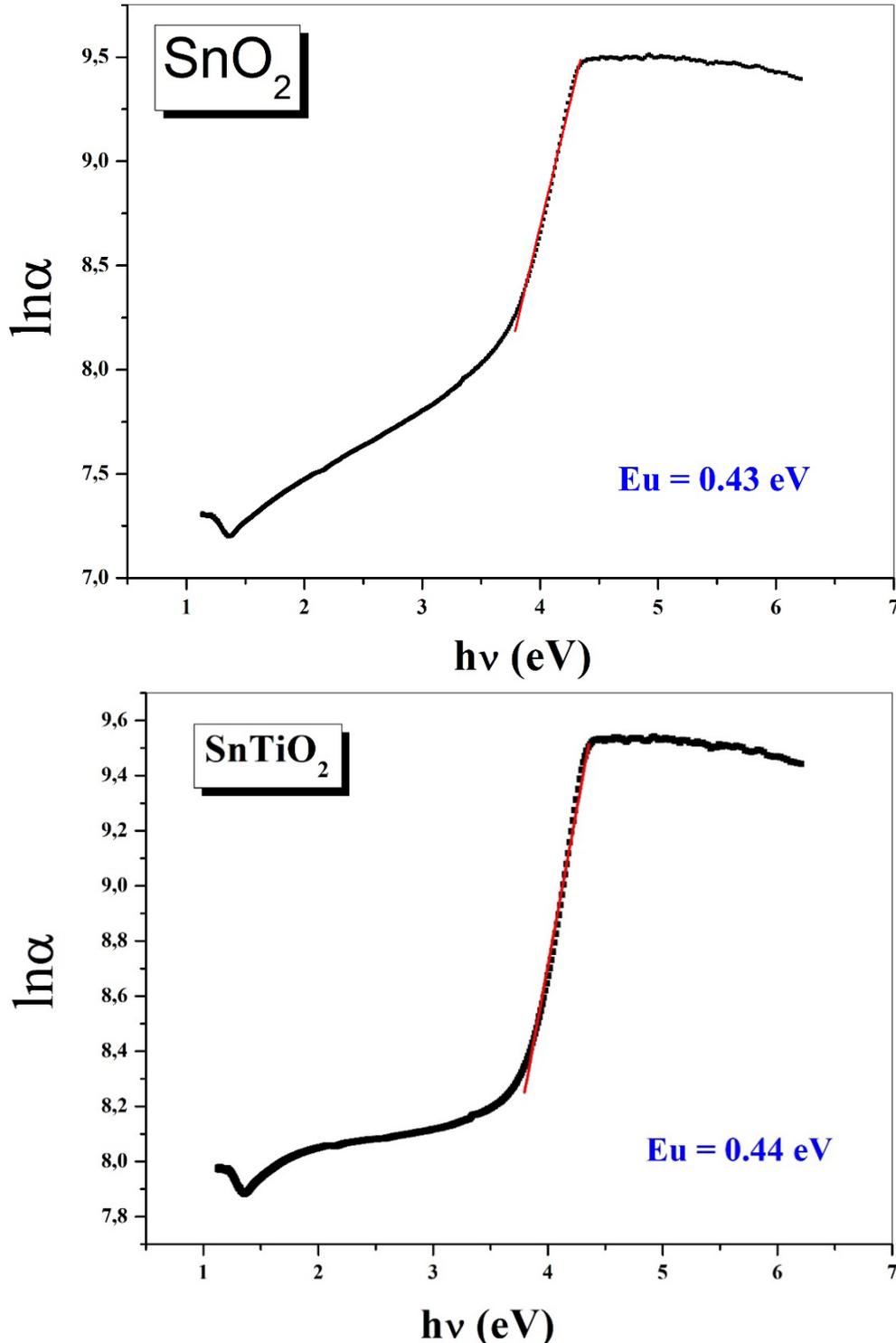
Figure 6. Urbach energy graphs for thin films.

The current-voltage graphs at various temperatures were given in Figure 7. In both graphs, it is seen that the current-voltage curves are linear and symmetrical. Linear curves indicate that thin films have ohmic properties. Although the decrease in the resistance values of the materials with the increase in temperature is clearly seen in the graph, the temperature-dependent resistance change graph in the structure is plotted for a more detailed examination and is given in figure 8.
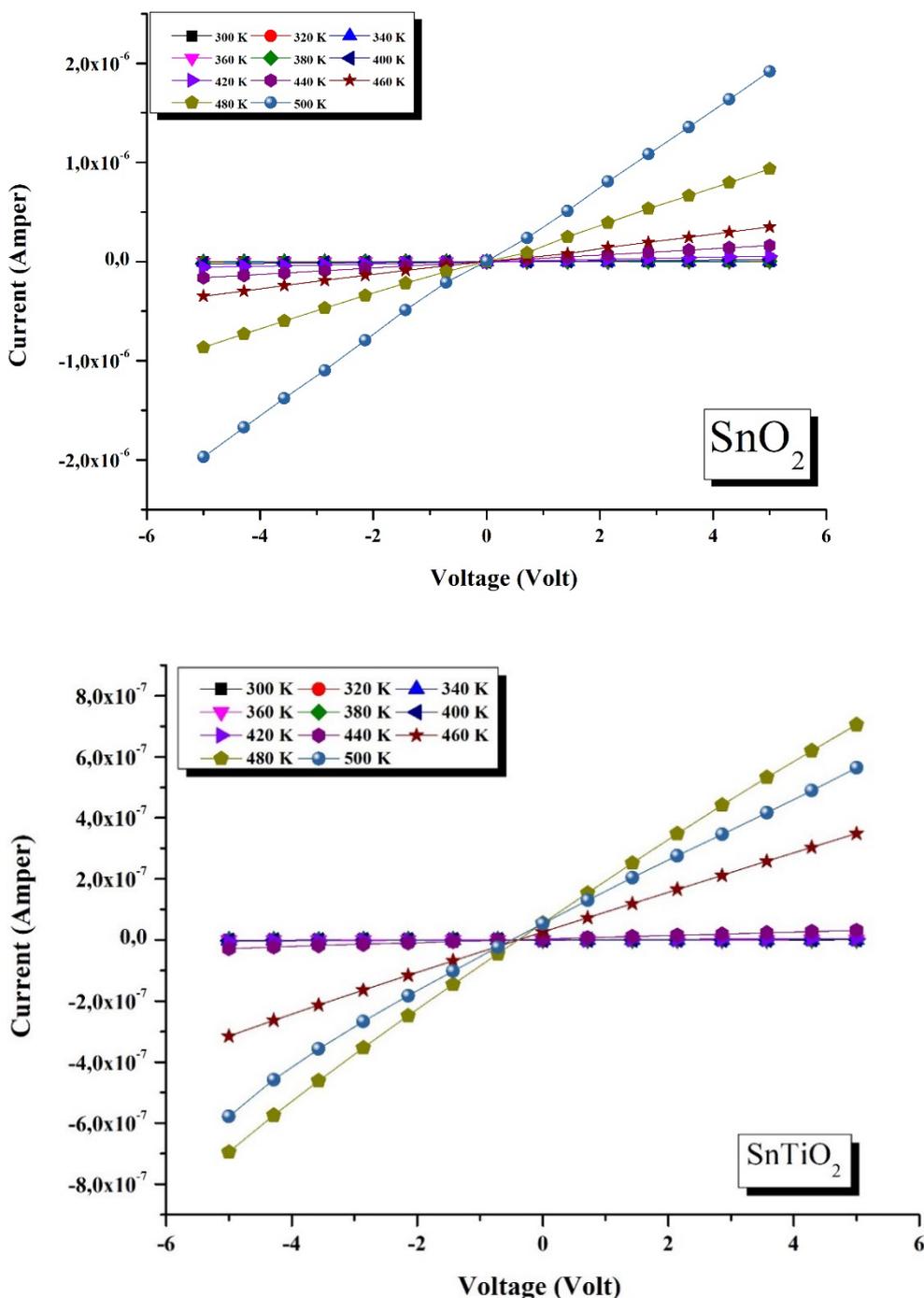
Figure 7. Current-Voltage plots at versus temperatures for SnO$_2$ and Sn-doped TiO$_2$ thin films

Figure 8 depicts the Lnρ versus 1000/T plot of the thin films produced. At the graph of the undoped SnO$_2$ thin film, it is seen that there is a linear decrease in resistivity after 320 °C. The

resistivity value of SnO_2 material at 500 °C was calculated as 9,22 Ω.cm. While it was observed that the resistivity value of the material decreased after 360 °C with titanium additive, the resistivity value of SnO_2 with Ti-doped at 500 °C was calculated as 10,45 Ω.cm.
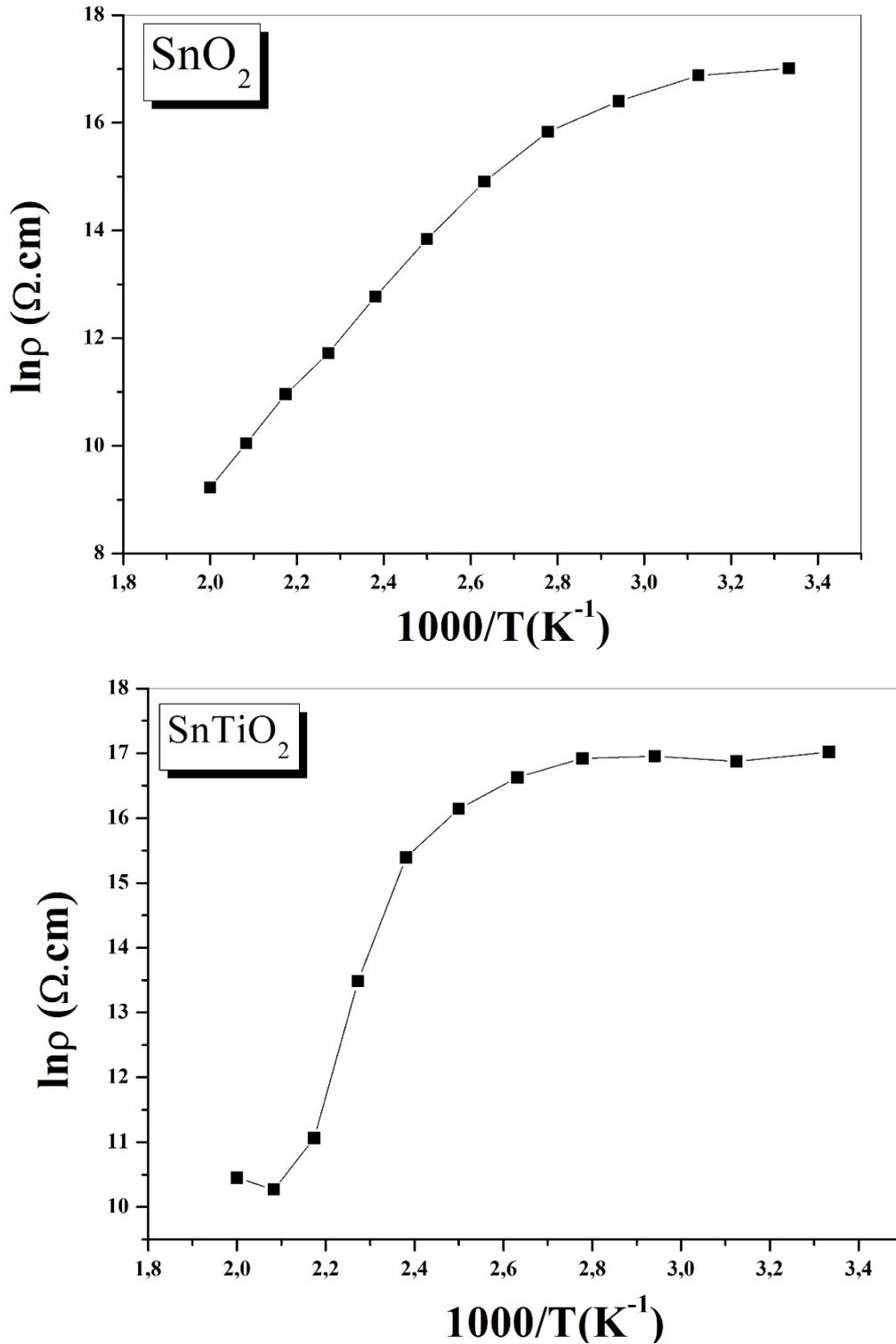
Figure 8. Lnρ-1000/T plots at versus temperatures for SnO_2 and Sn-doped TiO_2 thin films

6. CONCLUSIONS

SnO$_2$ and Ti-doped SnO$_2$ thin films successfully growth on the platinum interdigital contacts by SILAR method. The XRD patterns show that the structure transitioned from the semi-crystalline phase to the crystalline phase with the addition of titanium. Band gap energies calculated as 3.92 eV for undoped SnO$_2$ and 3.81 eV for Ti-doped SnO$_2$. Urbach energy results are in agreement with band gap values. The thin films current-voltage results have linear curves which indicate that thin films have ohmic properties. The resistivity values at 500 °C were calculated as 9,22 and 10,45 Ω.cm for undoped and Ti-doped thin films, respectively. It has seen that there are changes in the properties of the thin films depending on the use of titanium material. Depending on the usage area, titanium-doped SnO$_2$ thin films may show promise in commercial applications.

Conflict of Interest

No conflict of interest was declared by the authors.

REFERENCES

[1]   Alizadeh, A., Rajabi, Y., Bagheri–Mohagheghi, M. M., (2022). Effect of crystallinity on the nonlinear optical properties of indium–tin oxide thin films, Optic Materials, 131, 112589.

[2]   Li, Z., Song, J., Duana, X., Wua, H., Lian, N., Xue, J., Meng X., Yang, F., Li, J., Wang, Y., (2021). F and Al co-doped zinc oxide thin films deposited by ultrasonic spray pyrolysis: Effects of substrate temperature on physical properties, Journal of Alloys and Compound, 858, 158076.

[3]   Yates, H. M., Evans, P., Sheel, D. W., (2013). The influence of F-doping in SnO$_2$ thin films, Physics Procedia, 46, 19, 159–166.

[4]   Zhang, X., Yang, H., (2012). Structural characterization and gas sensing property of Cd-doped SnO$_2$ nanocrystallites synthesized by mechanochemical reaction, Sensors and Actuators B: Chemical, 173, 127–132.

[5]   Athira, M., Bharath, S. P., Angappane, S., (2022). SnO$_2$-NiO heterojunction based self-powered UV photodetectors, Sensors and Actuators A: Physical, 340, 113540.

[6]   Huang, C., Huang, Ni, Y., Lin, P., Fu, N., Fan, B., Xu, B., Zhang, W., (2021). Highly-Crystalline SnO$_2$ Thin Films for Efficient Planar Perovskite Solar Cells, ACS Applied Energy Materials, 5, 5704-5710.

[7]   Hassanien, A., Hashem, H., Kamel G., Soltan, Moustafa, A., Hammam, M., S., Ramadan, A. A., (2016). Performance of Transparent Conducting Fluorine-doped Tin Oxide Films for Applications in Energy Efficient Devices, International Journal of Thin Films Science and Technology, 65, 55–65.

[8]   Antonaia, A., Menna, P., Addonizio, M. L., Crocchiolo, M., (1992). Transport properties of polycrystalline tin oxide films," Solar Energy Materials and Solar Cells, 28, 167–173.

[9]   Sirohi, K., Kumar, S., Singh, V., Chauhan, N., (2020). Hydrothermal synthesis of Cd-doped SnO$_2$ nanostructures and their structural, morphological and optical properties, Materials Today Proceedings, 21, 1991–1998.

[10] Güldüren, M. E., Taşer, A., Güney, H., (2022). Effects of variable Cd doping concentrations on structural and optical properties of SILAR grown SnO_2 thin films, Micro and Nanostructures, 165, 207206.

[11] Saadeddin, I., Buffeteau, T., Campet, G., (2007). Synthesis and characterization of single- and Co-doped SnO_2 thin films for optoelectronic applications," Applied Surface Science, 253, 12, 5240–5249.

[12] Cho, Y., Parmar, N. S., Nahm, S., Choi, J. W., (2017). Full range optical and electrical properties of Zn-doped SnO_2 and oxide/metal/oxide multilayer thin films deposited on flexible PET substrate, Journal of Alloys and Compound, 694, 217–222.

[13] Hadri, A., Chafi, F. Z., Hat, A., Rouchdi, M., (2017). Structural, optical and electrical properties of Fe doped SnO_2 prepared by spray pyrolysis, Journal of Materials and Environmental Science, 8, 2, 420–425.

[14] Atay, F., Akyuz, I., (2022). Structural, optical, surface, and photocatalytic properties of SnO_2 films produced by ultrasonic spray pyrolysis, Journal of Sol-Gel Science and Technology, 102, 2, 303–312.

[15] Liu, P. Y., Chen, J. F., Sun, W. D., (2004). Characterizations of SnO_2 and SnO_2:Sb thin films prepared by PECVD," Vacuum, 76, 1, 7–11.

[16] Ferreira, M., Loureiro, J., Nogueira, A., Rodrigues, A., Martins, R., Ferreira, I., (2015). SnO_2 thin Film Oxides Produced by rf Sputtering for Transparent Thermoelectric Devices, Materials Today: Proceedings, 2, 2, 647–653.

[17] Liu, X. M., Wu, S. L., Chu, P. K., Zheng, J., S. L. Li, S. L., (2006). Characteristics of nano Ti-doped SnO_2 powders prepared by sol-gel method, Materials Science Engineerin A, 426, 1–2, 274–277.

[18] Khelifi, C., Attaf, A., (2020). Influence of Ti doping on SnO_2 thin films properties prepared by ultrasonic spray technique, Surfaces and Interfaces, 18, 100449.

[19] Karaduman Er, I., Çorlu, T., Yıldırım, M. A., Ateş, A., Acar, S., (2019). Low Concentration NO Gas Detection Of SnO_2 And $Zn_{0.50}Sn_{0.50}O$ Sensors, Journal of Polytechnic, 0900, 4, 1189–1196.

[20] Razeghizadeh, A. R., Rafee, V., Zalaghi, L., (2015). Effects of changes sol concentration on the structural and optical properties of SnO_2 nanoparticle by the sol-gel technique, Arxiv, 14.

[21] Choudhury, B., Choudhury, A., (2014). Oxygen defect dependent variation of band gap, Urbach energy and luminescence property of anatase, anatase-rutile mixed phase and of rutile phases of TiO_2 nanoparticles," Physica E: Low-Dimensional Systems and Nanostructures, 56, 364–371

[22] Bahade, S. T., Lanje, A. S., Sharma S. J. (2017). Synthesis of SnO_2 Thin Film by Sol-gel Spin Coating technique for Optical and Ethanol Gas Sensing Application, International Journal of Scientific Research in Science and Technology, 3, 7, ISSN: 2395-6011.

[23] Suriya, P., Prabhu, M., Jagannathan, K., (2022). Synthesis and structural, optical and photovoltaic characteristics of pure and Ag doped TiO_2 nanoparticles for dye sensitized solar cell application, Materials Today Proceedings, 65, 100–105.

Research Article

Residual Stress Analysis in Machining of a Near Beta Ti Alloy, Ti-5553 Under High Pressure Cooling and Lubrication

Authors: Lokman Yünlü (iD)

Residual Stress Analysis in Machining of a Near Beta Ti Alloy, Ti-5553 Under High Pressure Cooling and Lubrication

Lokman Yünlü*

[1]Burdur Mehmet Akif Ersoy University, Engineering Faculty, Mechanical Engineering Department, Turkey.

*Corresponding Author: lokmanyunlu@yahoo.com

ABSTRACT: Ti-5553 (Ti–5Al–5Mo–5V–3Cr) one of the titanium alloys, is a recently developed near beta Titanium alloy, which is frequently used in the aerospace industry such as landing gear. When machining these superalloys, surface integrity can be affected by cutting and cooling conditions. An experimental study was conducted on Ti-5553, also known as beta-like titanium alloy, to understand the role of High Pressure Cooling and Lubrication conditions on surface integrity. In this study, high pressure coolant levels and other machining parameters (cutting speed, feed rate) were chosen as variable factors. These various levels were selected in different values and used in the tests to emphasize the relations of the accepted shear conditions from the effective data in the formation of residual stresses, which is also a parameter of the surface integrity. The results demonstrate the need to prepare coolant pressure levels to improve work surface integrity in such a material. In order to reveal the consistency of the coolant pressure values with other determined cutting parameters and the accuracy of choice, a relationship optimization has been tried to be explained.

Keywords: Residual Stress, Ti-5553 Alloy, High Pressure Cooling, Surface integrity

1. INTRODUCTION

Titanium alloys generally have high ductility, strength and low fatigue properties. However, it is a heat treatable alpha-beta alloy produced to combine increased high temperature operating performance with high strength properties [1]. These alloys are known as two-phase titanium alloy with high corrosion resistance, good strength and ductility. Therefore, it is used in aerospace, automotive and other industries. Ti-5Al-5V-5Mo-3Cr (Ti-5553), also called beta-titanium alloy, has high strength, good temperature resistance and favorable ductility, depending on the heat treatment applied [2], [3]. This alloy has a higher tensile strength properties compared to other Ti alloys from the same family. Due to this superior ability, Ti-5553 is especially preferred in the aviation industry [4].

Titanium-based superalloys are widely used in many industries, including the aerospace, biomedical and automotive industries, due to their unique/superior properties. These alloys are frequently preferred especially in jet engines due to their good temperature resistance and higher corrosion resistance [5]. Titanium alloys are known as more expensive materials compared to other metals [2], [27]. The main reasons are due to the difficulties encountered in the extraction process, melting and workability. It makes these materials special is not only their place of use, but also that they are special in terms of manufacturing processes such as machining and cutting. Although the latest point in material technology has increased the use of these alloys, it is still considered an industrial problem in terms of machining and manufacturing [6], [7], [8]. These materials are known as hard-to-cut alloys. The main reasons for the hard machinability of titanium alloys are due to their high chemical reactivity, low thermal conductivity and modulus of elasticity. Recently, some cooling techniques have been developed to improve the cutting performance of low machinability alloys such as titanium [9]. These methods are; These are applications that provide better dimensional accuracy of the parts produced after machining, improve the increase the tool life and surface integrity of the material [10]. Research has focused on improving the machinability of titanium alloys, such as conventional cooling, dry cutting,

minimal lubrication (MQL), high pressure cooling/lubrication (HPC) and cryogenic cooling. In this study, the focused cooling strategy is the HPC system [11].

In machining difficult-to-cut materials, the effect of high-pressure jet coolant on the cutting zone can increase machining efficiency and ensure sustainability through better chip breaking and removal [12]. Proper selection of cutting method and parameters can increase the efficiency of the process while minimizing production costs. HPC is one of the methods aimed at increasing the machinability of hard-to-machine alloys by using high-pressure coolling water or an emulsion injected between to chip tool interface [11]. Some studies have revealed that directing the HPC system to the cutting zone provides control of chip formation, lowers temperatures in the cutting surface and facilitates chip removal [13]. This has also shown that it plays an important role in increasing tool life. However, High pressure cooling assisted cutting method offers an advanced method for achieving the desired surface quality finish and surface integrity of hard-to cut alloys such as titanium [14]. With this method, it is aimed to reduce the negativities such as cutting tool cost by preventing the dangerous situations in terms of health and environment in the traditional machining method.

Surface roughness, hardness, wear, internal stresses are also known as surface integrity factors that determine machining quality and fatigue life [8]. These factors are one of the most vital aspects of the quality of the machined surface, especially after processing very sensitive materials [15]. Therefore, determining the relationship between machining conditions and residual stresses, then revealing the most optimal machining parameters is one of the primary goals of the researchers [9]. Residual stress is the most common properties used to determine the quality of the machined workpiece surface, especially when manufacturing critical special structural components [6]. This is a feature that is emphasized in precision machining made of titanium alloys used in large proportions in the aerospace and medical industries [16].

Machining also known as surface integrity is an effective process on microstructural and topographic conditions of the machined surface [25]. Surface integrity, which expresses the state at the end of the cutting process in machining, covers the resulting microhardness, surface roughness, crystal structure, and all possible surface defects (microchip debris, material picking, tearing, dragging and contamination) [11], [17]. Residual stresses are the result of heat generated in the surface and subsurface layer as a result of the mechanical interaction between tool and workpiece during machining [3] [18]. In short, it is an effect of friction and heat on the surface and substrates in the machining process. The distribution of residual stress on the machined zone and substrate at the end of the cutting process reveals the functional performance of these components, including fatigue life and corrosion resistance.

Experimental design (DoE) defines the input parameters and levels, the response variable, the choice of test parameters, and a set of operations used to analyze the experimental results [18], [24]. This experimental method developed to evaluate the performance and effects of factor variables [19]. It defines the input parameter levels for optimal response variables and requires determination of appropriate experiment design, careful planning, correct experiment placement, and analysis of results [11] [18]. During the experiment, as the number of processing variables increases, so will the number of experiments that need to be done [20]. In Taguchi experimental design, the selection of an optimal orthogonal sequence should be made to describe the input variables (factors) and their interactions [14], [21]. Using statistically derived orthogonal arrays to plan experiments greatly reduces the number of tests in determining the quality of the analysis [22].

The aim of the current research: to reveal the effect of cutting parameters (feedrate f, depth of cut DoC, cutting speed Vc, and Coolant pressure P) on residual stress. The depth of cut of 2 mm was used as a fixed input parameter in the experiments. However, using the shear parameters determined by the experimental design method of the Ti-5553 alloy, to determine the optimum shear parameters that minimize the residual stress formation in the surface and subsurface layer [23]. In this study, three input factors were selected and a full factorial DoE consisting of three levels for each factor was designed and used to analyze the amount of residual stress produced at the end of machining. Turning of Ti-5553 was performed using a (Ti, Al) N+TiN carbide coated cutting inset.

2. EXPERIMENTAL PROCEDURES

Due to the high hardness of the new generation Ti-5553 alloys during machining, a chemical reaction occurs between the cutting insert and the workpiece material. This causes rapid wear on tool and thermal stresses on workpiece surface [28]. A process diagram related to the experiment plan is given Figure 1. below in order to anticipate this whole process and not to overlook possible problems.
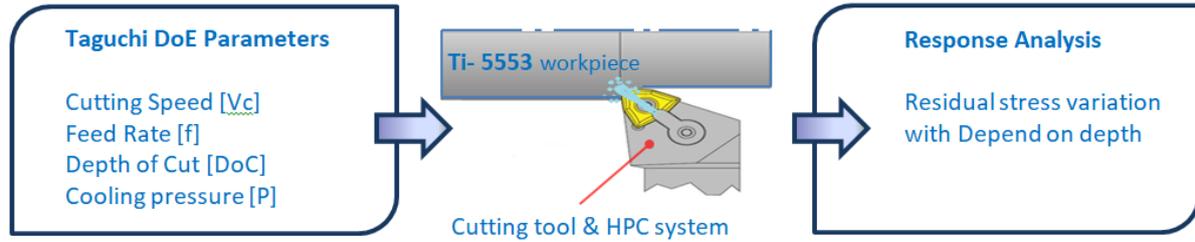
Figure 1. Schematic view of machining process.

2.1. Workpiece and Machine Tool

Ti-5Al-5V-5Mo-3Cr contains 20% of the α phase, this is known as a near β alloy. It has a Young's modulus similar to Ti64 in research. However, these two materials differ significantly in terms of mechanical property. Ti-5553 has 30% higher yield and tensile strength, but also lower ductility.

The workpiece used in the tests is a hot rolled cylindrical bar material made of Ti-5553 material, which is expressed as a titanium alloy close to β. The tests were carried out using Ti-5553 alloy with a diameter of 65 mm and a length of 200 mm. When this material is annealed, its tensile strength can reach up to 1080 MPa [26]. At the same time, when this material is heat treated, its tensile strength can exceed 1500 MPa. When Ti 5553 alloy is compared with other ti alloys; It stands out with its properties such as hardness, high strength and fracture toughness. The chemical composition and mechanical properties of this alloy are given in Tables 1 and 2, respectively.

Table 1. Chemical composition of Ti-5553 alloy.

Ti	Al	Mo	V	Cr	Fe	Si	O	C	Zr	H
Base.	4.4-5.7	4.0-5.5	4.4-5.5	2.5-3.5	0.3-0.5	≤0.15	≤0.18	≤0.1	≤0.30	≤0.015

Table 2. mechanical properties of Ti-5553 alloy.

Parameter	Value	Parameter	Value
Density (g/cm^3)	4.58	Specific heat capacity(J/(kg·k))	775
Melting point (K)	860	Young's modulus (GPa)	110
Poisson's ratio	0.31	Elongation (%)	11
Thermal conductivity (W·m^{-1} C^{-1})	8.3	Hardness (HV)	317±5

Machining experiments were carried out on an ANL-75 CNC machinin center with a spindle speed ranging from 35 to 3500 rpm and a motor power of 15 kW, supported by a high-pressure submersible pump providing a maximum pressure of 35 MPa and a flow rate of 21 l/min.

2.2. Cutting Tool and Application of Cooling Method

For use in the experiments, (Ti,Al)N+TiN coated carbide cutting insert were preferred by using the literature. The tool has a corner radius rε = 0.8 mm. A SECO Jet stream tool holder, cutting rake angle, γa = -6°, back rake angle, γb = –6°, approach angle is Kr = 95° and nozzle diameter d = 1,5 mm It is shown in Figure 2.
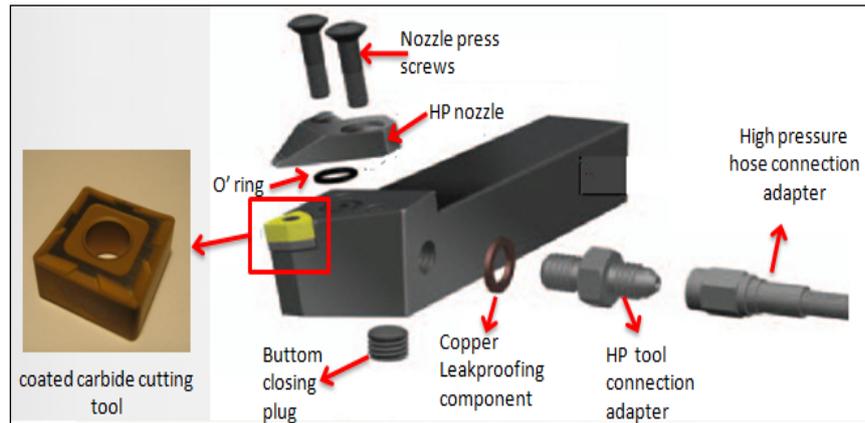
Figure 2. Cutting tool and HPC connection equipment

Before each cutting test, the worn tool was replaced with a new tool to maintain the surface integrity of the machined surface.Llubricating/Cooling fluid used in the experiments, 5% concentration, water-soluble oil chemical-based oil was used. Swisslube BCool 650 oil is injected at a low angle (tool rake angle of about 5 to 6°) to chip and tool interface.

2.3. Residual Stress Measurement Method and Application

Residual stress is elastic stress that remain in the part after various production/manufacturing stages. Plastic deformations or thermal changes that remain without homogeneous distribution in the material as a result of welded manufacturing, surface treatments, casting and heat treatments are the causes of residual stress. The residual stress subsurface can measured using the method of X-ray diffraction (XRD) [27]. Chemical etching is a common technique used in etching material to determine the amount of residual stress in the subsurface layers. In the study, residual stress was measured from the machined surfaces using the XRD method. The measured values in the σ_{xx} (axial) and σ_{yy} (radial) directions are calculated. In this process, residual stress values were calculated in ten reps from the surface of the material to a depth of 150 micrometers. Then, material was removed from the surface using the electropolishing process, measuring the residual stress value at every 10 micrometer depth. This method does not cause any damage to the internal structure of the material [29]. After the high pressure cooling assisted turning where the residual stress is measured and the schematic representation of the application of the HPC system are shown in the figure 3. The entire procedure regarding the experiment, material and method of the study is given below in table 3.
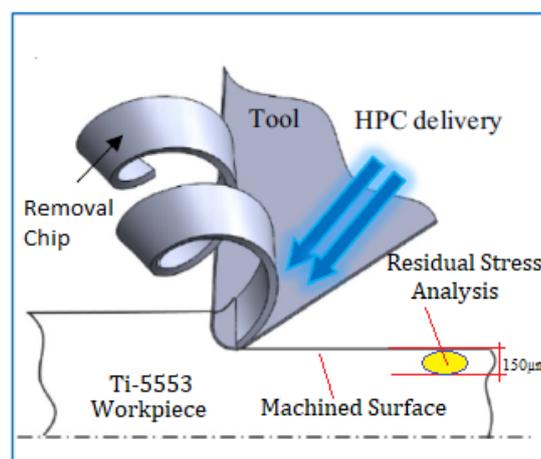
Figure 3. HPC processing and residual stress measured surface.

Table 3. Technical specifications of the machine tools, machining parameter factors, tool and cooling properties.

Category	Specifications
Machine tool	A general-purpose ALEX ANL-75 CNC lathe, (15 kW, speed range: 35 to 3500 rpm), Fanuc control system.
Work material	Ti-5Al-5V-5Mo-3Cr or known as near beta Ti alloy (Ti-5553)
Dimensions	Ø65 × 200 mm
Cutting Tool and Cutting Tool Holder	Rhombic shape CNMG 120408, (Ti,Al)N+TiN coated carbide SECO Jet stream PCLNR tool holder.
Cutting speed, Vc (m/min)	80, 100, 120
Feed, f (mm/rev)	0.1, 0.15, 0.2
Depth of cut, DoC (mm)	2 mm
Cooling environment	Conv (0.6), 15, 30 MPa The cooling/ lubrication fluid (CLF) chemical-based 5% concentration water soluble oil 5 to 6° with the cutting tool rake angle 21 l/min with 1,5 mm brass nozzle diameter.

2.4. Design of Experiment and Application of Machining Methods

A Taguchi orthogonal array, L_9 (3^4) is adopted in the turning process. Processing parameters selected in the application of the tests; Vc; 80-100-120 m/min, P; 0.6-15-30 MPa f; 0.1-0.15-0.2mm/rev, and a constant DoC; 2 mm. The response result parameter obtained of the tests is the average residual stress (axial and radial direction) values. Three levels were chosen for each input factor to increase the accuracy of the cutting parameters. The contents of the experimental design are given in Table 4.

Table 4. Cutting parameters and their levels

Symbol	Cutting parameters	Level 1	Level 2	Level 3
Vc (m/min)	Cutting speed	80	100	120
f (mm/rev)	Feed rate	0.1	0.15	0.2
P (MPa)	Cooling pressure	0.6	15	30

2.5. Empirical Model and Analysis of Residual Stress

The mean residual stress values measured at the end of each test were calculated according to Ri and Kij. Kij is calculated in Eq. (1) since the average residual stress is j at the selected level, of the machining parameter is i. At the end of these processes, Kij was calculated smaller is the best to obtain its desired effect compression stress [30].

The value calculated as the lowest level of Kij is the optimum level for each input factor. The calculated Ri value is Eq. (2) determines the order of importance of cutting parameters over residual stresses. As a result, by calculating the relationship between Kij and Ri, its effect on residual stress and its optimum levels can be determined [13] [30].

$$K_{ij} = \frac{\sum R_a(k)}{3} \tag{1}$$

$$R_i = max(K_{i1}, K_{i2}, K_{i3}) - min(K_{i1}, K_{i2}, K_{i3}) \tag{2}$$

in this equation; respectively; i = 1,2 and 3 (cutting speed, feed rate, and indicates cooling pressure), respectively; j = 1, 2, 3 shows level 1, 2 and 3, which are equal to the processing parameters, k = 1, 2, .. 9 is the test sequence number; Ra (k) represents the average stresses on the finished surface at the shear parameter;k.

Residual stresses at a distance of up to 150 micrometers in ten steps in total by descending 15 micrometers from the workpiece surface for each test; Ra was calculated and the average of these values was taken. These values are calculated in both axial and radial directionsis given in Table 5.

Table 5. Average residual stress results in axial and radial directions

The experimental design and response results for these three levels of cutting parameters using the L_9 (3^4) orthogonal array are given in Table 4 [12]. The average residual stress values (in both directions respectively) found according to equations 1 and 2 and their relations calculated for each level are given in the table 6 and 7 below.

Table 6. Average residual stresses in Axial direction of Kij and Ri calculations

Symbol	Cutting parameters	Kij			Ri
		Level 1	Level 2	Level 3	
Vc [m/min]	Cutting speed	-58.7	-207	-288	229.3
f [mm/rev]	Feed rate	-150	-206	-197.7	56
P [MPa]	Cooling pressure	-141.7	-189.7	-222.7	81

When the correlation between R values is calculated

$$Ri_{axial} = R1 > R3 > R2 \qquad (3)$$

Table 7. Average residual stresses in Radial direction of Kij and Ri calculations

Symbol	Cutting parameters	Kij			Ri
		Level 1	Level 2	Level 3	
Vc [m/min]	Cutting speed	-67.7	-188	-289	221.3
f [mm/rev]	Feed rate	-122.3	-194	-229	106.7
P [MPa]	Cooling pressure	-113.3	-191	-241	127.7

When the correlation between R values is calculated

$$Ri_{radial} = R1 > R3 > R2 \qquad (4)$$

To calculate the average residual stresses in both directions; the Kij equation is used. These results are written at levels of input parameters in field in tables 6 and 7, respectively.

K11 = (61 – 94 – 170) / 3

K12 = (–172 –134 – 259) / 3

K13 = (– 229 –345 –294) / 3

… ..

K33 = (–170 –259 –294) / 3 (5)

3. EXPERIMENT ANALYSIS and VALIDATION

There are many residual stress measurement methods in practice. The xrd method, which is the most preferred method in determining the residual stresses on the surface in metal cutting process, is a non-destructive measurement method. The surface and subsurface residual stress can be found using the Bragg law calculation used in the X-ray diffraction method. The chemical etching method is often preferred technique used in high pressure cooling-assisted metal cutting to remove layers from the surface to obtain residual stresses.

At the end of the cutting tests, the residual stress values in both directions (axial and radial) were calculated mathematically by using the $\sin^2\psi$ method [15]. In each test, two values were calculated for each layer of the workpiece, both in the axial and radial directions. In the electropolishing process, layers of 15 μm from the surface were etched each time using a solution of phosphoric and sulfuric acid. These processes were repeated in ten steps until a total of 150 μm was reached.

When the results are examined carefully; In general, tensile residual stresses reach near zero when the depth exceeds 150 μm. This situation; This leads to the conclusion that the mean residual stress can be characterized by the variation of residual stress with depth. In order to fully understand the HPC effect, instead of presenting all nine experiments graphically, three different cooling pressures at a constant shear rate were evaluated graphically and the residual stress profiles are shown in Figure 4.
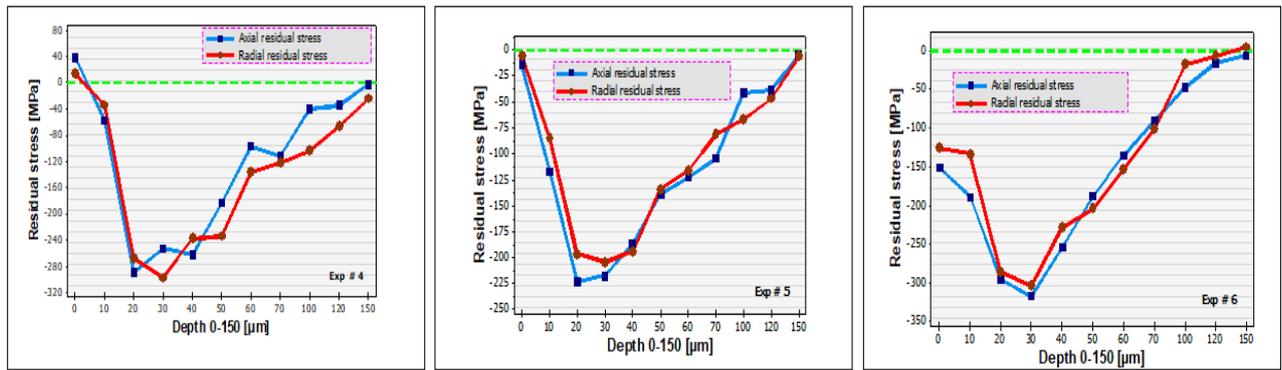
Figures 4. Residual stress variation in both directions of #4 #5 #6 tests

To better understand the residual stress change, one parameter at a time was assumed as a constant value. Thus, the effect of the other two parameters could be observed more easily. In these three graphs, the average residual stress changes at a constant shear, feed rate, and cooling pressure are presented graphically, respectively.

In the Taguchi experimental design method, optimal levels were determined for machining parameters (Vc;80- P;0.6-f;0.1) using the principle of smaller-better for Kij in the calculation of axial and radial residual stress values. The results indicates that the optimal Vc is common to the axial and radial compressive residual stress (see Figure 5). Ri value was calculated to determine the effect of shear parameters on residual stresses. Therefore, it has been observed that the feed rate has a decisive effect on the residual stress occurring in the axial direction.

When the Ri value given in Table 6 and Table 7 is examined, it is understood that the cutting speed has a greater effect on the residual stresses in both directions. However, cooling pressure and feed rate were found respectively to be the most effective factors on residual stress.
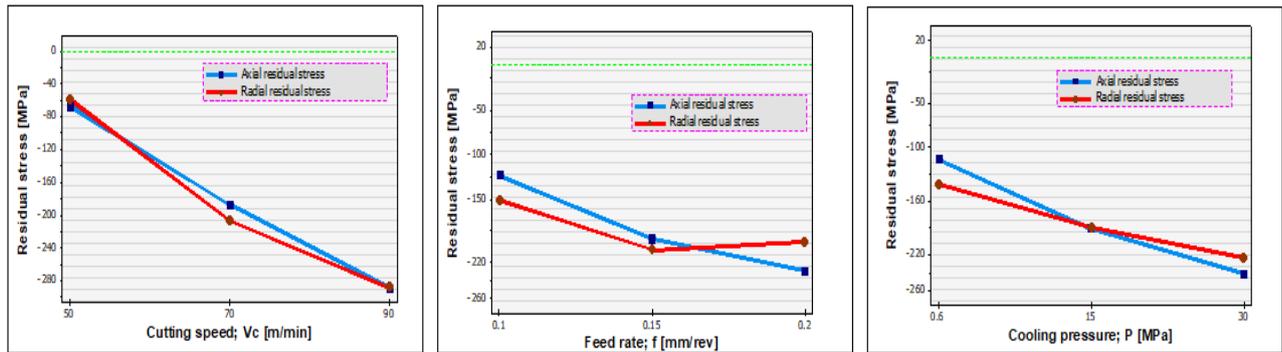
Figures 5. Kij value for each levels of cooling pressure, cutting speed and feed rate

4.CONCLUSION

According to these calculated results; we can reach the conclusion that machining parameters have different effects on residual stresses in both directions. The cooling pressure, which produces the lowest average residual stress value, appeared at level 3 of the cooling pressure for both the radial and axial directions. However, when the feed rate was selected at level 1, the minimum average residual stress value in both directions was obtained. Considering the effect of the feed rate on the average residual stress values formed in both directions; It was observed that the lowest stress occurred at the 3rd level and the highest average residual stress occurred at the 1st level. However, considering the effect of shear speed on the average residual stress, the maximum average stress value occurred at level 3 in the axial direction, while it occurred at level 2 in the radial direction.

The axial and radial determination of residual stresses in the turning process of Ti-5553 alloys, also known as difficult-to-machine materials, under high pressure cooling fluid support, was investigated experimentally.

Taguchi experimental design method was used in this process. Different levels of 3 input parameters were used in the experiments. Residual stress values in axial and radial directions were calculated from the results obtained and optimum machining parameters were proposed with a series of optimization processes.

If we evaluate the scientific results obtained from this study;

- When the effect of the feed rate parameter on the mean residual stress is examined, the level 1 value is slightly larger than the level 2. So we can select the feed rate as level 1 for the optimum machining level.

- When the average residual stress in the subsurface layer are examined, it is seen that the cutting speed; Vc is the most important parameter, respectively followed by the cooling pressure, and the feed rate in the radial direction,

- When the graphs are examined, the average residual stress when machining under the effect of cooling pressure is 0.6 MPa measured to be higher than the residual stress at 15 MPa cooling pressure.

- In the graphs showing the residual stress change depending on the depth, when the residual stresses in both directions are examined at 150μm from the surface, it is seen that the cooling pressure is more effective on the residual stress in the radial direction.

REFERENCES

[1] Niknam, S. A., Khettabi, R., & Songmene, V. 2014. Machinability and Machining of Titanium Alloys: a Review. Machining of Titanium Alloys, 1-30.

[2] Baili, Maher, et al. 2011. An Experimental Investigation of Hot Machining with Induction to Improve Ti-5553 Machinability. In: Applied Mechanics and Materials. Trans Tech Publications Ltd,. p. 67-76.

[3] Wagner, V., Baili, M., Dessein, G., & Lallement, D. 2009. Behaviour Laws Comparison For Titanium Alloys Machining: Application To Ti5553. In International Conference on Structural Analysis of Advanced Materials pp. Pp-1.

[4] Sun, Y., Huang, B., Puleo, D. A., & Jawahir, I. S. 2015. Enhanced Machinability of ti-5553 Alloy from Cryogenic Machining: Comparison with Mql and Flood-Cooled Machining and Modeling. Procedia Cirp, 31, 477-482.

[5] Mohd Hadzley, A B., Izamshah, R., Sarah, A. Siti. And Fatin, Nurul, M., 2013. "Finite Element Model of Machining with High Pressure Coolant for Ti-6Al-4V Alloy". Malaysian Technical Universities Conference on Engineering & Technology MUCET 2012. 53 p. 624-631.

[6] Kadir, G., & Antepli, A. 2020. Toz Metalurjisi Yöntemiyle Üretilen Al2024 ve Al6061 Matrisli, Grafen–Karbon Nanotüp Ve Titanyum Dioksik Takviyeli Kompozit Malzemelerin Mikroyapi Ve Mekanik Özelliklerinin Incelenmesi. Turan: Stratejik Arastirmalar Merkezi, 12(48), 282-290.

[7] Madyira, D. M., Laubscher, R. F., Van Rensburg, N. J., & Henning, P. F. J. 2013. High Speed Machining Induced Residual Stresses in Grade 5 Titanium Alloy. Proceedings of the Institution of Mechanical Engineers, part L: Journal of Materials: Design and Applications, 227(3), 208-215.

[8] Polvorosa, R., Suárez, A., de Lacalle, L. L., Cerrillo, I., Wretland, A., & Veiga, F. 2017. Tool Wear on Nickel Alloys with Different Coolant Pressures: Comparison of Alloy 718 and Waspaloy. Journal of Manufacturing Processes, 26, 44-56.

[9] Shokrani, A., Dhokia, V., & Newman, S. T. 2016. Investigation of The Effects of Cryogenic Machining on Surface Integrity in CNC End Milling of Ti–6Al–4V Titanium Alloy. Journal of Manufacturing Processes, 21, 172-179.

[10] Fang, Z., Obikawa, T., 2017. Turning of Inconel 718 Using Inserts with Cooling Channels Under High Pressure jet Coolant Assistance. Journal of Materials Processing Tech. 247 19–28.

[11] Liang, X., Liu, Z., Liu, W., Wang, B., & Yao, G. (2019). Surface Integrity Analysis for High-Pressure Jet Assisted Machined Ti-6Al-4V Considering Cooling Pressures and Injection Positions. Journal of Manufacturing Processes, 40, 149-159.

[12] Wang, Liang, et al. 2022. "Experimental Research on Chip Morphology of Ti-5553 Cutting under High-Pressure Cooling." Integrated Ferroelectrics 229.1 62-77.

[13] Liu, Erliang, et al. 2022. Surface Integrity Analysis Of Ti-5553 Under Different Cooling Strategies. Ferroelectrics, , 593.1: 51-62.

[14] Gündoğan, K., & Öztürk, D. K. 2021. Investigation of Properties ZnO, CuO, and TiO2 Reinforced Polypropylene Composites.

[15] Khoshaim, A. B., Elsheikh, A. H., Moustafa, E. B., vd. 2021. Prediction of Residual Stresses in Turning of Pure Iron Using Artificial Intelligence-Based Methods. Journal of Materials Research and Technology, 11, 2181-2194.

[16] Le Coz, G., Marinescu, M., Moufki, A., Dudzinski, D., 2010. Residual Stresses After Dry Machining of Inconel 718, Experimental Results and Numerical Simulation.

[17] Kamruzzaman, M., Dhar, N. R., 2009. Effect of High-Pressure Coolant on Temperature, Chip, Force, Tool Wear, Tool Life and Surface Roughness in Turning AISI 1060 Steel. Gazi University Journal of Science, 22(4), 359-370.

[18] Zhao, Xin, et al. 2022, Effect Of Cryogenic Cutting Surface Integrity On Fatigue Life Of Titanium Alloy Ti-5553. Ferroelectrics, 596.1: 115-125.

[19] Braham-Bouchnak, Tarek, et al. 2015. "Influence of High-Pressure Coolant Assistance on the Machinability of the Titanium Alloy ti555–3." Machining Science and Technology 19.1 2015, 134-151.

[20] Kock Filho, Tarcisio. 2021. Analysis of Different Ti5553 Alloy Cutting Strategies for the Improvement of Tool Life. Phd Thesis.

[21] Vishal S. Sharma, Manu Dogra, N.M. Suri, C., 2009. "Cooling Techniques for Improved Productivity in Turning." 49(6), p 435–453.

[22] Kui, G. W. A., Islam, S., Reddy, M. M., Khandoker, N., & Chen, V. L. C. 2021. Recent Progress and Evolution of Coolant Usages in Conventional Machining Methods: a Comprehensive Review. The International Journal of Advanced Manufacturing Technology, 1-38.

[23] Ezugwu, E. O. 2005. Key Improvements In The Machining Of Difficult-To-Cut Aerospace Superalloys. International Journal of Machine Tools and Manufacture, 45(12-13), 1353-1367.

[24] Sultana, Nazma, and Nikhil Ranjan Dhar. 2022."Effects of High-Pressure Coolant Jets on the Machinability of Ti-6Al-4V Alloy with External Rotary Liquid Applicator.

[25] Masmiati, N., Sarhan, A. A., Hassan, M. A. N., & Hamdi, M. 2016. Optimization of Cutting Conditions for Minimum Residual Stress, Cutting Force and Surface Roughness in End Milling of S50c Medium Carbon Steel. Measurement, 86, 253-265.

[26] Pimenov, D. Y., Mia, M., Gupta, M. K., vd. 2021. Improvement of Machinability of Ti and Its Alloys Using Cooling-Lubrication Techniques: A Review and Future Prospect. Journal of Materials Research and Technology, 11, 719-753.

[27] Roy, S., Joshi, K. K., Sahoo, A. K., & Das, R. K. 2018. Machining of Ti-6Al-4V ELI alloy: a Brief Review. In IOP Conference Series: Materials Science and Engineering Vol. 390, No. 1.

[28] Hatt, O., Crawforth, P., & Jackson, M. 2017. On The Mechanism Of Tool Crater Wear During Titanium Alloy Machining. Wear, 374, 15-20.

[29] Outeiro, J., Cheng, W., Chinesta, F., & Ammar, A. 2022. Modelling and Optimization of Machining of Ti-6Al-4V Titanium Alloy Using Machine Learning and Design of Experiments Methods. Journal of Manufacturing and Materials Processing, 6(3), 58.

[30] Yünlü, L., Çolak, O., et al. "Taguchi Doe Analysis of Surface Integrity for High Pressure Jet Assisted Machining of Inconel 718", Procedia CIRP, 2014

Research Article

EVALUATION OF THE ACTIVITIES CARRIED OUT IN A FURNITURE FACTORY THROUGH WORK AND TIME STUDY

Authors: Feyza AKARSLAN KODALOĞLU

International Journal of Engineering and Innovative Research

http://dergipark.gov.tr/ijeir

EVALUATION OF THE ACTIVITIES CARRIED OUT IN A FURNITURE FACTORY THROUGH WORK AND TIME STUDY

Feyza AKARSLAN KODALOĞLU[1]*

[1]Suleyman Demirel University Engineering Faculty, Textile Enginering , Isparta, Turkey.

*Corresponding Author: feyzaakarslan@sdu.edu.tr
(**Received:** 14.09.2022; **Accepted:** 05.12.2022)

ABSTRACT: Efficiency is one of the most important elements of competition. In order for the enterprises to maintain their competitiveness in the market, it is inevitable that they reduce the unit costs of the products they produce and increase the efficiency, depending on the collected study information. At the same time, it is important for businesses to know which product, how and in what time they produce so that they can use their resources in the best way. Work study; It is carried out in order to determine how a job is carried out with low capital, and to increase production profitability by using labor and equipment in the most appropriate way. Especially in the furniture sector, efficiency analysis is gaining importance with the increasing costs. Not enough work has been done in this area. For this reason, in this study, the effect of work and time study on productivity was investigated in a furniture factory. For this aim, a survey study was conducted in the form of face-to-face interviews with 90 people working as workers in the Imaj Furniture Factory operating in the province of Isparta. The survey results were interpreted using the SPSS 17 statistical analysis program. All collected data were evaluated using frequency analysis and Chi-square test. As a result of this research, some statistical results were obtained showing the productivity improvement with the work and time study in the factory.

Keywords: Productivity, Furniture industry, Time study, Work study

1. INTRODUCTION

The increase in competition day by day causes the profits to decrease as new competitors constantly enter the market. At this point, it is of great importance to reduce costs to a minimum. Cost improvement that can be made without allocating additional resources can primarily be achieved by using the workforce more efficiently. At the same time, it is an important requirement for businesses to know which product, how and in what time they produce in order to use their resources in the best way. It is a great need to determine all stages in the production process, together with their times, in detail, costing and controlling the process according to these data, both to keep the costs under control, to identify the problems in the process and to determine the improvement points [1-6]. "Work and time study" has an important place among the methods to be used.

If work study is considered as efforts to improve and facilitate people's working life, the history of work study is as old as humanity. These studies have accelerated due to industrialization. Work study is a technique that investigates all the factors that affect a particular event or activity in terms of economic and efficiency and examines human work in a wide scope in order to create opportunities for improvement [7-10]. The importance of ineffective periods for

businesses is very great. Revealing and eliminating these ineffective times lost in the production process and calculating the standard production times and assigning the labor times accordingly not only increases the efficiency of the production process, but also forms the basis for remuneration [11,12].

In technical terms, productivity is the ratio between the outputs produced by a service or manufacturing sector and the inputs used to create those outputs. Therefore, productivity is defined as the effective use of resources -labor, capital, land, materials, energy, information- in the production of various goods and services [13].

The aim is to obtain high efficiency by using the available resources in the best way. One of the most important problems of the countries of the world is the most appropriate use of raw material resources that are going towards depletion. Work study, which is a technique that investigates the factors affecting production activities in terms of economy and efficiency, and time study, which is a subsection of it, are directly related to productivity [14-17]. Efficiency, simplification of method, optimization by maximizing participation, thereby increasing the value-added content of products, reducing unit production costs or reducing unnecessary work and wasted time It is possible with the balancing of the production line [18,19].

The importance of ineffective periods for businesses is very great. Revealing and eliminating these ineffective times lost in the production process, and calculating standard production times and assigning labor times accordingly, increase the efficiency of the production process. In this study, it has been investigated that productivity can be increased without requiring an additional investment in the furniture industry by using work and time study techniques. In this study, a face-to-face interview was conducted with 90 people working as workers in a furniture factory in order to investigate the effect of work and time studies on productivity, and the survey results were statistically interpreted with the SPSS 17 statistical analysis program.

2. METHOD

A survey study was conducted in order to determine the level of knowledge and raise awareness on work, time study and productivity for the employees in the Özkutlu (Imaj) furniture factory operating in the province of Isparta. A total of 90 surveys were distributed to the workers in the factory, and 90 (100%) returned surveys were evaluated. Survey forms consist of two distinct sections. In the first section, there are demographic (population unit) characteristics of the employees, and in the second section, there are a total of 40 questions to be answered by the employees. In the second section, there are multiple-choice questions consisting of five options. The survey results were statistically evaluated by frequency analysis and Chi-square test using SPSS 17.0 statistical analysis program. In Table 1, the demographic characteristics of the employees who participated in the survey are given.

Table 1. Demographic properties of the employees who participated in the survey

Questions	Options	Frequency (n)	%
Gender	Male	72	80,0
	Female	18	20,0
Age	18-24	15	16,7
	25-34	38	42,2
	35-44	34	37,8

	45 and above	3	3,3
Marital Status	Single	21	23,3
	Married	69	76,7
Educational Status	Primary Education	22	24,4
	High School	58	64,4
	Undergraduate	10	11,1
Mountly Net Income	1600-1750 TL	62	68,9
	1751-2000 TL	18	20,0
	2001 TL and above	10	11,1
Operation Time	0-1 years	10	11,1
	1-2 years	13	14,4
	2-3 years	26	28,9
	3-5 years	24	26,7
	5 years and above	17	18,9

According to Table 1, 80% of the 90 people participating in the survey are men and 20% are women. It is seen that 16.7% of the 90 people participating in the survey are in the 18-24 age range, 42.2% are in the 25-34 age range, 37.8% are in the 35-44 age range and 3.3% are in the 45 and over age range. 23.3% of the respondents are single and 76.7% are married. 24.4% of the respondents are primary school graduates, 64.4% are high school graduates and 11.1% are associate degree-undergraduate graduates. 68.9% of the respondents are working with minimum wage, 20% are slightly above the minimum wage and 11% are workers with better salaries. 11.1% of the respondents are beginners, 14.4% are employees for 1-2 years, 28.9% are employees for 2-3 years, 26.7% are employees for 3-5 years, and 18% 9 of them are workers who have worked for 5 years or more. Accordingly, the majority of the survey consists of employees for more than 2 years.

The five options for the multiple choice questions in the second part of the survey are as follows:

Options:
1- I strongly disagree
2- I disagree
3- I'm undecided
4- I agree
5- I totally agree

3. FINDINGS

The survey results were statistically analyzed using the SPSS 17.0 statistical analysis program. The results obtained by frequency analysis and Chi-square test are given in the tables given between Table 2 and Table 9.

Table 2 shows the result of the Chi-square test evaluation of the relationship between the hypothesis that work study is one of the most effective ways to increase productivity and education status.

Table 2. Chi-square test evaluation result of the relationship between education status and the hypothesis that work study is one of the most effective ways to increase productivity

Work study is one of the most effective ways to increase productivity.			1	2	3	4	5	Total	p
Education Status	Primary Education	Number	3$_a$	9$_a$	6$_a$	4$_b$	0$_b$	22	
		%	60,0%	64,3%	54,5%	8,5%	0,0%	24,4%	
	High School	Number	2$_a$	5$_a$	5$_a$	38$_b$	8$_{a,b}$	58	
		%	40,0%	35,7%	45,5%	80,9%	61,5%	64,4%	0,00
	Undergraduate	Number	0$_{a,b}$	0$_b$	0$_b$	5$_b$	5$_a$	10	
		%	0,0%	0,0%	0,0%	10,6%	38,5%	11,1%	
Total		Number	5	14	11	47	13	90	
		%	100,0%	100,0%	100,0%	100,0%	100,0%	100,0%	

As can be seen in Table 2, since p <0.05, it was observed that there was a significant difference between the question posed and their education level, those with low education levels did not participate, and as the education level increased, the level of participation in the posed opinion increased.

Table 3 shows the result of the Chi-square test of the hypothesis that the measurement will increase the workload and the relationship between education status.

Table 3. Chi-square test evaluation result of the relationship between the hypothesis that the measurement will increase the workload and the educational status

I think measurement will increase the workload.			1	2	3	4	5	Total	p
Educational Status	Primary Education	Number	3$_a$	3$_a$	11$_b$	5$_b$	0$_b$	22	
		%	9,4%	8,8%	68,8%	62,5%	0,0%	24,4%	
	High School	Number	21$_{a,b}$	29$_b$	5$_c$	3$_{a,c}$	0$_b$	58	
		%	65,6%	85,3%	31,3%	37,5%	0,0%	64,4%	
	Undergraduate	Number	8$_a$	2$_b$	0$_b$	0$_{a,b}$	0$_b$	10	0,00
		%	25,0%	5,9%	0,0%	0,0%	0,0%	11,1%	
Total		Number	5	32	34	16	8	90	
		%	100,0%	100,0%	100,0%	100,0%	100,0%	100,0%	

As it can be seen from Table 3, since p <0.05, it is seen that there is a significant difference between the education level and the question asked. While the answers of those with a low level of education were negative, the answers of those with a higher education level were positive. Table 4 shows the hypothesis that there is a link between work study and productivity, and the result of the evaluation with the Chi-square test of the relationship between genders.

Table 4. Chi-square test evaluation result of the hypothesis that there is a link between work study and productivity and gender status

There is a link between work study and productivity.			1	2	3	4	5	Total	p
Gender	Male	Number	10_a	$10_{b,c}$	$27_{a,c}$	8_b	$17_{a,b,c}$	72	
		%	100,0%	66,7%	90,0%	57,1%	81,0%	80,0%	
	Female	Number	0_a	$5_{b,c}$	$3_{a,c}$	6_b	$4_{a,b,c}$	18	0,031
		%	0,0%	33,3%	10,0%	42,9%	19,0%	20,0%	
Total		Number	10	15	30	14	21	90	
		%	100,0%	100,0%	100,0%	100,0%	100,0%	100,0%	

As it can be seen in Table 4, since $p < 0.05$, there is a significant difference between the question asked and the gender status, and the majority of the men who participated in the survey answered that they do not agree with the opinion. It is seen that the majority of women give the answer "I agree".

In Table 5, the result of the Chi-square test evaluation of the hypothesis that measurement will make the workflow healthier and the relationship between genders can be seen.

Table 5. Chi-square test evaluation result of the hypothesis that the measurement will make the workflow healthier and the gender status relationship

I think measurement will make the workflow more streamlined.			1	2	3	4	5	Total	p
Gender	Male	Number	$7_{a,b,c}$	8_c	5_b	$21_{a,c}$	$31_{a,c}$	72	
		%	87,5%	100,0%	45,5%	84,0%	81,6%	80,0%	
	Female	Number	$1_{a,b,c}$	0_c	6_b	$4_{a,c}$	$7_{a,c}$	18	0,029
		%	12,5%	0,0%	54,5%	16,0%	18,4%	20,0%	
Total		Number	8	8	11	25	38	90	
		%	100,0%	100,0%	100,0%	100,0%	100,0%	100,0%	

As can be seen in Table 5, since $p < 0.05$, it is seen that there is a important distinction between the question posed and the gender status, and that men and women give different answers.

In Table 6, the Chi-square test evaluation result of the relationship between the hypothesis that work study is one of the most effective ways to increase productivity and age groups can be seen.

Table 6. Chi-square test evaluation result of the relationship between age groups and the hypothesis that work study is one of the most effective ways to increase productivity

Work study is one of the most effective ways to increase productivity.			1	2	3	4	5	Total	p
Age	18-24	Number	$0_{a,b}$	0_b	0_b	9_b	6_a	15	
		%	0,0%	0,0%	0,0%	19,1%	46,2%	16,7%	
	25-34	Number	1_a	3_a	5_a	24_a	5_a	38	
		%	20,0%	21,4%	45,5%	51,1%	38,5%	42,2%	
	35-44	Number	$2_{a,b,c}$	10_c	$6_{b,c}$	$14_{a,b}$	2_a	34	0,000
		%	40,0%	71,4%	54,5%	29,8%	15,4%	37,8%	
	45 ve üzeri	Number	2_a	$1_{a,b}$	0_b	0_b	0_b	3	
		%	40,0%	7,1%	0,0%	0,0%	0,0%	3,3%	
Total		Number	5	14	11	47	13	90	
		%	100,0%	100,0%	100,0%	100,0%	100,0%	100,0%	

As it is seen in Table 6, since $p < 0.05$, it can be said that there is a significant difference between the age groups and the question asked, and those younger in age give positive answers to the posed idea, and negative answers are given as the age range increases.

In Table 7, the Chi-square test evaluation result of the relationship between the hypothesis that I think time is wasted while taking measurements and age groups is seen.

Table 7. Chi-square test evaluation result of the relationship between age groups and the hypothesis that I think time is wasted while taking measurements.

I think time is wasted when taking measurements.			1	2	3	4	5	Total	p
Age	18-24	Number	5_a	4_a	4_a	2_b	0_b	15	
		%	50,0%	26,7%	33,3%	5,4%	0,0%	16,7%	
	25-34	Number	$3_{a,b}$	8_b	$4_{a,b}$	20_b	3_a	38	
		%	30,0%	53,3%	33,3%	54,1%	18,8%	42,2%	
	35-44	Number	2_a	3_a	$4_{a,b}$	$15_{a,b}$	10_b	34	0,000
		%	20,0%	20,0%	33,3%	40,5%	62,5%	37,8%	
	45 ve üzeri	Number	$0_{a,b}$	$0_{a,b}$	$0_{a,b}$	0_b	3_a	3	
		%	0,0%	0,0%	0,0%	0,0%	18,8%	3,3%	
Total		Number	10	15	12	37	16	90	
		%	100,0%	100,0%	100,0%	100,0%	100,0%	100,0%	

As it can be seen in Table 7, since $p < 0.05$, it was determined that there was a significant difference between the age groups and the question asked, and the people between the ages of

18-24 did not agree with the idea, while the employees after the age of 25 agreed and said that time was wasted while taking measurements.

In Table 8, the result of the Chi-square test evaluation of the relationship between the hypothesis that work study is a way of increasing the efficiency of a factory by rearranging the work and the working hours is seen.

Table 8. Chi-square test evaluation result of the working time relationship with the hypothesis that work study is a way of increasing the efficiency of a factory by rearranging the work

Work study is a way of increasing the efficiency of a factory by reorganizing work			1	2	3	4	5	Total	p
Operation Time	0-1 year	Number	0_a	1_a	1_a	6_a	2_a	10	
		%	0,0%	12,5%	11,1%	11,1%	12,5%	11,1%	
	1-2 years	Number	0_a	0_a	0_a	9_a	4_a	13	
		%	0,0%	0,0%	0,0%	16,7%	25,0%	14,4%	
	2-3 years	Number	0_a	1_a	1_a	19_a	5_a	26	
		%	0,0%	12,5%	11,1%	35,2%	31,3%	28,9%	0,049
	3-5 years	Number	2_a	1_a	3_a	13_a	5_a	24	
		%	66,7%	12,5%	33,3%	24,1%	31,3%	26,7%	
	5 years and above	Number	$1_{a,b}$	5_b	4_b	$7_{a,c}$	0_c	17	
		%	33,3%	62,5%	44,4%	13,0%	0,0%	18,9%	
Total		Number	3	8	9	54	16	90	
		%	100,0%	100,0%	100,0%	100,0%	100,0%	100,0%	

As it can be seen in Table 8, since $p < 0.05$, it was observed that there was a significant difference between the question asked and the working time, and that the newcomers agreed with the idea that "work study is a way to increase the efficiency of a factory by rearranging the work", while older employees did not agree with the idea.

In Table 9, the Chi-square test evaluation result of the relationship between the hypothesis that I think time is wasted while taking the measurement and the working time is seen.

Table 9. Chi-square test evaluation result of the relationship between the hypothesis that time is wasted while taking the measurement and the working time

I think time is wasted when taking measurements.			1	2	3	4	5	Total	p
Operation Time	0-1 year	Number	2_a	2_a	1_a	3_a	2_a	10	
		%	20,0%	13,3%	8,3%	8,1%	12,5%	11,1%	
	1-2 years	Number	4_a	$3_{a,b}$	$2_{a,b}$	4_b	0_b	13	0,131
		%	40,0%	20,0%	16,7%	10,8%	0,0%	14,4%	
	2-3 years	Number	3_a	6_a	4_a	11_a	2_a	26	

			30,0%	40,0%	33,3%	29,7%	12,5%	28,9%
	%		30,0%	40,0%	33,3%	29,7%	12,5%	28,9%
3-5 years	Number		1a	4a	3a	11a	5a	24
	%		10,0%	26,7%	25,0%	29,7%	31,3%	26,7%
5 years and above	Number		0a	0a	2a, b	8a, b	7b	17
	%		0,0%	0,0%	16,7%	21,6%	43,8%	18,9%
Total		Number	10	15	12	37	16	90
		%	100,0%	100,0%	100,0%	100,0%	100,0%	100,0%

As it can be seen in Table 9, since $p > 0.05$, it was seen that there was no significant difference between the question asked and the duration of the study.

4.RESULTS AND DISCUSSION

The concept of efficiency is an important element in our country, especially for businesses. Efficiency increase in enterprises can be achieved to a large extent by the work study technique and the application of studies based on this technique. The most important thing that businesses should do before starting this application is to provide relevant information from the top-level manager to the lowest-level employee. Otherwise, the desired results may not be obtained from the application. The person who will carry out the study should have sufficient knowledge and skills.
In the application study, work and time studies were carried out in Özkutlu (IMAJ) Furniture operating in Isparta, the answers given to the questions in the survey for workers in the position of workers were handled and the results were analyzed and interpreted by using the SPSS 17.0 statistical analysis program.

According to the data obtained, it is seen that the majority of the workers participating in the survey working at Imaj Furniture are male, between the ages of 25-44, married, primary and high school graduates, experienced workers working with minimum wage.

According to the Chi-square test evaluation result of the relationship between the hypothesis 'Work study is one of the most effective ways to increase productivity' and educational status; It was observed that there was a significant difference between the education level and the given hypothesis, and as the level of education increased, the participation in the thought increased, which is an expected result.

According to the Chi-square test evaluation result of the relationship between the hypothesis 'I think the measurement will increase the workload' and the educational status; It is seen that there is a significant difference between the education level and the hypothesis given with the education level. While the answers of those with a low level of education were negative, the answers of those with a higher education level were positive.

According to the Chi-square test evaluation result of the hypothesis of "There is a link between work study and productivity" and gender status; It is seen that there is a significant difference between the hypothesis given and the gender status, and the majority of the men who participated in the survey gave the answer that I did not agree with the opinion, while the majority of the women gave the answer of I agree.

According to the Chi-square test evaluation result of the relationship between gender status and the hypothesis "I think the measurement will make the workflow healthier"; It is seen that there is a significant difference between the question and the gender status, and that men and women give different answers.

According to the Chi-square test evaluation result of the relationship between the hypothesis 'Work study is one of the most effective ways to increase productivity' and age groups; It is seen that there is a significant difference between the given hypothesis and the age groups, that the younger ones respond positively to the thought, and that the negative answers are given as the age range increases.

According to the Chi-square test evaluation result of the relationship between the hypothesis 'I think time is wasted when taking measurements' and age groups; It has been determined that there is a significant difference between the age groups with the given hypothesis and that people between the ages of 18-24 do not agree with the idea, while employees after the age of 25 agree with the idea and think that time is wasted when taking measurements.

According to the Chi-square test evaluation result of the relationship between the hypothesis "Work study is a way of increasing the efficiency of a factory by rearranging the work" and the working hours; It was observed that there was a significant difference between the given hypothesis and the duration of the study, and that the newcomers agreed with the given idea, while the older employees did not.

According to the Chi-square test evaluation result of the relationship between the hypothesis that I think time is wasted while taking the measurement and the working time; It was found that there was no significant difference between the question asked and the duration of the study.

REFERENCES

[1] Şenyiğit, E., Karakaş, S., Uçar, S., Akbal, S., 2021. Analysis of Work-Study-Productivity Practice for Enterprise Resource Planning in a Furniture Firm: Case Study, *European Journal of Science and Technology,* Special Issue 28, pp. 476-480.

[2] Cengiz, T. G., Orbak, A. Y., (2010). Increasing Efficiency with Work and Time Study in a Milk and Dairy Products Factory, International Journal of Engineering Research and Development, Vol.2, No.2.

[3] Doğruer, İ., (2014). Work study. 2nd Edition, Açılım Bookstore , İstanbul.

[4] Acar, N., (2001). Production Planning Methods and Practices, National Productivity Center Publication No:280, 8th Edition
Ankara.

[5] Baş, İ.M., Artar, A., (1991). Productivity Control in Businesses, National Productivity Center Publications, Ankara.

[6] Ayyıldız, İ., (2001). Work Study Technique and an Application in Increasing Efficiency in Businesses. Master Thesis, Sivas Cumhuriyet University, Institute of Social Sciences.

[7] Bezen, A., (2007). The Relationship between Work Study Techniques and Quality and Customer Satisfaction, An Application in the Packaging Industry. Dumlupınar University, Institute of Science and Technology. Master Thesis, 84s, Kütahya.

[8] Bilen, G., (2007). The Effect of Work Study on Productivity in Textile Business and Applied Study in a Textile Factory, Master Thesis, Bolu Abant İzzet Baysal University, Institute of Social Sciences.

[9] Demir, M., (2003). The Effect of Work Study on Increasing Productivity and Its Application in Textile Industry. Master Thesis, Istanbul Marmara University, Institute of Social Sciences,

[10] Demirbaş, Z., (2010). The Effects of Application of Method Study as an Efficiency Improvement Technique in a Garment Business on Business Performance. Master Thesis, Dokuz Eylul University, Institute of Social Sciences.

[11] Dizdar, E., Özen R., (2001). Work Study Practices for Production Efficiency in the Wood Furniture Industry, Journal Technology, Issue
 1-2, 1-9.

[12] Durgun, Y., (2000). Work Study-Work Measurement Techniques and an Application in Textile Industry. Master Thesis, Kocaeli University, Institute of Social Sciences.

[13] Kovancı, Ü., (2018). The effect of occupational health and safety practices on productivity. Master Thesis, Katip Celebi University, Institute of Science.

[14] Öncer, M., Asil N., (1992). Detection and Prevention of Lost Time in Four Modern Furniture Factories by Work Sampling, MPM Publications
: 458, Ankara.

[15] Seri, K., (2010). The Effect of Time Study on Long-Term Efficiency An Empirical Evaluation in a Food Company. Master Thesis, Adnan Menderes University, Institute of Social Sciences.

[16] Sabır, E.C., Dönmez, U., (2013). Application of Work Study Method in Yarn Spinning Mill, Tekstil ve Mühendis, 20: 92, 11-26.

[17] Şahin, E., (2003). Determination of Efficiency by Method and Time Study in a Workplace. Journal of Technology, 3-4, 59-66.

[18] Moktadir, M. A., Ahmed, S., Zohra, F. T., & Sultana, R. (2017). Productivity improvement by work study technique: a case on leather products industry of Bangladesh. Ind. Eng. Manag, 6(1), 1000207.

[19] Kumaş, Z., Sabır, E.C., Duru Baykal, P., (2016). The Using of Work Study Technique for Process Productivity of Apparel Plant. Çukurova University Journal of the Faculty of Engineering and Architecture, 31(1), pp. 175-189.

Research Article

THERMODYNAMIC ANALYSIS OF A NOVEL COMBINED SUPERCRITICAL CO2 AND ORGANIC RANKINE CYCLE

Authors: Ahmet Elbir (iD) Mehmet Erhan Şahin (iD) Arif Emre Özgür (iD)
Hilmi Cenk Bayrakçı (iD)

International Journal of Engineering and Innovative Research

http://dergipark.gov.tr/ijeir

THERMODYNAMIC ANALYSIS OF A NOVEL COMBINED SUPERCRITICAL CO₂ AND ORGANIC RANKINE CYCLE

Ahmet Elbir[1]* , Mehmet Erhan Şahin[2] , Arif Emre Özgür[3] , Hilmi Cenk Bayrakçı[3]

[1]Suleyman Demirel University, YEKARUM, Isparta, Turkey.
[2] Isparta Applied Science University, Technical Vocational High School, Isparta, Turkey.
[3]Isparta Applied Science University, Technology Faculty, Isparta, Turkey.

*Corresponding Author: ahmetelbir@sdu.edu.tr

ABSTRACT: Sustainable and innovative technologies offer us the inevitable opportunity to use the last drop of energy. In this study, gradual compression and gradual expansion were carried out with intermediate heat exchangers in single and double stage S-CO₂ brayton cycles operating at the same operating temperature ranges. The ORC (Organic Rankine Cycle) is integrated from the system's waste heat source. The performance characteristics of the S-CO₂ power systems and the combined ORC system, as well as the energy and energy analysis results of the system components for each component, are presented in tables. The performance of the gradual compression and gradual expansion systems, the operating conditions of the stepless system operating under the same operating conditions, were examined. It has been reported that there is an increase in electricity generation of 136% and an increase in thermal efficiency of 22% when switching from single-stage to double-stage. The addition of the ORC system to the single-stage and double-stage systems increased the thermal efficiency by 10.2% and the net work by 39.75KW. When switching from single stage to double stage, exergy destruction increased by 86% and energy efficiency decreased by 1%. The addition of the ORC system to the single-stage and double-stage systems increased the energy efficiency by 15% and the exergy destruction by 44.27KW. As a result, nature-friendly CO₂ shows us that it is an alternative, innovative, and sustainable source in low temperature applications.

Keywords: Brayton cycle, S-CO₂, ORC, Enegy analysis, Exergy analysis.

1. INTRODUCTION

In recent days, we have seen that global problems increase the demand for energy needs with the effects of the pandemic. The common views of international agencies say that the demand for electricity will increase further, the need for primary fossil resources will increase to meet this demand, and the result will be met mostly by coal. The use of coal pollutes our atmosphere with high levels of CO₂, SO₂, NOx, and CO₂. We know that the main elements of the environmental problems faced by humanity are the improvement of energy efficiency and the reduction of carbon emissions. In this context, it has led us to use traditional fossil fuel energy sources in a more sustainable and rational way, not in an alarming way. As a result, the environmental friendliness of energy and the increase in its efficiency have led us to combined power systems. When choosing environmentally friendly energy sources, we should choose renewable energy sources such as solar, wind, biomass and geothermal. In power generation

systems, S-CO$_2$ (Supercritical carbon dioxide) is the most promising and environmentally friendly system. When we look at the latest studies, ensuring that unused waste heat is converted into energy without being thrown into the environment will reduce the negative environmental effects. We see that it provides additional benefits, especially in converting waste heat sources to power generation systems with ORC systems. If we look at how environmentally friendly CO$_2$ systems are used in electricity generation in the literature; Wang, et al., suggested CO$_2$ power cycles in their work. If the source temperature is high, CO$_2$ power systems have better efficient than the Rankine cycle having ultra-supercritical operating conditions. CO$_2$ power cycles are also an innovative approach to power production, notedly for low-grade heat sources. [1]. Mishra and Kumar, studied the thermodynamic performance of the Brayton Cycle. They claim that the Brayton cycle powered by R123 outperforms R245fa and R134a in terms of thermodynamic performance. They studied how various performance parameters, such as pressure ratio, maximum temperature in the cycle, and compressor inlet temperature, affect the Brayton cycle [2]. Bellos, and Tzivanidis, investigated a transcritical refrigeration cycle connected to a Brayton cycle with a CO$_2$ recompression fed by a biomass boiler [3]. Deng et al., compared the application of thermal source temperatures in the Brayton cycle (recompression, intercooling, and reheating). They said that with increasing temperature of the heat source, the efficiency of the recompression model gradually increased [4]. Zhang et al., performed the related system design and thermodynamic analysis to analyze the energetic and exergetic performance of the supercritical power cycle. They investigated the parametric values of turbine inlet temperatures and operating pressures. They said that high pressure increases the turbine's temperature and increases cycle efficiency while reducing output work. In this case, for the effect of low pressure turbine inlet temperature, it is said that the cycle efficiency and output work increase with increasing temperature. They stated that the waste heat recovery efficiency in the system they studied increased to 74.83% [5]. Hoang et al., In their evaluation of S-CO$_2$ Brayton Energy Conversion Systems, they investigated the effects of changing thermodynamic assumptions and investigated the effect of non-ideal fluid behavior on heat exchanger performance [6]. Wang et al., evaluated the effects of key thermodynamic parameters on the performance of combined S-CO$_2$, T-CO$_2$ cycles. They showed that the thermal efficiency of the simple S-CO$_2$, T-CO$_2$ cycle at S-CO$_2$ turbine pressure ratio and compressor inlet temperature increased [7]. Yari and Sirousazar, This study investigated the performance of the pre-cooler recompression S-CO$_2$ Brayton cycle used in a transcritical carbon dioxide (T-CO$_2$) cycle to improve the performance of the cycle. They also made a comparison between S-CO$_2$ and a simple S-CO$_2$ cycle. They said that both the energetic and exergetic efficiencies of the new S-CO$_2$ cycle are about 5.5 percent to 26 percent higher than the simple S-CO$_2$ cycle [8]. Al-Sulaiman and Atıf made a comparison five different supercritical carbon dioxide Brayton cycles operated with the energy obtained from a solar tower. Split expansion Brayton cycle, precompression Brayton cycle, recompression Brayton cycle, regenerative Brayton cycle, and Brayton cycle analyses were carried out. They showed that recompression Brayton cycle have the highest thermal efficiency. The regenerative Brayton cycle, although leaner in configuration, performs comparable to the recompression Brayton cycle. [9]. Yu et al., They said that the internal combustion engine (ICE) with waste heat recovery and S-CO$_2$ cycle is considered a promising technology [10]. Casanova et al., Transcritical carbon dioxide cycles and the Rankine cycle have arised as alternatives for power generation in low-temperature applications. The low heat removal temperatures required for CO$_2$ condensation are prohibitive for many locations. They studied the S-CO$_2$ Brayton cycle [11]. Zhoua et al., presented the second law analysis of a single-reheated S-CO$_2$ Brayton cycle for coal-fired power plant. They emphasized that the optimum parameters of the turbines provide a higher expansion rate for the low pressure turbine (LPT) than for the high pressure turbine (HPT). They showed that the overall energy efficiency of a reheated 1000MW S-CO$_2$ coal-fired power

plant is higher than that of a conventional ultra-high critical steam plant [12]. Chowdhury et al., The S-CO$_2$ Brayton cycle S-CO$_2$, triple cycle (TLC), and ORC examined the performance of the cycles under constant heat input conditions. They showed that a higher thermal efficiency (26.5%) can be achieved in the case of the ORC cycle with n-pentane as the working fluid, compared with S-CO$_2$ and TLC with its thermal efficiency [13]. Wang et al., stated that the intercooling loop layout and sub-cooling loop layout usually provide the best performances, followed by the recompression loop layout and precompression loop layout, while the simple recovery loop layout has the worst performances. They said that the advantages of partial refrigeration loop layout and intercooling loop layout are more pronounced in the case of high compressor inlet temperatures compared to other loop layouts [14]. Wei et al., analyzed the S-CO$_2$ Brayton cycle and the ORC combined system [15]. Ma and Liu., it is said that it will be a creative power system by integrating the S-CO$_2$ Brayton cycle with the transcritical ORC. They said that the ORC turbine and the CO$_2$ turbine have a priority of improvement over the compressor and pump. They showed that the ORC increases the maximum system energy efficiency by changing the turbine inlet pressure [16]. Wang et al., in their study, they presented comparative research on the supercritical carbon dioxide power cycle for waste heat recovery of gas turbines. From cycles, energy and exergy analyses were optimized according to single and multi-objective optimization results from the perspective of system efficiency, configuration complexity, and economic cost. They emphasized the importance of increasing the thermal efficiency of the gas turbine waste heat recovery system. They emphasized the use of a double-heated cascade cycle to ensure high system efficiency [17]. Purjam, et al., projecting new and efficient heat machines and increasing their efficiency is one of the interests of researchers in the field of thermodynamics. In this context, they designed a cycle with the favorable features of familiar cycles, such as less emission and higher power-to-weight ratio and efficiency. The supercritical carbon dioxide cycle (SCDC) is assumed that one of the most promising cycle. The main aim of this research is to design a high efficiency SCDC with an efficiency of 45% to 47%. They said that this article includes the entire designed loop, designing and discussing efficiency improvement methods, comparing, designing, and discussing SCDC with other power loops. The sensitivity of loop efficiency to some important parameters was also examined [18]. Padilla et al., In this paper, thermodynamic analyses are performed separately for each component of a supercritical CO$_2$ recompression Brayton cycle. As a result, they showed that the energy efficiency reached its maximum value at 600 °C and that the first law efficiency increased with the temperature of the cycle. [19]. Besarati at al. In this study, S-CO$_2$ Brayton cycle, recompression S-CO$_2$ Brayton cycle and partial cooling S-CO$_2$ Brayton cycles are compared with the studies in the literature. They have added an ORC to each configuration to take advantage of the waste heat source. Different working fluids were used for these integrated cycles and the working conditions were analyzed. showed that the combined recompression-ORC cycle provides higher thermodynamic efficiency than other systems. [20]. Akbari at al., presented an exergoeconomic analysis analyzed for a new combined S-CO$_2$ recompression Brayton and organic Rankine cycle (SCRB/ORC). In this project, waste heat from the SCRBC is used by an ORC to generate power. Thermodynamic and exergoeconomic analyzes are also studied to make comparisons for eight different ORC working fluids with models were developed. The results showed that the best energy efficiency and lowest product unit cost for SCRB/ORC were obtained when isobutane and RC318 ORC working fluid were considered, respectively [21]. Khan and Mishra, This study performed a performance analysis of a combined pre-compression S-CO$_2$ cycle and ORC powered by a solar tower for waste heat recovery. The results showed that the net power output and thermal efficiency of the pre-compression loop were improved by 4.51% and 4.52%, respectively, using ORC. They said that the combined cycle's highest thermal, energy efficiency and power output increased with 1000 W/m^2 of solar radiation using R227ea, and the solar radiation with the highest values was

51.83 – 74.06%, and 278.5 kW. They emphasized that the efficiency of the heat exchanger increases the waste heat recovery rate. They found the best value as 0.5673 at 0.95 efficacy according to R227ea [22]. Chacartegui at al., In this study, low-temperature ORC was investigated as a sub-cycle in medium and large-scale combined cycle power plants. As organic fluids, cyclohexane, R245, isobutene, R113, toluene, and isopentane toluene were used. Of these, competitive results were obtained for the cyclohexane ORC combined cycles. [23].

When S-CO$_2$ systems are examined in the literature, it is seen that they are either single-stage or double-stage. In our study, the thermodynamic analysis of the single-stage, single-expansion S-CO$_2$/ORC system, operating at the same lower and upper temperatures as the single-stage, double-expansion S-CO$_2$/ORC system, was investigated. In the study, environmentally-friendly R600a refrigerant was used in the ORC system. Recent system improvements for CO$_2$ have been made in supercritical Brayton cycles with intermediate heat exchangers, gradual compression, and gradual expansion. In the waste heat sources of the system, the gradual expansion of the ORC cycles is provided by the intermediate heat exchangers. Performance characteristics of S-CO$_2$ power systems and combined ORC systems are aimed at energy and exergy analysis of system components.

2. METHODS

2.1. System Description

Figure 1 gives a schematic of a single-stage S-CO$_2$ cycle for a closed-cycle supercritical CO$_2$ using CO$_2$ as the working fluid.
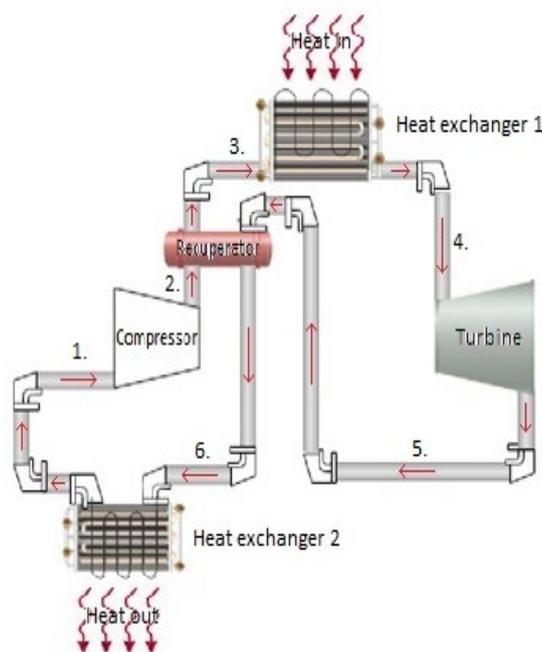
Figure 1. Single-stage S-CO$_2$ cycle.

The process location in the design is as follows:
1. 1→2: Adiabatic compressor increases fluid pressure and converts it to supercritical fluid,
2. 2→3: adiabatic heat transfer with counterflow recuperator.
3. 3→4: The working fluid receives heat from the heat source,

4. 4→5: expanding the adiabatic turbine to generate work

5. 5→6: adiabatic heat removal with counterflow recuperator.

6. 6→1: return to State I by isobaric transfer of the heat of the fluid to an ORC system

Combining a S-CO$_2$ closed loop cascade compression and cascade expansion system using CO$_2$ as the working fluid with the ORC system Figure 2 gives a schematic of the cycle.
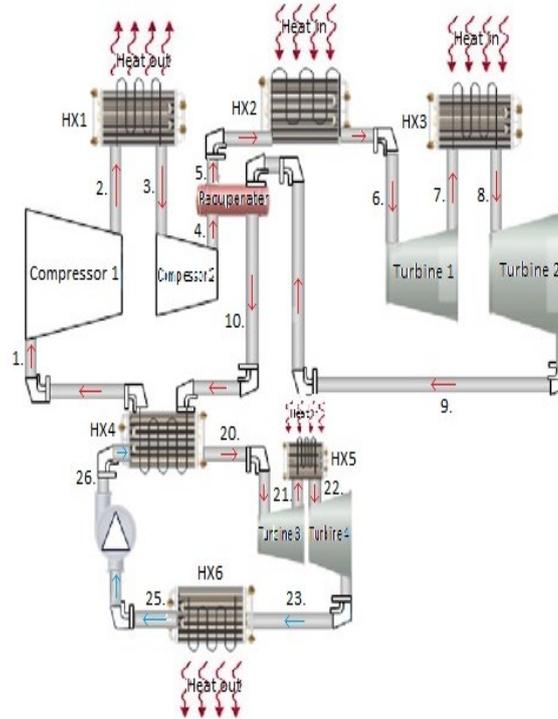
Figure 2. Double-stage expansion and double-stage compression combined with ORC in the S-CO$_2$ cycle.

The process location in the design is as follows:

1. 1→2: Adiabatic compressor-I increases the fluid pressure and converts it to supercritical fluid,

2. 2→3: lowering the isobaric temperature of the supercritical fluid in the heat exchanger,

3. 3→4: again increasing the fluid pressure of the Adiabatic compressor-II,

4. 4→5: adiabatic heat transfer with counter flow recuperator.

5. 5→6: The working fluid receives heat from the heat source,

6. 6→7: expanding the adiabatic turbine-I to generate work

7. 7→8: Reheating the working fluid up to the turbine-I inlet temperature,

8. 8→9: expanding the adiabatic turbine-II to generate work

9. 9→10: adiabatic heat removal with counter flow recuperator.

10. 10→1: return to State I by isobaric transfer of heat of the fluid to an ORC system.

11. 26→20: heat transfer from adiabatic and mixed flow heat exchanger to R600a ORC system

12. 20→21: expanding the adiabatic turbine-III to generate work

13. 21→22: Reheating the working fluid to turbine-III inlet temperature,

14. 22→23: Expanding the adiabatic turbine to generate IV work

15. 23→25: heat removal by heat exchanger as isobar.

16. 25→26: increasing the pressure of the saturated liquid with the adiabatic pump.

Thermodynamic equations

The following assumptions were taken into account while making the thermodynamic analysis of the system:

• Pure substance is used in the system.

• The compression in the compressor is adiabatic.
• Pressure drops in system components and on the pipeline and the heat transfer process are also neglected.
• All heat exchangers are counter flow.
• System performance is assumed to be constant and regular.
• Gravitational potential energy and kinetic energy are not taken into account.
• It has been calculated by taking the pressure ratio in the compressors and turbines, which are used in stages, as 1.8 as a constant.
• Isentropic efficiency of the compressors and pumps in the systems ηiz =0.85
• Isentropic efficiency for turbines in systems ηiz =0.90
• Ambient temperature is taken as 20 ℃.
• There was 40% more heat transfer from the source and 40% less heat transfer from all heat exchangers except the recuperator and heat exchanger 4.
• Calculations were made by taking the heat source and instantaneous surface temperature differences in the heat source heat exchangers, 10 K in the brayton cycle, and 2 K in the ORC.

2.2. Energy and exergy analyzes

For steady state in thermodynamic analysis, the basic mass balance equation can be given as follows;

$$\sum \dot{m}_{in} = \sum \dot{m}_{ex} \tag{1}$$

where $\dot{m}$ is the mass flow rate, the in and ex indices represent the inlet and outlet states, respectively. The energy balance is given as:

$$\dot{Q}_{in} + \dot{W}_{in} + \sum_{in} \dot{m}\left(h + \frac{v^2}{2} + gz\right) = \dot{Q}_{ex} + \dot{W}_{ex} + \sum_{ex} \dot{m}\left(h + \frac{v^2}{2} + gz\right) \tag{2}$$

Here, $\dot{Q}$ is the heat transfer rate, , $\dot{W}$ is the power, h is the specific enthalpy, v is the velocity, z is the height, and g is the gravitational acceleration. The entropy balance equation for steady-state conditions is written as:

$$\sum_{in} \dot{m}_{in}s_{in} + \sum_{k} \frac{\dot{Q}}{T_k} + \dot{S}_{gen} = \sum_{ex} \dot{m}_{ex}s_{ex} \tag{3}$$

where s is the specific entropy and $\dot{S}_{gen}$ is the entropy generation rate. The exergy balance equation can be written as:

$$\sum \dot{m}_{in} ex_{in} + \sum \dot{E}x_{Q,in} + \sum \dot{E}x_{W,in} = \sum \dot{m}_{ex}ex_{ex} + \sum \dot{E}x_{Q,ex} + \sum \dot{E}x_{W,ex} + \dot{E}x_D \tag{4}$$

The specific flow exergy can be written as:

$$ex = x_{ph} + ex_{ch} + ex_{pt} + ex_{kn} \tag{5}$$

The kinetic and potential parts of the exergy are assumed to be negligible. Also, the chemical exergy is assumed to be negligible. The physical or flow exergy (ex_{ph}) is defined as:

$$ex_{ph} = (h - h_o) - T_o(s - s_o) \tag{6}$$

where h and s represent specific enthalpy and entropy, respectively, in the real case. h_o and s_o are enthalpy and entropy at reference medium states, respectively.

The instantaneous temperature T(K) value for the surfaces was calculated as follows:

$$T = \frac{h_2 - h_1}{s_2 - s_1} \tag{7}$$

Exergy destruction is equal to specific exergy times mass;

$$\dot{E}x_D = ex * m \tag{8}$$

or

$$\dot{E}x_D = T_0 \dot{S}_{gen} \tag{9}$$

$\dot{E}x_W$, are work-related exergy ratios and are given as:

$$\dot{E}x_W = \dot{W} \tag{10}$$

$\dot{E}x_Q$, are the exergy rates related to heat transfer and are given as below.

$$\dot{E}x_Q = \left(1 - \frac{T_o}{T}\right)\dot{Q} \tag{11}$$

What work comes out of the system;

$$\dot{W}net_{out} = \dot{Q}_{in} - \dot{Q}_{out} \tag{12}$$

efficiency for the Brayton system;

$$\eta th_{,} = \frac{\dot{W}net_{out}}{\dot{Q}_{in}} \tag{13}$$

The exergy efficiency (ψ) can be defined as follows;

$$\psi = \frac{\sum useful\ output\ exergy}{\sum input\ exergy} = 1 - \frac{\sum exergy\ loss}{\sum input\ exergy} \tag{14}$$

The mass balance, energy balance, entropy balance, exergy balance and exergy efficiency equations for each component are presented in Table 1.

Table 1. Mass balance, energy balance, entropy balance, exergy balance and exergy efficiency equations

Component	Mass balance	Energy balance	Entropy balance	Exergy balance	Exergy efficiency
CO_2-Comp1 (1-2)	$\dot{m}_1 = \dot{m}_2$ $= \dot{m}_{CO2}$	$\dot{W}_{Comp1.} = \dot{m}_{CO2}(h_2 - h_1)$	$\dot{S}_{gen,Comp1.}$ $= \dot{m}_{CO2}(s_2 - s_1)$	$\dot{E}x_{D,Comp1}$ $= \dot{m}_{CO2}(ex_1 - ex_2)$ $+ \dot{W}_{Comp1}$	ψ_{copm1} $= \frac{\dot{m}_{CO2}(ex_2 - ex_1)}{\dot{W}_{Comp1}}$
	$\dot{m}_2 = \dot{m}_3$ $= \dot{m}_{CO2}$	$\dot{Q}_{HXI}^{out}$ $= \dot{m}_{CO2}(h_2 - h_3)$			

CO_2-heat exchanger I (2-3)		$\dot{Q}_{HX1}^{in} = \dot{m}_{CO2}(h_2 - h_3)/1,4$	$\dot{S}_{gen.,HX1} = \dot{m}_{CO2}(s_2 - s_3) + \left(\frac{\dot{Q}_{CO2}^{in}}{T_{HX1} - 10}\right)$	$\dot{Ex}_{D,HX1} = \dot{m}_{CO2}(ex_2 - ex_3) - \dot{Q}_{CO2}^{in}\left(1 - \frac{T_0}{T_{HX1} - 10}\right)$	$\psi_{cond.} = \frac{\dot{Q}_{CO2}^{in}\left(1 - \frac{T_0}{T_{HX1}*1,03}\right)}{\dot{m}_{CO2}(ex_2 - ex_3)}$
CO_2-Comp2 (3-4)	$\dot{m}_3 = \dot{m}_4 = \dot{m}_{CO2}$	$\dot{W}_{\mathbf{Comp2}} = \dot{m}_{CO2}(h_4 - h_3)$	$\dot{S}_{gen,Comp2.} = \dot{m}_{CO2}(s_4 - s_3)$	$\dot{Ex}_{D,\mathbf{Comp2}} = \dot{m}_{CO2}(ex_3 - ex_4) + \dot{W}_{Comp2}$	$\psi_{comp2} = \frac{\dot{m}_{CO2}(ex_4 - ex_3)}{\dot{W}_{Comp2}}$
CO_2-Recuperator (4-5)	$\dot{m}_4 = \dot{m}_5 = \dot{m}_9 = \dot{m}_{10} = \dot{m}_{CO2}$	$\dot{m}_{CO2}(h_9 - h_{10}) = \dot{m}_{CO2}(h_5 - h_4)$	$\dot{S}_{gen,Rekü.} = \dot{m}_{CO2}(s_{10} - s_9) + \dot{m}_{CO2}(s_5 - s_4)$	$\dot{Ex}_{D,Rekü.} = \dot{m}_{ORC}(ex_4 - ex_5) + \dot{m}_{ORC}(ex_9 - ex_{10})$	$\psi_{Rekü.} = \frac{\dot{m}_{CO2}(ex_5 - ex_4)}{\dot{m}_{CO2}(ex_9 - ex_{10})}$
CO_2-heat exchanger II (5-6)	$\dot{m}_5 = \dot{m}_6 = \dot{m}_{CO2}$	$\dot{Q}_{HX2}^{in} = \dot{m}_{CO2}(h_6 - h_5) * 1,4$ $\dot{Q}_{HX2}^{out} = \dot{m}_{CO2}(h_6 - h_5)$	$\dot{S}_{gen.,HX2} = \dot{m}_{CO2}(s_6 - s_5) + \left(\frac{\dot{Q}_{CO2}^{in}}{T_{HX2} + 10}\right)$	$\dot{Ex}_{D,HX2} = \dot{m}_{CO2}(ex_5 - ex_6) + \dot{Q}_{CO2}^{in}\left(1 - \frac{T_0}{T_{HX2} + 10}\right)$	$\psi_{comp.} = \frac{\dot{m}_{CO2}(ex_5 - ex_6)}{\dot{Q}_{CO2}^{in}\left(1 - \frac{T_0}{T_{HX2} + 10}\right)}$
CO_2-Turbine I (6-7)	$\dot{m}_6 = \dot{m}_7 = \dot{m}_{CO2}$	$\dot{W}_{turb1.} = \dot{m}_{CO2}(h_6 - h_7)$	$\dot{S}_{gen,turb1.} = \dot{m}_{CO2}(s_7 - s_6)$	$\dot{Ex}_{D,turb1.} = \dot{m}_{CO2}(ex_6 - ex_7) - \dot{W}_{turb1.}$	$\psi_{turb1.} = \frac{\dot{W}_{turb1.}}{\dot{m}_{CO2}(ex_6 - ex_7)}$
CO_2-heat exchanger III (7-8)	$\dot{m}_7 = \dot{m}_8 = \dot{m}_{CO2}$	$\dot{Q}_{HX3}^{in} = \dot{m}_{CO2}(h_7 - h_8) * 1,4$ $\dot{Q}_{HX3}^{out} = \dot{m}_{CO2}(h_7 - h_8)$	$\dot{S}_{gen.,HX3} = \dot{m}_{CO2}(s_8 - s_7) + \left(\frac{\dot{Q}_{CO2}^{in}}{T_{HX3} + 10}\right)$	$\dot{Ex}_{D,HX3} = \dot{m}_{CO2}(ex_7 - ex_8) + \dot{Q}_{CO2}^{in}\left(1 - \frac{T_0}{T_{HX2} + 10}\right)$	$\psi_{HX3} = \frac{\dot{m}_{CO2}(ex_8 - ex_7)}{\dot{Q}_{CO2}^{in}\left(1 - \frac{T_0}{T_{HX3} + 10}\right)}$
CO_2-Turbine II (8-9)	$\dot{m}_8 = \dot{m}_9 = \dot{m}_{CO2}$	$\dot{W}_{turb2.} = \dot{m}_{CO2}(h_8 - h_9)$	$\dot{S}_{gen,turb2.} = \dot{m}_{CO2}(s_9 - s_8)$	$\dot{Ex}_{D,turb2.} = \dot{m}_{CO2}(ex_8 - ex_9) - \dot{W}_{turb2.}$	$\psi_{turb2.} = \frac{\dot{W}_{turb2.}}{\dot{m}_{CO2}(ex_8 - ex_9)}$
CO_2-R600a heat exchanger IV (10-1) (20-26)	$\dot{m}_{10} = \dot{m}_1 = \dot{m}_{CO2};$ $\dot{m}_{26} = \dot{m}_{20} = \dot{m}_{R600a}$	$\dot{Q}_{R600a}^{in} = \dot{m}_{R600a}(h_{20} - h_{26}) * 1,4$ $\dot{Q}_{HX4}^{out} = \dot{m}_{CO2}(h_{10} - h_1)$	$\dot{S}_{gen.,HX4} = \dot{m}_{CO2}(s_{11} - s_{10}) - \dot{m}_{R600a}(s_{26} - s_{20})$	$\dot{Ex}_{D,HX4} = \dot{m}_{CO2}(ex_{10} - ex_{11}) - \dot{m}_{R600a}(ex_{20} - ex_{26})$	$\psi_{HX4} = \frac{\dot{m}_{R600a}(ex_{20} - ex_{26})}{\dot{m}_{CO2}(ex_{10} - ex_{11})}$
R600a-Turbine III (20-21)	$\dot{m}_{20} = \dot{m}_{21} = \dot{m}_{R600a}$	$\dot{W}_{turb3.} = \dot{m}_{R600a}(h_{20} - h_{21})$	$\dot{S}_{gen,turb3.} = \dot{m}_{CO2}(s_{20} - s_{21})$	$\dot{Ex}_{D,turb3.} = \dot{m}_{CO2}(ex_{20} - ex_{21}) - \dot{W}_{turb3.}$	$\psi_{turb2.} = \frac{\dot{W}_{turb3.}}{\dot{m}_{CO2}(ex_{20} - ex_{21})}$
R600a-heat exchanger V (21-22)	$\dot{m}_{21} = \dot{m}_{22} = \dot{m}_{R600a}$	$\dot{Q}_{HX5}^{out} = \dot{m}_{R600a}(h_{22} - h_{21})$ $\dot{Q}_{HX5}^{in} = \dot{m}_{R600a}(h_{22} - h_{21}) * 1,4$	$\dot{S}_{gen.,HX5} = \dot{m}_{R600a}(s_{22} - s_{21}) + \left(\frac{\dot{Q}_{CO2}^{in}}{T_{HX5} + 2}\right)$	$\dot{Ex}_{D,HX5} = \dot{m}_{R600a}(ex_{21} - ex_{22}) + \dot{Q}_{CO2}^{in}\left(1 - \frac{T_0}{T_{HX5} + 2}\right)$	$\psi_{HX5} = \frac{\dot{m}_{R600a}(ex_{22} - ex_{21})}{\dot{Q}_{CO2}^{in}\left(1 - \frac{T_0}{T_{HX5} + 2}\right)}$

R600a-Turbine IV (22-23)	$\dot{m}_{22}$ $= \dot{m}_{23}$ $= \dot{m}_{R600a}$	$\dot{W}_{turb4.} = \dot{m}_{R600a}(h_{22} - h_{23})$	$\dot{S}_{gen,turb4.}$ $= \dot{m}_{CO2}(s_{22} - s_{23})$	$\dot{Ex}_{D,turb4.}$ $= \dot{m}_{CO2}(ex_{22} - ex_{23})$ $- \dot{W}_{turb3.}$	$\psi_{turb4.}$ $= \dfrac{\dot{W}_{turb3.}}{\dot{m}_{CO2}(ex_{22} - ex_{23})}$
R600a-heat exchanger VI (23-25)	$\dot{m}_{23}$ $= \dot{m}_{25}$ $= \dot{m}_{R600a}$	$\dot{Q}_{HX6}^{out}$ $= \dot{m}_{R600a}(h_{23} - h_{25})$ $\dot{Q}_{HX6}^{in}$ $= \dot{m}_{R600a}(h_{23} - h_{25}) * 1,4$	$\dot{S}_{gen.,HX6}$ $= \dot{m}_{R600a}(s_{23} - s_{25})$ $+ \left(\dfrac{\dot{Q}_{CO2}^{in}}{T_{HX6} - 2}\right)$	$\dot{Ex}_{D,HX6}$ $= \dot{m}_{R600a}(ex_{23} - ex_{25})$ $- \dot{Q}_{CO2}^{in}\left(1 - \dfrac{T_0}{T_{HX6} - 2}\right)$	ψ_{HX5} $= \dfrac{\dot{m}_{R600a}(ex_{23} - ex_{25})}{\dot{Q}_{CO2}^{in}\left(1 - \dfrac{T_0}{T_{HX6} - 2}\right)}$
R600a-pump (25-26)	$\dot{m}_{25}$ $= \dot{m}_{26}$ $= \dot{m}_{R600a}$	$\dot{W}_{pump}$ $= \dot{m}_{R600a}(h_{26} - h_{25})$	$\dot{S}_{gen,pump}$ $= \dot{m}_{R600a}(s_{26} - s_{25})$	$\dot{Ex}_{D,pump}$ $= \dot{m}_{R600a}(ex_{25} - ex_{26})$ $+ \dot{W}_{pump}$	ψ_{pump} $= \dfrac{\dot{m}_{R600a}(ex_{26} - ex_{25})}{\dot{W}_{pump}}$

3. RESULTS

In Figure 3, the T-s diagram of the ideal brayton cycle for single stage (with regeneration) and double stage (with regeneration, intercooling and reheating) is given.
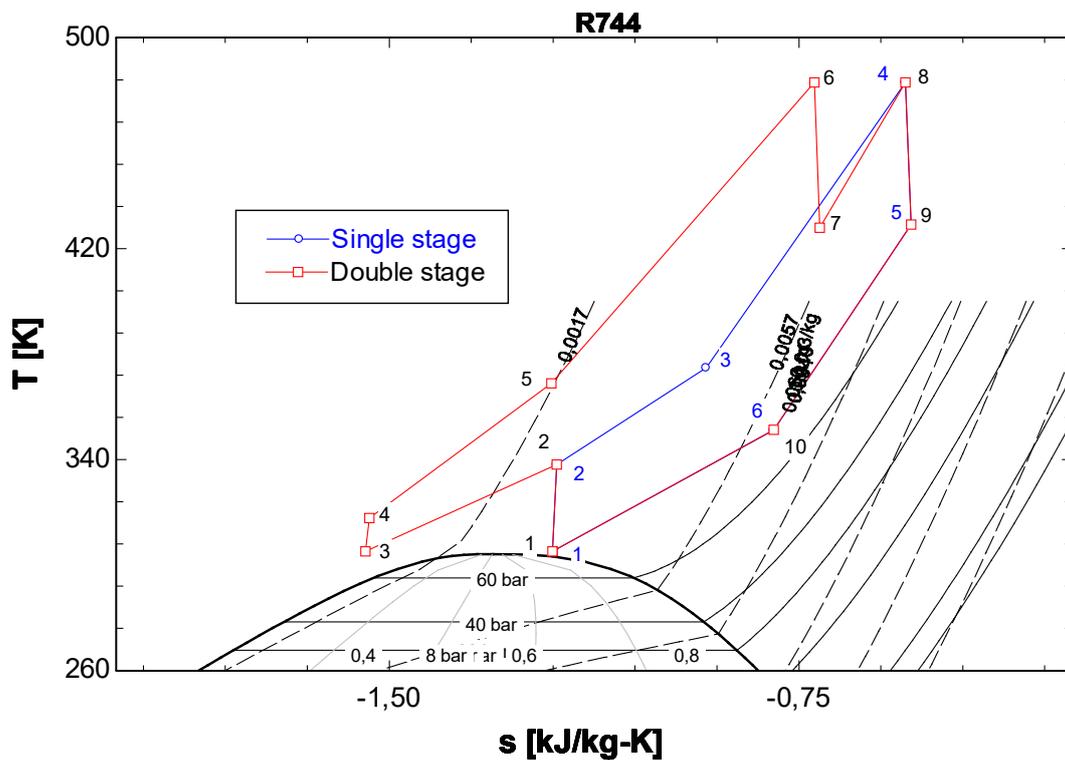
Figure 3. Single-stage and double-stage T-s cycle in the ideal brayton cycle

The cooling process at the 10th to 1st point of the T-s diagram in Figure 3 corresponds to the heat transfer between the 26th and 20th points in the system operating with the R600 refrigerant used in the ORC system in Figure 4.
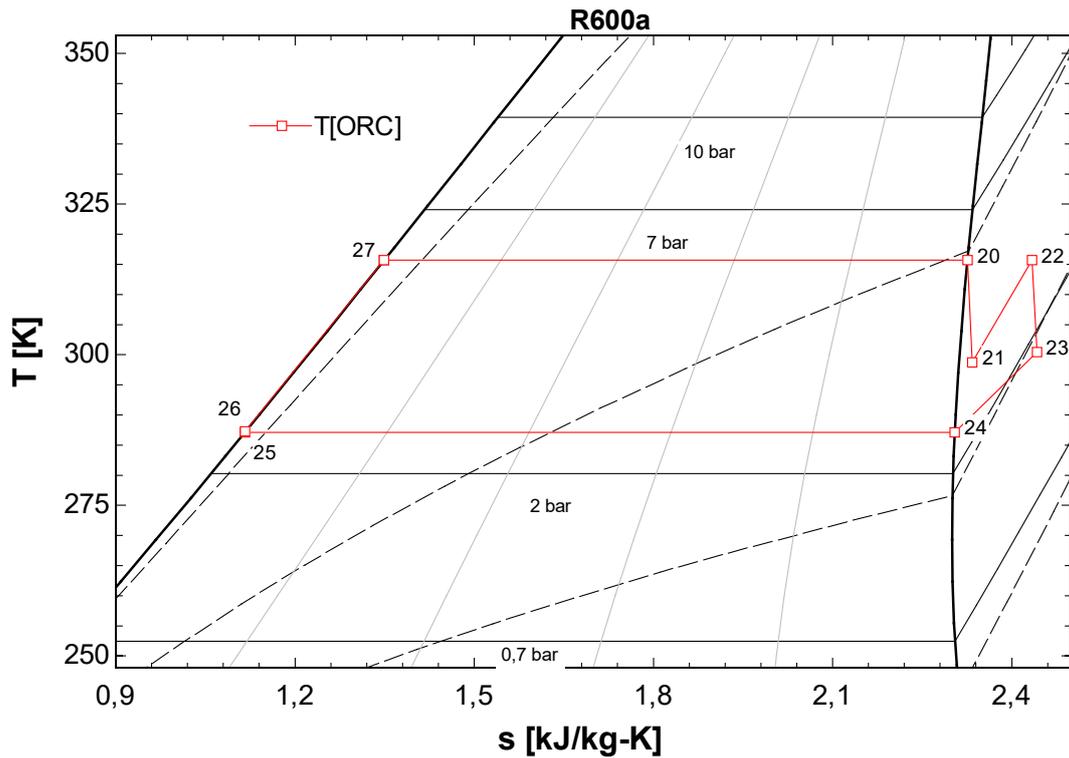
Figure 4. ORC system with R600a refrigerant

In Table 2, the thermodynamic values of the single-stage (regeneration) system are given according to the operating temperature data. (T_0(Dead state))

Table 2. Thermodynamic values of a single-stage (regeneration) system

Single stage	Temperature T [K]	Specific entropy s [kJ/kg.K]	Pressure P [bar]	Specific entalpy h [kJ/kg]	Exergy destruction Ex [kJ/kg]	Mass m [kg/s]
1	305.2	-1.201	75	-142.5	632.1	3
2	338.1	-1.194	135	-126	675.3	3
3	375.2	-0.9179	135	-28.3	725.7	3
4	483	-0.5551	135	125.3	867.3	3
5	429.2	-0.5445	75	84.6	735.9	3
6	351.2	-0.7966	75	-13.09	664.5	3
T_0	293.2	-0.01389	1	-5.125		

The thermodynamic results presented in Table 2 and the exergy destruction, exergy efficiencies and energy exchanges of each component of the system for the ideal single-stage (regeneration) Brayton cycle are shown in Table 3.

Table 3. Thermodynamic results of the one-stage (regenerated) ideal brayton cycle

Component	Exergy destruction Ex(KW)	Heat in Q(KW)in	Heat out Q(KW)out	Power W(KW)	Efficiency φ
1-2 compressors	6.454	-	-	49.57	0.87
2-3 Recuperators	20.94	293.1	293.1	-	0.70
3-4 Heat exchanger 1	66.95	645.1	460.8	-	0.68
4-5 Turbine1	9.311	-	-	122.1	0.93
5-6 Heat exchanger 2	47.29	277.3	388.3	-	0.46

As seen in Table 3, exergy destruction in the single-stage (with regeneration) system is seen in heat exchanger 1 with a maximum of 66.95KW. The best exergy efficiency was seen in turbine 1 with 93%. With a power of 72.53kw, it provided an electricity production efficiency of 40%. The thermodynamic data of the temperature results in the ideal brayton cycle in two stages (with regeneration, intercooling and reheating) are presented in Table 4.

Table 4. Thematic values of the double stage (regeneration, intercooling and reheating) cycle.

Double stage	Temperature T [K]	Specific entropy s [kJ/kg.K]	Pressure P [bar]	Specific entalpy h [kJ/kg]	Exergy destruction Ex [kJ/kg]	Mass m [kg/s]
1	305.2	-1.201	75	-142.5	632.1	3
2	338.1	-1.194	135	-136	675.3	3
3	305.2	-1.544	135	-239	644.4	3
4	317.8	-1.537	243	-223.8	683.4	3
5	361.6	-1.249	243	-126.1	723.6	3
6	483	-0.7217	243	92.28	914.7	3
7	427.9	-0.7118	135	54.08	791.4	3
8	483	-0.5444	135	125.3	867.3	3
9	429.2	-0.7965	75	84.63	735.9	3
10	351.2	-1.201	75	-13.05	664.5	3
T_0	293.2	-0.01389	1	-5.125		

The thermodynamic values of the cycle temperatures of the R600a refrigerant ORC system are presented in Table 5.

Table 5. Thermodynamic values of the cycle temperatures of the R600a refrigerant ORC system

ORC	Temperature T [K]	Specific entropy s [kJ/kg.K]	Pressure P [bar]	Specific entalpy h [kJ/kg]	Exergy destruction Ex [kJ/kg]	Mass m [kg/s]
20	315.7	2.326	5.668	611.7	65.09	0.951
21	298.7	2.333	3.149	591.1	43.38	0.951
22	315.7	2.434	3.149	621.9	44.70	0.951
23	300.4	2.442	1.749	600	21.61	0.951
25	287.1	1.116	2.503	232.7	41.89	0.951
26	287.3	1.116	5.668	233.4	42.42	0.951
T_0	293.2	2.487	1	590.6		

The thermodynamic calculation results of the cycles resulting in the combination of the two-stage (regeneration. intercooling and reheating) cycle and the ORC system are presented in Table 6.

Table 6. Thermodynamic results of the combination of the double stage (regeneration, intercooling and reheating) cycle with the ORC system.

Component	Exergy destruction Ex(KW)	Heat in Q(KW)in	Heat out Q(KW)out	Power W(KW)	Efficiency φ
1-2 compressors1	6.454	-	-	49.57	0.87
2-3 Heat exchanger 1	13.29	242.1	338.9	-	0.48
3.4 compressor2	6.305	-	-	45.49	0.86
4-5 Recuperators	31.28	293	293	-	0.56
5-6 Heat exchanger 2	91.84	917.3	655.2	-	0.67
6-7 Turbine1	8.756	-	-	114.6	0.93
7-8 Heat exchanger 3	32.5	299.2	213.7	-	0.68
8-9 Turbine2	9.311	-	-	122.1	0.93
10-1 Heat exchanger 4	9.72	359.8	388.4	-	0.70
20-21 Turbine 3	2.14	-	-	19.58	0.90
21-22 Heat exchanger 5	0.78	40.99	29.28	-	0.62

22-23 Turbine 4	2.26	-	-	20.83	0.90
23-25 Heat exchanger 6	3.87	249.5	349.3	-	0.80
25-26 Pump	0.09	-	-	0.628	0.84

In the ORC system, which is added by making use of waste heat in the regeneration, intercooling and reheating system, heat exchanger 1, which is used as the main heat source, followed by the recuperator, heat exchanger 1, heat exchanger 4, the heat exchangers have been subjected to exergy destruction. In terms of exergy efficiency, Turbine1, Turbine 2, Turbine 3, Turbine 4, respectively, were used with the highest efficiency.

The net work output and thermal efficiencies with the addition of the ORC system in the single and double-stage operating cycle are given in Table 7.

Table 7. Thermal efficiency of single and double stage cycle

Cycle	Heat input $\dot{Q}(kW)$	Heat output $\dot{Q}(kW)$	Net power $\dot{W}(kW)$	Energy efficiency $\eta th,$
Single stage	$(h_4 - h_3) * \dot{m}_{co2}$	$(h_6 - h_1) * \dot{m}_{co2}$	72.57	0.157
Double stage	$[(h_6 - h_5) + (h_8 - h_7)] * \dot{m}_{co2}$	$[(h_{10} - h_1) + (h_2 - h_3)] * \dot{m}_{co2}$	171.45	0.197
ORC	$[(h_{20} - h_{26}) + (h_{22} - h_{21})] * \dot{m}_{R600a}$	$(h_{23} - h_{25}) * \dot{m}_{R600a}$	39.75	0.102

As can be seen in Table 7, when switching from single-stage to double-stage, there was an increase in electricity production of 136% and an increase in thermal efficiency of 22%. Adding ORC system to single-stage and double-stage system will increase thermal efficiency by 10,2% and net work by 39,75KW.

The exergy destruction and exergy efficiencies for each system are given in Table 8 with the addition of the ORC system in the single and double stage operating cycle.

Table 8. Exergy destruction and yields of single and double stage cycles

Cycle	Exergy in Ex(kW)	Exergy out Ex(kW)	Exergy desruction Ex(kW)	Exergy efficiency φ_{Ex}
Single stage	$(ex_4 - ex_3) * \dot{m}_{co2}$	$(ex_6 - ex_1) * \dot{m}_{co2}$	109,2	0,77
Double stage	$[(ex_6 - ex_5) + (ex_8 - ex_7)] * \dot{m}_{co2}$	$[(ex_{10} - ex_1) + (ex_2 - ex_3)] * \dot{m}_{co2}$	203.7	0.76
ORC	$[(ex_{20} - ex_{26}) + (ex_{22} - ex_{21})] * \dot{m}_{R600a}$	$(ex_{23} - ex_{25}) * \dot{m}_{R600a}$	44.27	0.15

Table 8 When switching from single stage to double stage, exergy destruction increased by 86% and exergy efficiency decreased by 1%. Adding ORC system to single-stage and double-stage system will increase exergy efficiency by 15% and exergy destruction by 44.27KW.

4. CONCLUSIONS

Increasing and changing energy demand reminds us of the sustainable and most efficient use of energy day by day. In this context, it is inevitable that regenerative systems will provide us with more usable results. This study provides us with the final system improvements of CO_2 in supercritical Brayton cycles with intermediate heat exchangers, gradual compression, and gradual expansion. The performance characteristics of the CO_2 power systems and the

combined ORC system, and the energy and energy analysis results of the system components, by transferring the system from the waste heat source to the ORC cycle:

In the single-stage (with regeneration) system, exergy destruction is observed in heat exchanger 1 with a maximum of 66.95KW. The best energy efficiency was seen in turbine 1, with 93%. With a power of 72.53 kw, it provided an electricity production efficiency of 40%.

In the ORC system, which is added by making use of waste heat in the regeneration, intercooling, and reheating systems, heat exchanger 1 is used as the main heat source, followed by the recuperator, heat ext. 1, temp. At 4, the heat exchangers are subject to energy destruction. In terms of energy efficiency, turbine 1, turbine 2, turbine 3, and turbine 4, respectively, were used with the highest efficiency.

When switching from single-stage to double-stage, electricity production increased by 136% and thermal efficiency increased by 22%.Adding an ORC system to single-stage and double-stage systems will increase thermal efficiency by 10.2% and net work by 39.75KW.

When switching from single stage to double stage, increased by 86% and energy efficiency decreased by 1%. Adding an ORC system to single-stage and double-stage systems will increase energy efficiency by 15% and exergy destruction by 44.27KW.

More sustainable and environmentally friendly system designs can be developed by integrating ORC systems into recompression and reexpansion systems. The results obtained in this study show us that waste heat sources are of great importance in increasing the efficiency of integrated systems by combining energy conversion power plants and providing us with a more sustainable energy source.

REFERENCES

[1] Wang, E., Peng, N., & Zhang, M. (2021). System design and application of supercritical and transcritical CO_2 power cycles: A review. Frontiers in Energy Research, 699.

[2] Mishra, R. S., & Kumar, M. (2019). Thermodynamic analysis of brayton cycle for power generation.

[3] Bellos, E., & Tzivanidis, C. (2021). Parametric Analysis of a Polygeneration System with CO_2 Working Fluid. Applied Sciences, 11(7), 3215.

[4] Zhang, L., Deng, T., Klemeš, J. J., Zeng, M., Ma, T., & Wang, Q. (2021). Supercritical CO_2 Brayton cycle at different heat source temperatures and its analysis under leakage and disturbance conditions. Energy, 237, 121610.

[5] Zhang, R., Su, W., Lin, X., Zhou, N., & Zhao, L. (2020). Thermodynamic analysis and parametric optimization of a novel S–CO_2 power cycle for the waste heat recovery of internal combustion engines. Energy, 209, 118484.

[6] Hoang, H. T., Corcoran, M. R., & Wuthrich, J. W. (2009). Thermodynamic study of a supercritical CO_2 Brayton cycle concept. In Proceedings of supercritical CO_2 power cycle symposium.

[7] Wang, X., Wang, J., Zhao, P., & Dai, Y. (2016). Thermodynamic comparison and optimization of supercritical CO2 Brayton cycles with a bottoming transcritical CO_2 cycle. Journal of Energy Engineering, 142(3), 04015028.

[8] Yari, M., & Sirousazar, M. (2010). A novel recompression S-CO_2 Brayton cycle with pre-cooler exergy utilization. Proceedings of the Institution of Mechanical Engineers, Part A:

Journal of Power and Energy, 224(7), 931-946.

[9] Al-Sulaiman, F. A., & Atif, M. (2015). Performance comparison of different supercritical carbon dioxide Brayton cycles integrated with a solar power tower. Energy, 82, 61-71.

[10] Yu, W., Gong, Q., Gao, D., Wang, G., Su, H., & Li, X. (2020). Thermodynamic analysis of supercritical carbon dioxide cycle for internal combustion engine waste heat recovery. Processes, 8(2), 216.

[11] Ruiz-Casanova, E., Rubio-Maya, C., Pacheco-Ibarra, J. J., Ambriz-Díaz, V. M., Romero, C. E., & Wang, X. (2020). Thermodynamic analysis and optimization of supercritical carbon dioxide Brayton cycles for use with low-grade geothermal heat sources. Energy Conversion and Management, 216, 112978.

[12] Zhou, J., Zhang, C., Su, S., Wang, Y., Hu, S., Liu, L., ... & Xiang, J. (2018). Exergy analysis of a 1000 MW single reheat supercritical CO_2 Brayton cycle coal-fired power plant. Energy conversion and management, 173, 348-358.

[13] Chowdhury, J. I., Asfand, F., Hu, Y., Balta-Ozkan, N., Varga, L., & Patchigolla, K. (2019, January). Waste heat recovery potential from industrial bakery ovens using thermodynamic power cycles. In ECOS 2019-Proceedings of the 32nd International Conference on Efficiency, Cost, Optimization, Simulation and Environmental Impact of Energy Systems (pp. 2435-2441). Institute of Thermal Technology.

[14] Wang, K., Li, M. J., Guo, J. Q., Li, P., & Liu, Z. B. (2018). A systematic comparison of different S-CO_2 Brayton cycle layouts based on multi-objective optimization for applications in solar power tower plants. Applied energy, 212, 109-121.

[15] Gao, W., Yao, M., Chen, Y., Li, H., Zhang, Y., & Zhang, L. (2019). Performance of S-CO_2 Brayton cycle and organic Rankine cycle (ORC) combined system considering the diurnal distribution of solar radiation. Journal of Thermal Science, 28(3), 463-471.

[16] Ma, H., & Liu, Z. (2022). An Engine Exhaust Utilization System by Combining CO_2 Brayton Cycle and Transcritical Organic Rankine Cycle. Sustainability, 14(3), 1276.

[17] Li, B., Wang, S. S., Wang, K., & Song, L. (2021). Comparative investigation on the supercritical carbon dioxide power cycle for waste heat recovery of gas turbine. Energy Conversion and Management, 228, 113670.

[18] Purjam, M., Goudarzi, K., & Keshtgar, M. (2017). A new supercritical carbon dioxide brayton cycle with high efficiency. Heat Transfer—Asian Research, 46(5), 465-482.

[19] Padilla, R. V., Benito, R. G., & Stein, W. (2015). An exergy analysis of recompression supercritical CO_2 cycles with and without reheating. Energy Procedia, 69, 1181-1191.

[20] Besarati, S. M., & Yogi Goswami, D. (2014). Analysis of advanced supercritical carbon dioxide power cycles with a bottoming cycle for concentrating solar power applications. Journal of solar energy engineering, 136(1).

[21] Akbari, A. D., & Mahmoudi, S. M. (2014). Thermoeconomic analysis & optimization of the combined supercritical CO_2 (carbon dioxide) recompression Brayton/organic Rankine cycle. Energy, 78, 501-512.

[22] Khan, Y., & Mishra, R. S. (2021). Performance evaluation of solar based combined pre-compression supercritical CO_2 cycle and organic Rankine cycle. International journal of Green energy, 18(2), 172-186.

[23] Chacartegui, R., Sánchez, D., Muñoz, J. M., & Sánchez, T. (2009). Alternative ORC bottoming cycles for combined cycle power plants. Applied Energy, 86(10), 2162-2170.

[24] Dincer, I., & Rosen, M. A. (2012). Exergy: energy, environment and sustainable development. Newnes.

[25] Cengel, Y. A., Boles, M. A., & Kanoğlu, M. (2011). Thermodynamics: an engineering approach (Vol. 5, p. 445). New York: McGraw-hill.

[26] Klein, S. A., & Alvarado, F. L. (2002). Engineering equation solver. F-Chart Software, Madison, WI, 1.

Modeling and Economic Analysis of Greenhouse Top Solar Power Plant with Pvsyst Software

Authors: Muhammet Raşit SANCAR ⓘD Ahmet Buğrahan BAYRAM ⓘD

International Journal of Engineering and Innovative Research

http://dergipark.gov.tr/ijeir

Modeling and Economic Analysis of Greenhouse Top Solar Power Plant with Pvsyst Software

Muhammet Raşit SANCAR [1],[*],[**] ⓘ, Ahmet Buğrahan BAYRAM [1],[**] ⓘ

[1] Isparta University of Applied Sciences, Graduate School of Education, Department of Energy Systems Engineering, Isparta, Turkey.

[*]Corresponding Author: d1840640001@isparta.edu.tr
[**] The authors are YOK 100-2000 scholarship holders.

ABSTRACT: Due to increasing wars and global warming, the issue of providing the supply-demand balance in energy and food is becoming more important daily. When the issue of providing the electricity needed in modern greenhouses and consuming the energy where it is produced are evaluated together, rooftop applications in greenhouses become important. In this study, a photovoltaic system on a greenhouse in an area of 5031.6 m^2 was modeled three-dimensionally using PVsyst software in north-south, and east-west orientations at 10°, 20° and 35° angles, and 6 different simulation studies were performed. By determining the cost of the greenhouse and above-greenhouse photovoltaic system to be constituted, an economic analysis study was performed at the point of OG single-term and OG double-term tariffs in the Energy Market Regulatory Authority (EPDK) tariff tables. As a result, the highest electricity production of the power plant was eventuated as 1579.2 MWh at 10° east-west orientation. In the case of the sale of electricity produced in the photovoltaic system installed above the greenhouse, it has been calculated that the OG single-term tariff brings 2 162 443.087 TL, and the OG double-term tariff 2 203 707.83 TL annual income. The lowest electricity generation was at 35° north-south orientation and was 1392.3 MWh. Based on this production value, it has been calculated that in the case of electricity sales, the OG monomial tariff brings an annual income of 1 894 757.401 TL, and the OG binomial tariff brings 1 930 914.04 TL.

Keywords: Above Greenhouse SEPP, Above Greenhouse Photovoltaic System, Greenhouse SEPP

1. INTRODUCTION

With the growing world population, the demand for food is increasing rapidly. In line with this demand, sustainable agriculture gains tremendous importance in the production of high-quality products economically by environmentally friendly techniques. While environmental problems such as human activities, urbanization, climate change, and desertification threaten agricultural productivity and food security, they necessitate improving agricultural activities. Modern greenhouses are one of the areas where sustainable agriculture is applied. Control of the growth medium in light, water, temperature, relative humidity, CO_2 concentration, and ventilation provides optimal growing conditions for plants while improving crop yield and quality in greenhouse plant production. Many interrelated parameters can affect the environmental parameters in greenhouses, such as the size and location of the greenhouses, the type of cover material, the heat storage method, the amount and quality of the materials used, the type of cultivation, and the desired day and night temperature [1].

Since the sun is the essential tool for plants and photovoltaic panels, combining the two and establishing photovoltaic greenhouses has been the subject of considerable research and studies. In a study conducted in China, translucent photovoltaic panels were installed to cover 20% of the greenhouse roof area with a 30° inclination towards the south. It has been interpreted that the shading effect caused by the panels prevents overheating in summer, and the integration of shaded greenhouses may be more suitable for growing tomatoes in hot climates. It has been determined that the annual generated electrical energy of the used photovoltaic panels is 637 kWh and the payback period is 9 years [2].

It has been determined that covering 19.2% of the roof with photovoltaic panels will reduce annual natural gas consumption, electricity demand, and CO_2 emissions, respectively, by 3.57%, 45.5%, and 30.56 kg/m2, and annual electricity production of panels is approximately 42.7 kWh/m^2 [3].

The experiment was performed in Agadir, on the Atlantic coast of Morocco, using two greenhouses. On the roof of one of the equipped greenhouses, photovoltaic panels are used with 32 East-West oriented, covering 10% of the total surface area. The other greenhouse was accepted as a control and only covered with plastic cover. Tomato plants were planted in each greenhouse, and it was interpreted that the yield of tomatoes collected in the photovoltaic greenhouse was higher than in the control greenhouse and sometimes nearly the same degree as in the control greenhouse [4].

In the study performed in Izmir, Turkey, a greenhouse with an area of 150m^2 and a roof angle of 38.4° were modeled using Design Builder software. Tomato, cucumber, and lettuce cultivation in the greenhouse is examined. In order not to overshadow the plants, it is equipped with 66 photovoltaic panels covering 50% of the south face of the roof area. Annual electricity production was found as 21510.4 kWh [5].

The experiment conducted on a 1024 m^2 greenhouse in Spain was carried out with the installation of two photovoltaic panel arrays, each with a surface area of 192 m^2. It was analyzed that the shading caused by the panels placed on the greenhouse roof did not affect the yield of the tomato plant, and the plant morphology did not change, but it caused a decrease in the fruit diameter [6].

An experiment in Italy was carried out by placing photovoltaic (PV) modules on 50% of the roof area of a commercial greenhouse with an area of 960 m^2. The tomato plant was chosen as the test crop to confirm the greenhouse solar radiation distribution due to its high sensitivity to light. The existing greenhouse has a roof slope of 22°. The maximum nominal power of the photovoltaic panels used is 68 kWp, and ıt is stated that the polycrystalline silicon module covers an area of 475m^2. As a result of the experiment, it was measured that the annual average outdoor temperature was 17 °C, and the temperature inside the greenhouse was 19.8 °C. It has been determined that this temperature difference is higher in the winter and spring seasons (from November to April). A decrease was observed in the yield of the tomato plant. It was determined that the annual electricity production was 107 885 kWh, with the highest production in June and the lowest in December [7].

Based on a farm greenhouse with an area of approximately 1.50 hectares located on the northwest coast of Sicily, the study performed an economic analysis of the use of photovoltaic panels. It was stated that the white asparagus plant was cultivated because 0.5 hectares of the

greenhouse would adapt well to the weak light conditions caused by the solar panels. The greenhouse is covered with polycrystalline silicon panels, and its installed power is declared to be 300 kW. Assuming that the annual electricity efficiency produced decreases by 0.8% every year, an annual average of 417 387.19 kWh of electricity production is analyzed [8].

Shading simulation was carried out using Autodesk software in a tunnel greenhouse at the University of Tuscia in Viterbo, Italy. The greenhouse is 8 m wide, 30 m long, and 3.20 m high. The photovoltaic panels used have a rectangular shape of 1.116 m × 0.165 m, 2 mm thick, and are placed on the greenhouse roof both parallel and equidistant from each other. According to the analyzed results, it was observed that from March to September, the shadows were inside the greenhouse at midday and partially inside and outside the greenhouse tunnel in the remaining months. It is interpreted that the shading depends on the distance between the panels and the slope [9].

Established in Kunming, China, the experimental greenhouse was installed on the roof of an east-west-oriented solar energy research institute building. The greenhouse is heated by a solar collector combined with a heat pump with opaque photovoltaic modules mounted on its roof with an area of 77.50 m^2. Opaque photovoltaic modules placed on the greenhouse roof with an inclination angle of 30° covered 25.9% of the total surface area of the roof. Layout was made using an order with a gap of 1.1 m between each module. The plant variety tested in the greenhouse was selected as 'Jingzangxiang' strawberry, which had a high survival rate during the trial. To compare the effects of shaded and unshaded light, thirteen pots were placed under the photovoltaic modules, and thirteen different pots were placed between the modules. In addition, twenty potted strawberry plants were used for the unshaded control samples. According to the results, it was observed that the chlorophyll content of the shaded strawberry leaves was 1.3 times higher than the unshaded strawberry leaves, the 'Jingzangxiang' strawberry plants in the shade grew better than the unshaded ones, and the strawberry fruit grown in the shade had a sweeter taste than the strawberry fruit grown without the shade [10].

"Unlicensed Electricity Generation Regulation in the Electricity Market" was published in the Official Gazette dated 12/5/2019 and numbered 30772 [11]. The purpose of this regulation is explained as "In the electricity market, consumers meet their electricity needs from their production facility closest to the point of consumption, bring small-scale generation facilities to the country's economy to ensure supply security, and reduce the number of losses in the electricity grid by ensuring effective use of small-scale generation resources". For this purpose, generating electricity where it is consumed has great importance in terms of minimizing losses.

Supporting sustainable agriculture with renewable energy will be an environmentalist approach. Applications such as supplying the electricity needed in greenhouses, operating irrigation systems, heating greenhouses, heating, cooling, ventilation, and lighting can be provided to the greenhouse in an environmentally friendly way using photovoltaic panels. If there is no suitable land near the greenhouse where the photovoltaic panel application is desired, the greenhouse roof can be considered a suitable location for the assembly and installation of this application.

In this study, a greenhouse solar power plant with two different designs and three different angles for the province of Isparta was simulated using PVsyst software. With 6 different simulation studies, electricity production values were compared with each other in 2 different designs at different angles, using identical equipment and equal installed power conditions. Obtained electricity production values were analyzed economically over electricity unit price

using June tariff tables of Energy Market Regulatory Authority (EPDK). Thus, the electricity production values and economic evaluation that can be obtained from the greenhouses to be established in different designs at different angles in the province of Isparta were made and it was aimed to create a foresight for agricultural investors.

2. MATERIAL AND METHOD

This study was performed in Bozanönü village, located at 37.87° latitude and 30.58° longitude, in the central district of Isparta province. By using the PVsyst software, a greenhouse photovoltaic system simulation was made for the greenhouse designs with east-west and north-south orientation, and the income to be obtained in the case of selling all the electricity produced to the grid was examined for 2 different tariff situations in the field of "Agricultural Activities" using the EPDK tariff table.

2.1 PVsyst Simulation

In the study. 7.2.15 version of PVsyst software was used. The software is a computer software package for modeling, sizing, inspection, and data analysis of photovoltaic systems [12]. There are options for photovoltaic system designs, including pump use and off-grid and grid-connected systems in the software. In addition, there is a comprehensive climate data infrastructure with many climate data sources in the software interface. The software is widely used in the private sector and academically. The interface of the software is presented in Figure 1.
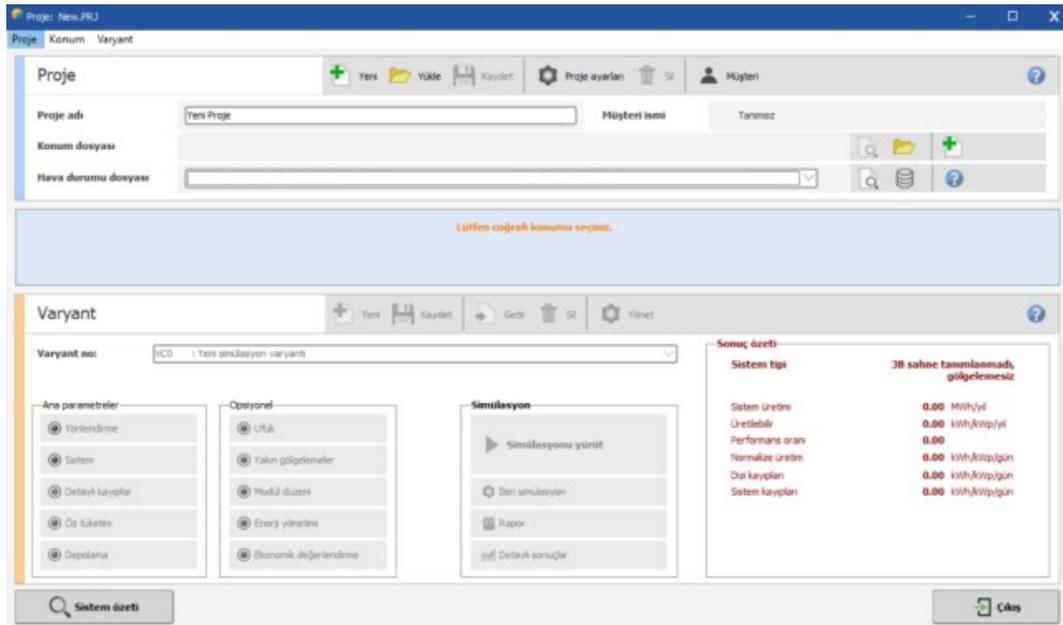
Figure 1. PVsyst software interface

The PVsyst simulation study for the greenhouse photovoltaic system was performed following the steps below.

- It will be a system connected to the grid, and the electricity generated will be supplied to the grid. For this reason, under the heading "Project design and simulation," the system was determined by checking the "Connected to the Network" system option.
- Under the steering button, the photovoltaic system's orientation angle and azimuth angle values are entered. Due to settlement, for greenhouse designs with an east-west

orientation, the azimuth angle values are entered as 70°, -110° and azimuth angle values as -20°, 160° for greenhouse designs with a north-south orientation.

- Under the "System" button, the Inverter and panel properties are entered. After these properties are entered, the serial and parallel numbers of the power plant panels are adjusted. The Inverter, panel, and other system specifications are given in Table 1.

Table 1. Photovoltaic system specifications

Photovoltaic Panel		Inverter Specifications	
Panel Model	JKM-610N-78HL4-BDV	Model	SUN2000-100KTL-M1-480Vac
Panel Power	610 Wp	Unit Power	100 kWac
Impp	13.38 A	Operating voltage	200-1000 V
Vmpp	45.6 V	Maximum AC Power	110 Kva
Voc	55.31 V	Absolute Maximum PV Voltage	1100 V
Isc	14.03 A	Mains Voltage	480 V
Photovoltaic System Properties			
Gross power	1098 kWac	Number of Sequences in the System	100
Maximum rated power (DC:AC)	1.098	Number of Panels in Array	18
Number of Panels Used	1800	Rated for total PV power (STC)	1098 kWp
Number of Inverters Used	10	Total Area	5031.6 m^2

It is modeled in three dimensions, based on the azimuth angle and plane angle properties, which were previously defined under the "orientation" button under the "close shadings" button. There are two different designs related to three-dimensional models. The first of these designs is the north-south design presented in Figure 2, and the second is the east-west design presented in Figure 3.
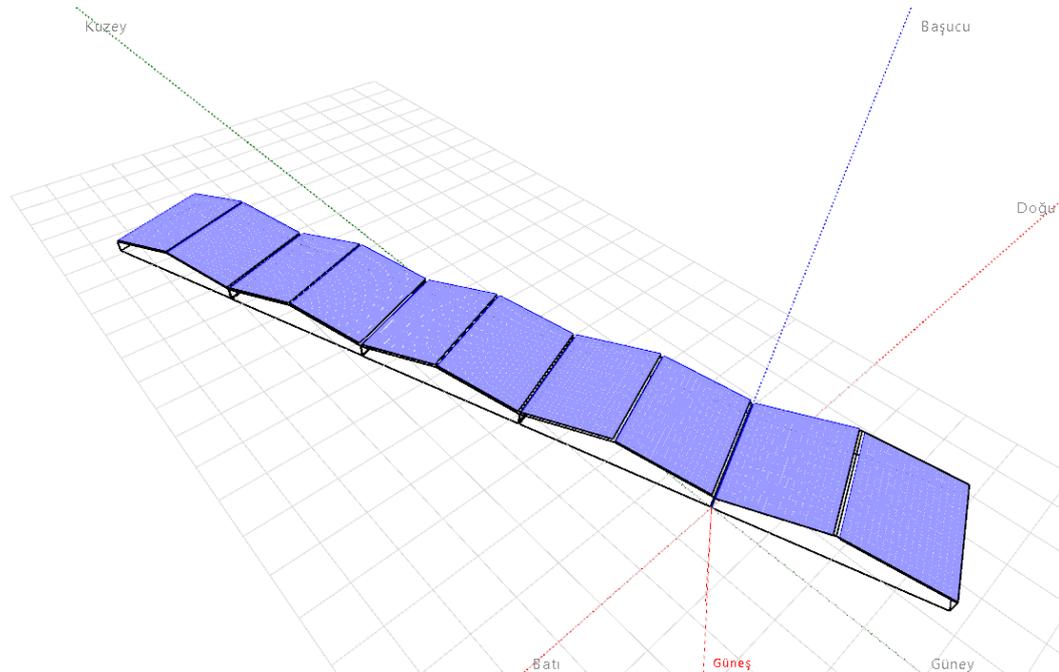
Figure 2. Design of North-South orientation [12]
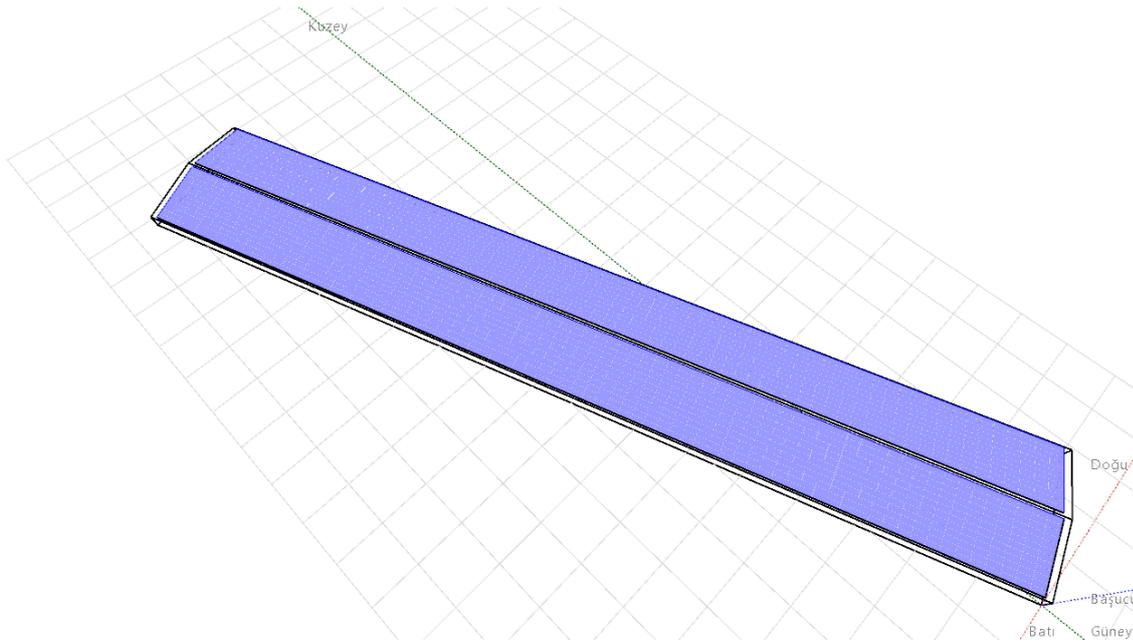
Figure 3. Design of east-west orientation [12]

The above steps were performed separately for each design at plane angles of 10°, 20°, and 35.6° different simulation studies were performed. As a result of the simulation studies, monthly and annual electricity production values were taken from the report presented by the software.

2.1 Economic Analysis

There are three main components in the greenhouse and greenhouse photovoltaic system designed in this study. These are transformer, greenhouse, and photovoltaic systems. Information on the cost of all systems is presented in Table 2.

Table 2. Greenhouse and greenhouse photovoltaic system cost

Photovoltaic System	14875000 TL
Transformer (1000 kVA)	1400000 TL
Greenhouse Installation Cost	3850000 TL
Subscription Deposit	70000 TL

In the regulation dated 12/5/2019 and numbered 30772, the expression "set-off" defines the process of "finding the net production or net consumption value in kWh as a result of deducting the production and consumption from each other within a certain period". In the "a" clause of the 24th paragraph of the same regulation, "The net electrical energy produced in the production facility or facilities located at the same place as the consumption facility and given to the grid in each billing period is ten years to be evaluated within the scope of Renewable Energy Resources Support Mechanism (YEKDEM) at a price determined by the supply company in charge as surplus electrical energy and purchased for a period of time". Within the scope of these statements, a consumption facility can produce electrical energy at the point where it consumes electrical energy and sells the excess for 10 years by offsetting. In companies that sell electricity by set-off, the selling prices of electricity are the same as the purchase prices. These prices are regularly published on EPDK's website [13].

For this study, 2 separate economic analyzes were carried out for "Agricultural Activities" users from the EPDK tariff table presented in Table 3, within the scope of "Single-term" and "binomial-term" subscription groups at medium voltage. The net income obtained as a result of

the sales of electricity produced in the analysis was calculated with the help of Equation 1. The annual net income is calculated with the help of Equation 2.

$$AG = AE\ddot{U} \times (PTZEB - DB) \qquad (1)$$

$$YG = \sum_{n=12}^{n} AG \qquad (2)$$

In Equations 1 and 2, "AG" expresses the monthly net income value in TL. "AEU" represents the monthly electricity generation value. These electricity generation values are taken from the simulation results. The term "PTZEB" defines the retail one-time energy price for the applied tariff. Finally, the expression "DB" refers to the distribution price for the determined tariff. ROI value is the annual income value in TL. In Equation 3, the formula for the payback period is given.

$$G\ddot{O}S = \frac{\dot{I}YM}{YG} \qquad (3)$$

The GDS value defines the payback period in years. The expression ICE defines the initial investment cost. Acceptances made in the following items are presented.

- Electricity consumption in the greenhouse is neglected.
- When calculating the payback period, the greenhouse installation cost was not calculated since only the calculations were made for the photovoltaic system.
- All electricity produced was sold to the grid.
- Yield losses in the coming years have been neglected.
- Electricity sales prices are assumed to be constant for all years.

Table 3. Tariff Table Based on EPDK Electricity Bills [12].

| | Activity Based Tariffs Approved by EPDK and Approved as of June 1 June 2022 | | | | | | | | |
| 1/6/2022 | Activity Based Consumer Tariffs (kr/kWh) | | | | | Total Tariffs Excluding Power Fee (kr/kWh) | | | |
Transmission System Users Receiving Energy from the Incumbent Supply Company	Retail One-Time Energy Cost	Retail Daytime Energy Fee	Retail Rush Hour Energy Cost	Retail Night Energy Fee	Distribution Fee	Single Time	Daytime	Puant	Night
Consumer	245,3607	248,3693	392,2113	132,2746	0,0000	245,3607	248,3693	392,2113	132,2746
Distribution System Users	Retail One-Time Energy Cost	Retail Daytime Energy Fee	Retail Rush Hour Energy Cost	Retail Night Energy Fee	Distribution Fee	Single Time	Daytime	Puant	Night
Medium Voltage						Medium Voltage			
Double-Term						Double-Term			
Industry	248,3714	251,3801	395,2221	135,2853	14,7972	263,1686	266,1773	410,0193	150,0825
Public and Private Services Sector and Other	230,2455	232,5236	363,0085	128,7021	23,0611	253,3066	255,5847	386,0696	151,7632
Residential	152,9207	155,4131	246,1925	82,8186	22,8419	175,7626	178,2550	269,0344	105,6605
Agricultural Activities	157,6777	159,2914	251,4048	85,6839	18,9925	176,6702	178,2839	270,3973	104,6764
Lighting	212,2218				22,1336	234,3554			
Monomial									
Industry	256,6870	259,8001	408,5735	139,7250	16,3448	273,0318	276,1449	424,9183	156,0698
Public and Private Services Sector and Other	235,0787	237,3568	367,8417	133,5347	28,7660	263,8447	266,1228	396,6077	162,3007
Residential	154,5685	157,0611	247,8392	84,4656	28,2039	182,7724	185,2650	276,0431	112,6695
Agricultural Activities	159,7360	161,3497	253,4633	87,7413	23,6477	183,3837	184,9974	277,1110	111,3890
Lighting	216,7131				27,6100	244,3231			
Low Voltage						Low Voltage			
Monomial						Monomial			
Industry	262,2851	265,2400	406,5304	151,2050	25,2888	287,5739	290,5288	431,8192	176,4938
Public and Private Services Sector and Other (30 kWh/day and below)	174,6438	246,0159	376,5007	142,1943	34,2716	208,9154	280,2875	410,7723	176,4659
Public and Private Services Sector and Other (over 30 kWh/day)	243,7383	246,0159	376,5007	142,1943	34,2716	278,0099	280,2875	410,7723	176,4659
Residential (8 kWh/day and below)	95,5452	161,7720	252,5509	89,1764	33,5187	129,0639	195,2907	286,0696	122,6951
Residential (over 8 kWh/day)	159,2790	161,7720	252,5509	89,1764	33,5187	192,7977	195,2907	286,0696	122,6951
Families of Martyrs and Disabled Veterans	38,7776				22,7335	61,5111			
Agricultural Activities	164,3828	168,6088	258,1106	92,3882	28,1603	192,5431	196,7691	286,2709	120,5485
Lighting	224,9134				32,8247	257,7381			
General Lighting	204,7600				32,8247	237,5847			

4. RESULTS

The electricity generation data obtained from the simulation results carried out in the study were applied using the equations 1, 2 and 3 given above. Figure 4 presents the annual gain graph at OG binomial tariff point for different designs. Since the highest electricity production values for all designs were realized in July, the gain values for this month again reached the highest value. The highest electricity generation was for the 10° east-west design, with a value of approximately 1589 MWh. The annual income amount for this design is 2 142 131.6 TL. The lowest electricity generation value was for the 35° north-south design, and the annual electricity generation value was calculated as 1392.3 MWh for this design. The annual income amount for this design is 1 879 045.77 TL.
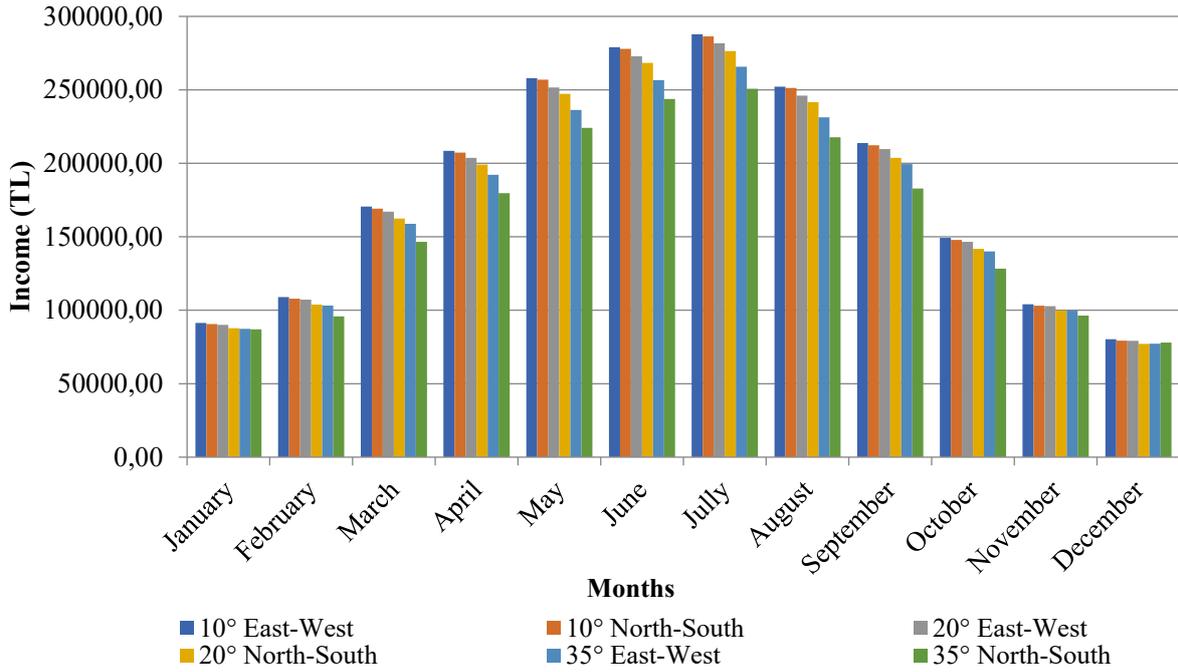
Figure 4. Monthly income values for OG binomial tariff

Figure 5 shows the annual gain graph for different designs at the OG mononomial tariff point. Since the lowest electricity production values for all designs occurred in December, the gain values for this month still seem to be at the lowest value. The lowest gain value among the designs was realized for the 35° north-south design and was calculated as 1 894 757.04 TL. The highest gain was for the 10° east-west design. The annual income amount for this design is 2 162 443.09 TL.
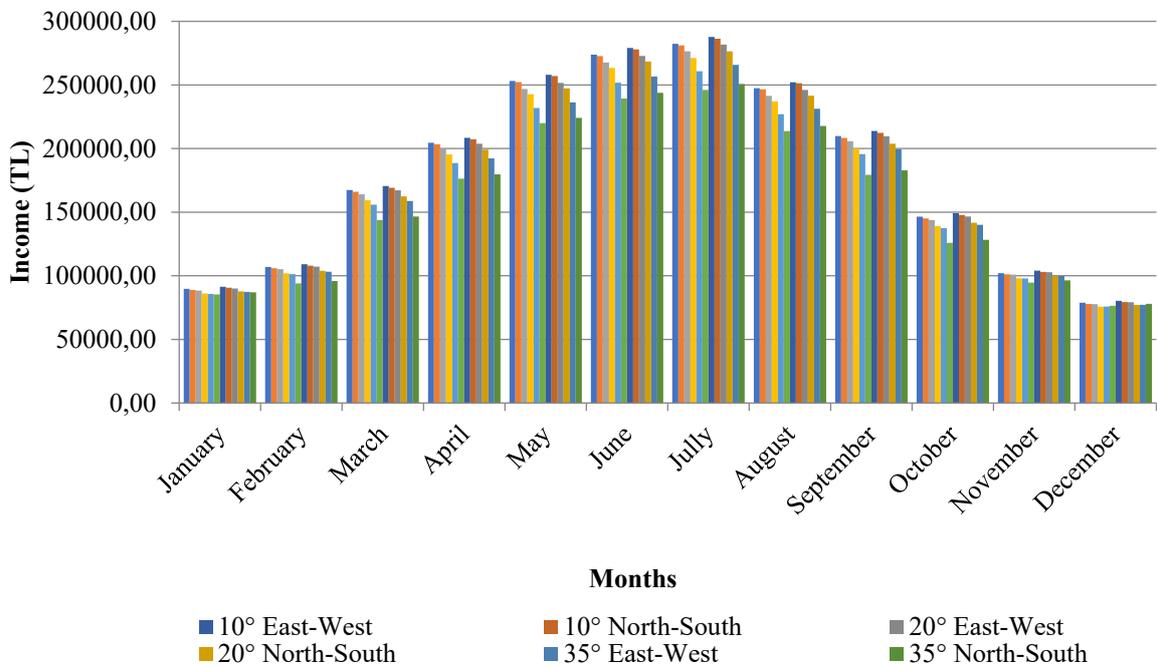
Figure 5. Monthly income values for the OG monomial tariff

Table 4 presents the payment terms for the greenhouse photovoltaic system for different greenhouse designs within the scope of the OG binary tariff. Among the calculations made for

different designs within the scope of this tariff, the minimum payback period was 7.63 years, and the highest was 8.7 years.

Table 4. OG binomial payback periods.

Design	Payback Periods (Year)
10° East -West	7.63
10° North- South	7.68
20° East -West	7.79
20° North- South	7.94
35° East -West	8.21
35° North- South	8.70

Table 5 shows the payback periods for different greenhouse designs under the OG monomial tariff. For this tariff, the highest payback period is 8.63 years, while the lowest is 7.56 years.

Table 5. OG monomial payback periods

Design	Payback Periods (Year)
10° East -West	7.56
10° North- South	7.61
20° East -West	7.72
20° North- South	7.90
35° East -West	8.13
35° North- South	8.63

5. CONCLUSION

In this study, photovoltaic system designs have been performed for different types of greenhouses in order to examine the food and energy issues together, which have gained significant importance in recent years. The realized designs were simulated using PVsyst software. The electricity generation data obtained in the simulation results were analyzed economically at the point of monomial and binomial tariff groups for the "Agricultural Activities" subscription in the EPDK tariff tables. The difference between the highest electricity generation value and the lowest electricity generation value among the designs was determined as approximately 196.7 MWh. It has been calculated that the difference between the lowest annual income value and the highest annual income value within the scope of the OG binomial tariff is 272 793.79 TL. Within the OG monomial tariff scope, the difference between the lowest annual income and the highest annual income has been calculated as 267 685.69 TL. When the design and tariff parameters are evaluated together, it has been calculated that the difference between the highest and lowest values on the basis of annual income is 308 950.4271 TL. Again, when the tariffs and designs are evaluated together, it has been determined that a period of 1.14 years occurs when the highest and lowest values of the payback period are considered.

In the literature review, it has been determined that many studies have been carried out on using greenhouse photovoltaic systems. It is thought that such systems will become widespread in Turkey in the near future. Within the scope of the study, a study that will create a foresight on different designs and different subscriber groups for a greenhouse established on an area of 5031.6 m^2 has been presented, and a guideline study has been presented for investors considering agriculture and renewable energy investments together. With agricultural support mechanisms supporting such investments, payback periods can be shortened, and agricultural investors' investments in renewable energy can be encouraged. Orientation to greenhouse photovoltaic systems can be realized more quickly by directing the specialized organized industrial zones based on agriculture on these issues.

In addition, considering the increase in food prices and the supply gap, it is thought that if the following steps are taken, it can be a precaution against the food crisis that may be experienced.

- Determining the greenhouse-sourced food type and the need for these species throughout the country.
- Determining the greenhouse installation zones for the product, taking into account the climatic factors for the determined food type and need
- Designing greenhouse projects according to the standards determined for the products in the selected regions and designing greenhouse projects suitable for installing photovoltaic systems.
- Organizing the transformer capacities in the regions with the capacity to make applications to all areas where photovoltaic systems can be installed
- Opening the projects to the private sector investment in the determined regions at the point of the selected agricultural products, on the condition of continuous production.
- Encouraging investments in rural and agricultural development supports
- Purchasing the electricity production of investors who continuously produce agricultural products in the desired amount with the realization of the applications
- Fixing domestic sales prices at regular intervals by imposing a quota on the import of products.
- Increasing the electricity purchase prices and reducing the distribution costs .from the subscribers of "Agricultural Activities" presented in EPDK tariff tables.

With the realization of the above-mentioned items, energy investors, who have difficulties in finding viable photovoltaic system installation areas in the current situation, can be directed to the agricultural sector and the way of directing investments in two areas where there is a supply deficit in the world can be paved. If the condition of growing the target products determined in the greenhouse is met, the continuity of their earnings can be ensured by enabling them to sell electricity in the same place by the offsetting method. Thus, agricultural investors cannot reach sufficient income from time to time due to the fluctuations in the market. With the determination of food prices by the government, price stability can be achieved by reducing food inflation in the market. With the application of different renewable energy-based applications in agricultural areas, it can be predicted that rapid, sustainable progress can be realized in both agricultural and energy fields.

6. ACKNOWLEDGEMENTS

Conflict of Interest

No conflict of interest was declared by the authors.

REFERENCES

[1]   Koçar, G., Eryaşar A., Gödekmerdan E., Özgül S., Düzenli M. (2018). A Prospect on Integration of Solar Technology to Modern Greenhouses. Dokuz Eylul University-Faculty of Engineering Journal of Science and Engineering, 20, 58, 245-258.

[2] Hassanien, R. H. E., Li, M., Yin, F. (2018). The integration of semi-transparent photovoltaics on greenhouse roof for energy and plant production. Renewable Energy, 121, 377-388.

[3] Alinejad, T., Yaghoubi, M., Vadiee, A. (2020). Thermo-environomic assessment of an integrated greenhouse with an adjustable solar photovoltaic blind system. Renewable energy, 156, 1-13.

[4] Ezzaeri, K., Fatnassi, H., Bouharroud, R., Gourdo, L., Bazgaou, A., Wifaya, A., Bouirden, L. (2018). The effect of photovoltaic panels on the microclimate and on the tomato production under photovoltaic canarian greenhouses. Solar Energy, 173, 1126-1134.

[5] Yildirim, N., Bilir, L. (2017). Evaluation of a hybrid system for a nearly zero energy greenhouse. Energy Conversion and Management, 148, 1278-1290.

[6] Aroca-Delgado, R., Pérez-Alonso, J., Callejón-Ferre, Á. J., Díaz-Pérez, M. (2019). Morphology, yield and quality of greenhouse tomato cultivation with flexible photovoltaic rooftop panels (Almería-Spain). Scientia Horticulturae, 257, 108768.

[7] Cossu, M., Murgia, L., Ledda, L., Deligios, P. A., Sirigu, A., Chessa, F., Pazzona, A. (2014). Solar radiation distribution inside a greenhouse with south-oriented photovoltaic roofs and effects on crop productivity. Applied Energy, 133, 89-100.

[8] Sgroi, F., Tudisca, S., Di Trapani, A. M., Testa, R., Squatrito, R. (2014). Efficacy and efficiency of Italian energy policy: The case of PV systems in greenhouse farms. Energies, 7(6), 3985-4001.

[9] Marucci, A., Zambon, I., Colantoni, A., Monarca, D. (2018). A combination of agricultural and energy purposes: Evaluation of a prototype of photovoltaic greenhouse tunnel. Renewable and Sustainable Energy Reviews, 82, 1178-1186.

[10] Tang, Y., Ma, X., Li, M., Wang, Y. (2020). The effect of temperature and light on strawberry production in a solar greenhouse. Solar Energy, 195, 318-328.

[11] Official Gazette of the Republic of Turkey, 12 May 2019, number: 30772. https://www.resmigazete.gov.tr/eskiler/2019/05/20190512-1.htm [Access Date: 30.10.2022].

[12] PVsyst. (2022). Programme Interface. http://www.pvsyst.com/en/html [Access Date: 08.03.2022].

[13] EPDK, Repuclic of Turkiye Energy Market Regulatory Authority. (2022). https://www.epdk.gov.tr/Detay/Icerik/3-1327/elektrik-faturalarina-esas-tarife-tablolari.html [Access Date: 08.07.2022].

Authors: Muhammet Raşit SANCAR (iD)   Ali Kemal YAKUT (iD)

Comparative Analysis of SAM and PVsyst Simulations for a Rooftop Photovoltaic System

Muhammet Raşit SANCAR[1*,**] , Ali Kemal YAKUT [2]

[1] Isparta University of Applied Sciences, Faculty of Technology, Department of Energy Systems Engineering, Isparta, Turkey.
[2] Isparta University of Applied Sciences, Faculty of Technology, Department of Mechanical Engineering, Isparta, Turkey.

[*]Corresponding Author: d1840640001@isparta.edu.tr
[**]One of the authors, Muhammet Raşit SANCAR, is a scholarship holder of YOK 100-2000.

ABSTRACT: Turkiye is a country rich in renewable energy resources, one of which is its tremendous potential, especially in solar energy. Investments in photovoltaic systems are increasing day by day in order to evaluate this potential The simulations of these systems, which will be established while making investment plans, are very important in terms of investment return times. In this study, information and data were obtained from a working rooftop photovoltaic system and simulations were carried out using PVsyst and system advisor model (SAM) software. The simulation data was compared with the power plant's electricity generation data using statistical analysis methods of deviation, Root Mean Square Error (RMSD), and Mean Absolute Deviation (MAD). When all these analysis methods were evaluated, it was seen that the error and deviation values of the SAM software were lower on an annual basis. On the other hand, it has been determined that the error and deviation values of the PVsyst software are lower on a monthly basis.

Keywords: Rooftop photovoltaic system, SAM, Pvsyst

1. INTRODUCTION

The need for energy has been increasing daily with the developments in industry and technology. An inclination toward non-renewable energy sources has been observed when responding to this increase. Due to this tendency, the problem of global warming has intensified. In order to prevent the global warming problem and to meet the ever-rising energy demand, a rapid trend towards renewable energy sources has been taking place, and the use of many sources, such as solar energy, wind energy, and geothermal energy, has become widespread.

The utilization of solar energy is being realized with both thermal systems and photovoltaic (PV) systems. Photovoltaic systems; Today, it is seen in many areas, from open lands to rural areas away from the grid. According to the International Energy Agency (IEA) December 2021 data, the installed power capacity of photovoltaic systems worldwide is 894.3 GW, and electrical energy production from photovoltaic systems is 994 TWh/Year. For Turkey, these values are 8 GW and 12.9 TWh/Year, respectively [1]. While 240107 MW of this 8 GW

installed power belongs to the energy investments in 2020, this value has become 498050 MW for 2021 [2].

In the installation of photovoltaic systems, it is of great importance that the projecting phase is carried out in the most accurate way to ensure that the system's energy production is at the highest level. For this reason, many factors, such as the location of installation, the slope, power & orientation of the panels, and the power of the inverters, need to be analyzed. Many software with different tools has been developed to carry out these analyses, including different climate databases, shading analysis, and many other factors that would affect the quality of production result in the projection phase [3].

In a related study, simulation was done using PVSyst, SAM, and PVLib software for a 75 MWp plant in Kalkbult, Northern Cape Province of South Africa. The results obtained from all three software were compared with the production results of the facility in 2014. PVLib software was rated the best regarding modeling flexibility, followed closely by SAM software. However, when other general features and functions are considered, SAM would be the most suitable among these three software packages [4]. In another study, simulation and efficiency analysis were performed using PVsyst software for a grid-connected photovoltaic system with an annual energy production of 1109 MWh at Umm Al-Qura University. It has been verified by the PVsyst software that 1109 MWh of energy can be met by a 100 MW photovoltaic power plant [5].

In a study conducted for the International Solar Energy Institute in Tashkent, Uzbekistan, analyses of the 2.24 kW photovoltaic system connected to the grid were done using PVsyst simulation software for 2018. Eight modules with a power of 280 W and four micro-inverters with a power of 580 W were used in the system installed in the field. It was observed that the power plant produces 14.65 kW of power under the best conditions. The performance rate of the system was calculated as 79.7% in the PVsyst software, and the actual performance rate was calculated as 95.5% [6]. A study was conducted for the photovoltaic system planned to be installed in Borg El Arab, an industrial city in Egypt. The system is designed for a commercial building with a total power capacity of 1.47 MW DC. SAM and PVWatt software were used to simulate the system's electricity generation, which was created with 4608 modules and two inverters to form 18 serial modules and 256 parallel arrays [7]. Again, a PVsyst simulation study was conducted for India's Bikaner Engineering Faculty machinery department office. The annual energy demand for the Mechanical Engineering Department was determined to be 1086.24 kWh; It was calculated that the current produced energy with the solar panels is 1143.6 kWh, and the energy provided to the user due to different losses is 1068.12 kWh [8]. In another study, instead of analyzing the annual optimum inclination angle of the panels in the photovoltaic system, the monthly or seasonal optimum inclination angles were analyzed, and the effect of this scenario on energy efficiency was studied. For this, the geographical location of the University College of Science and Technology in Gaza Strip-Palestine was chosen. The System simulation was done using the Photovoltaic Geographical Information System (PVGIS) software. It was observed that the energy produced increased by 5.82% and 4.77%, respectively, when the monthly and seasonal optimum slope angles were used in the system. Results were then validated with SAM. The results obtained from the SAM were close to those obtained from the PVGIS software tool [9]. In another study, the design and performance analysis of the 700 kWp photovoltaic system connected to the grid in Daikundi city of Afghanistan was done using Pvsyst. As a result of the simulation, the system production was calculated to be 1266 MWh/year, the performance ratio as 0.797, and the system losses as 0.10 kWh/kWp/day. If the power factor is between (0.7–0.9), it is stated that the system works efficiently [10]. In another study for a photovoltaic system having different operating conditions, a grid-connected solar roof system was designed in Bhubaneswar, Odisha. With the help of SAM and Solar Edge

software, various studies such as site selection, roof selection, panel layout, and array electrical design were carried out, so the roof of the building and the total efficiency loss was calculated with design and simulation [11]. In a study for photovoltaic solar energy planned on the roof of an agricultural farm in the city of Elazig, analyses and designs were done using PVsyst software. According to the analysis results, it was observed that the system would produce 1601 MWh of energy for 10 years, reducing approximately 164,547 tons of carbon emissions. The amortization period of the photovoltaic system was calculated to be 4.6 years [12]. In another study, a hybrid photovoltaic system of a 17-digit village in India with google coordinates of 14.13°N and 75.42°E was investigated using PVsyst software. The system was designed for 3 different applications: 13.84 kWh/daylighting, 30 m³ water pumping, and a combination of both energy needs. After comparing the hybrid system with the individual systems, it was seen that a reduction of 1.32 kWp in photovoltaic capacity and a payback period of eight years resulted in a 21.87% savings in the total project cost [13].

In this study, the electricity generation data for one year for the photovoltaic sourced Solar Power Plant (SPP), located on the roof of cold storage in Elmalı district in the province of Antalya, was taken from the power plant's remote monitoring system. The plant was simulated separately in PVsyst and SAM (System Advisor Model) software. By comparing the results of the simulations and the production data with each other, the similarity rates of the programs to the actual production data were calculated. Thus, in the preliminary estimation of electricity generation data for an SPP to be established in Elmalı, one of the two different software gave production results closer to the actual production data determined, in particular, the climate data package used in the study. A study has been carried out that will guide commercial investments and academic studies of power plants of similar capacities in the district.

2. MATERIAL AND METHOD

This study was carried out in Turkey, Antalya province, Elmalı district. The actual data of the power plant for 2021 were used for the Simulation. According to the General Directorate of Meteorology data, Elmalı district has a semi-arid-semi-humid second-degree mesothermal climate type. Winters are cool, and summers are hot. The highest temperature was measured as 45 °C and the lowest temperature as -4.6 °C between 1930-2021 for the province of Antalya, where Elmalı district is affiliated. The annual average temperature is 18.8 °C, the annual highest and lowest temperatures are 24.2 °C and 13.8 °C, respectively, and the average number of rainy days is 83.5 days [14]. In Figure 1 and Figure 2, graphs showing the global radiation values and sunshine durations of the Elmalı district are given [15].
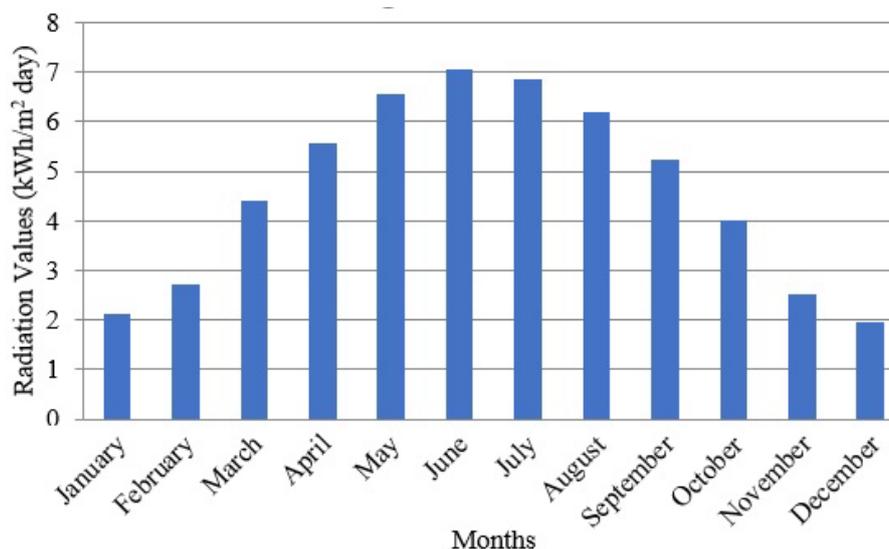
Figure 1. Global monthly radiation values graph of Elmalı district.
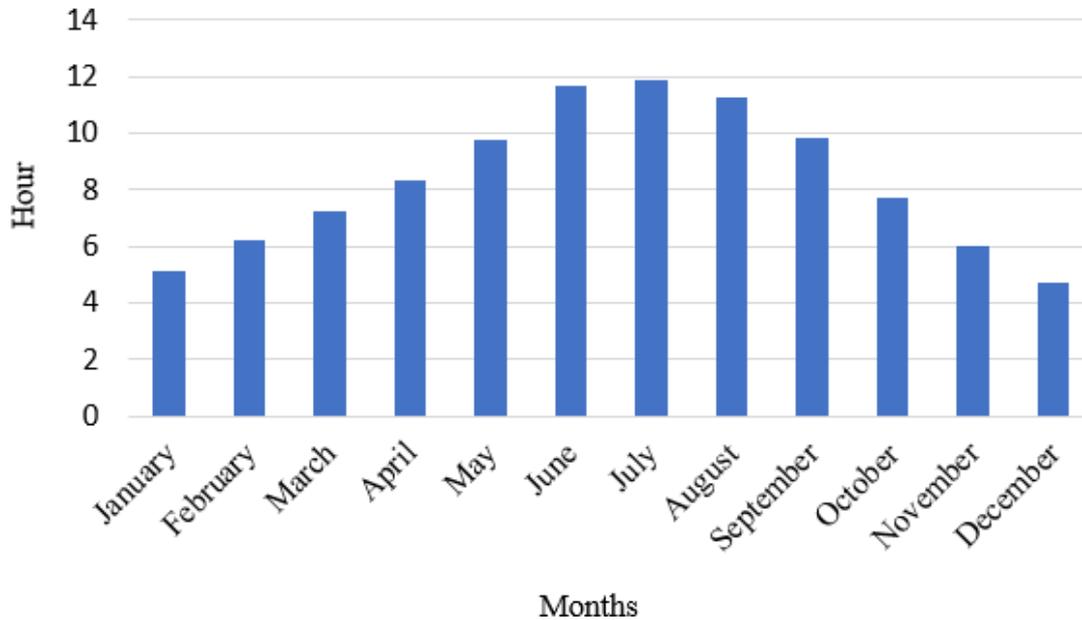
Figure 2. Sunshine duration of Elmalı district.

2.1 General Features Of The Powerplant

The study was carried out for the solar power plant installed on the roof of cold storage in the Elmalı district. The view of the power plant is presented in figure 3.

Figure 3. A picture of the power plant being studied.

The roof where the power plant is installed has 2 different orientations. Both of these orientations are inclined at 10 degrees. A total of 360 panels and 2 inverters were installed on the roof of the power plant. The characteristics of the panels and inverter are given in table 1 and table 2. The panels used in the power plant consist of 18 rows, and there are 20 panels in each row.

Table 1. Technical and mechanical properties of the panels used in the power plant

Technical Properties of the Panels	
Number of Strings in the System	18
Number of Panels in the System	20
Total Number of Panels	360
Panel Type	Monocrystal Panel
Panel Angle	East-West 10°
Maximum Power	325 Wp
Maximum Voltage Vmpp	33.68 V
Maximum Current Impp	9.65 A
Open-Circuit Voltage Voc	40.55 V
Short-Circuit Voltage Isc	10.26 A
Mechanical Properties of the Panels	
Panel dimensions	1670mm x 1000mm x 35mm
Cell	Monocrystalline
Cell number	60
Weight	18kg ± 1kg
Front Glass	3.2mm, tempered glass with high transmittance and low iron content
Back Protection	Polyester PET Film
Frame	Anodized Aluminium
Junction Box	3 Bypass Diode
Connector	MC4 Compatible

Table 2. Technical specifications of the inverter used in the plant

Technical Properties of the Inverter Used in Elmali Power Plant	
Number of Inverters Used	2
Number of Series per Inverter	9
Rated Power of Inverter	50 kW
Maximum Input Voltage DC	1000 V
Starting Voltage DC	420 V
MPTT Starting Voltage Range DC	480-800 V
MPTT Number	3
Maximum Input Current	108 A
Maximum Short Circuit current	165 A
Nominal Output Power AC	50 kW
Maximum Output Power AC	55 kW
AC Voltage	400 / 230 V
Maximum Current Flow AC	80 A
Frequency	50Hz/ 60Hz

In the study, the power plant project was examined, and simulations were carried out using PVsyst and SAM programs in accordance with reality. In the simulation studies, the climatic data package of the NSRDB resource in the climate interface of the SAM program was used. Some data on climatic characteristics are given in Table 3.

Table 3. Climatic data sourced from NSRDB

	Global Radiation (kWh/m^2)	Diffuse Radiation (kWh/m^2)	Average Temp (°C)	Wind Speed (m/s)
January	65.9	26.97	1.51	1.8
February	100.3	33.36	4.38	1.5
March	137.9	46.23	7.74	1.8
April	181.4	57.69	11.14	1.6
May	196.2	75.21	15.68	1.6
June	224.2	59.36	21.95	1.5
July	254.8	49.22	26.7	1.8
August	199.8	57.09	25.36	1.5
September	187.3	39.96	23.1	1.6
October	136.3	30.25	14.66	1.6
November	88.3	26.55	9.04	1.4
December	61.6	23.27	6.78	1.6
Total	1833.9	525.16	14.06	1.6

The panels in the power plant have 2 different azimuth angles since the roof has two different orientations. The azimuth values are 53° and -127° for the PVsyst program, 53° and 307° for the SAM program, and the panel slope is 10°, the same as the roof slope. The numbers and total powers of the panel group with each azimuth angle in the power plant are equal to each other. Panel groups with different orientations in this power plant are connected to different inverters. By comparing the simulation results with the plant data, deviation rates from the plant data were calculated. Simulation steps are presented under separate headings for the software used.

2.2 Procedure of Simulation

In this study, PVsyst software version 7.2.12 was used. PVsyst is a computer software package for inspecting, sizing, and data analysis of PV systems. It deals with grid-connected, off-grid, photovoltaic systems involving the use of pumps. In the analyses done, it includes a very comprehensive background on meteorological data and photovoltaic system component data. This software is very useful in both industry and education. The interface of the software is presented in Figure 4 [16].
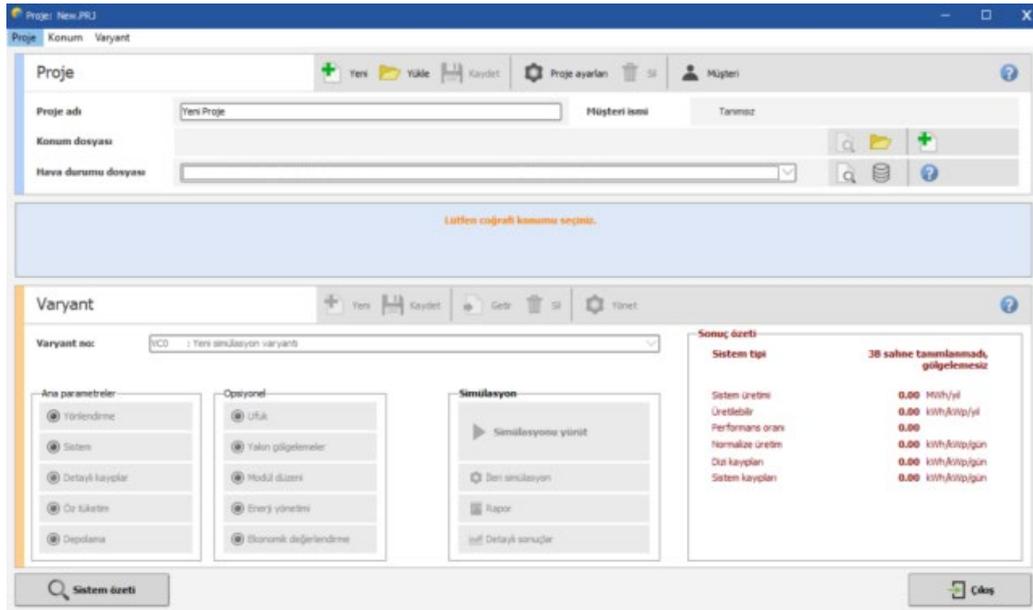
Figure 4. The interface of PVsyst software

Since the power plant where the study was carried out is a system connected to the grid, the "Grid-Connected" system option and then the location of the power plant were selected in the "Project design and simulation" section. Since the same climate data should be used for both software after location selection, the climate data selection process was performed using the import option in PVsyst software of NRSDB climate data from the SAM software repository. In the software, the azimuth angle Azimuth values and the current inclination angle of the panel are entered under the orientation button, and the panel orientation number is defined as two. Then, by entering the system button interface, the panel and inverter options used in the switchboard were selected from the system database, and the serial and parallel connection numbers and shapes of the panels in the power plant were defined here, and the simulation was completed. The process flow chart for this study is presented in Figure 5.
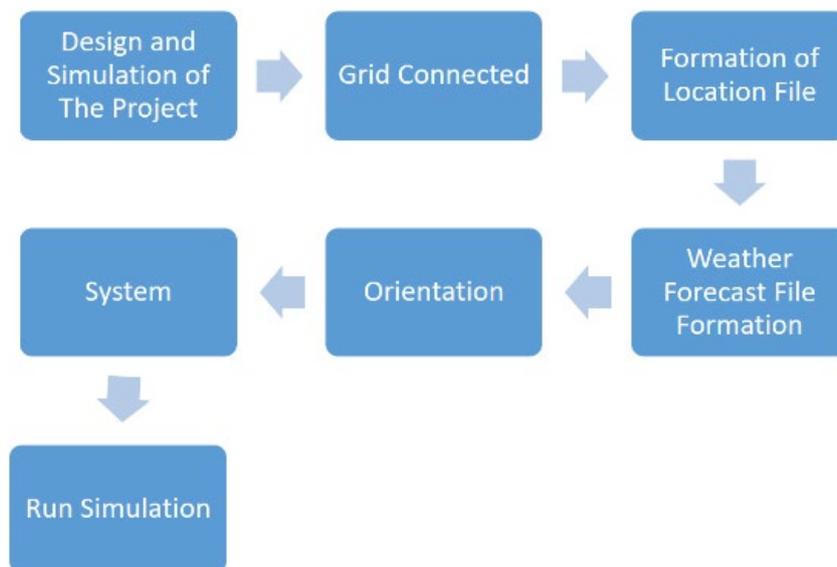
Figure 5. Process flow chart of PVsyst software.

2.3. Simulation Procedure in SAM

SAM software has a wide range of educational and sectoral uses by offering different renewable energy systems simulations and energy storage simulations. This study was carried out using SAM version 2021.12.2. The software interface is presented in figure 6 [17].
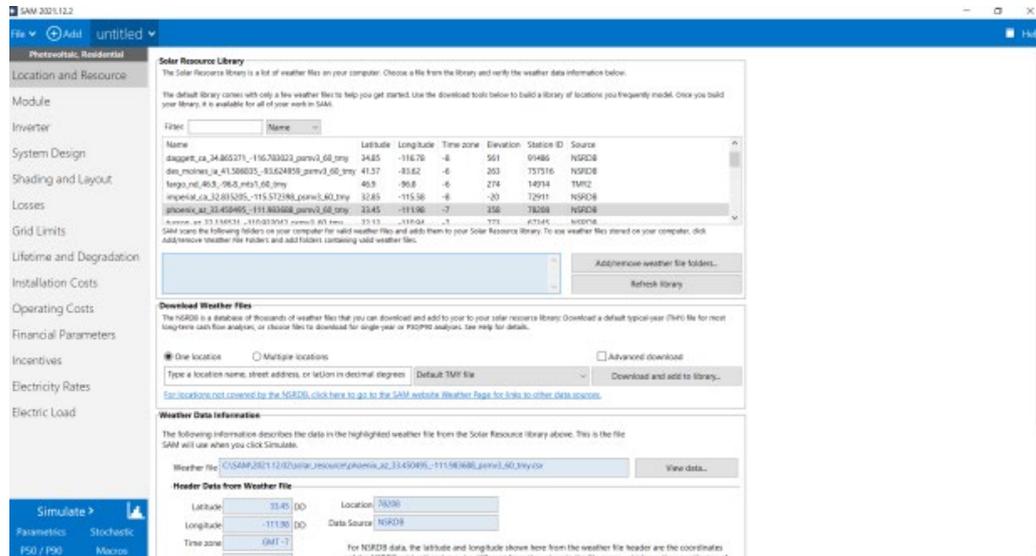
Figure 6. SAM software interface

After selecting the file button in the software interface, the new project option was selected, and then the photovoltaic section was entered. A detailed PV model option was selected under the Photovoltaic option, and a grid-connected option was selected since the current plant is a grid-connected system. The project interface was switched over to the individual user interface. The location determination process, the first step of project simulation, was carried out by entering the coordinates of the power plant into the system. The data from the NSRDB climate data catalog were drawn and defined in the system for simulation. After this stage, the panel and inverter data used in the power plant are entered into the program, and the panel and inverter steps are completed. Under the system design button, 2 different orientations were selected, and azimuth angles, panel angles, and the number of inverters were processed. Features such as the number of panels in an array and the number of arrays were entered into the software. The simulation is completed by performing all these operations. The process flow chart of the simulation is presented in Figure 7.
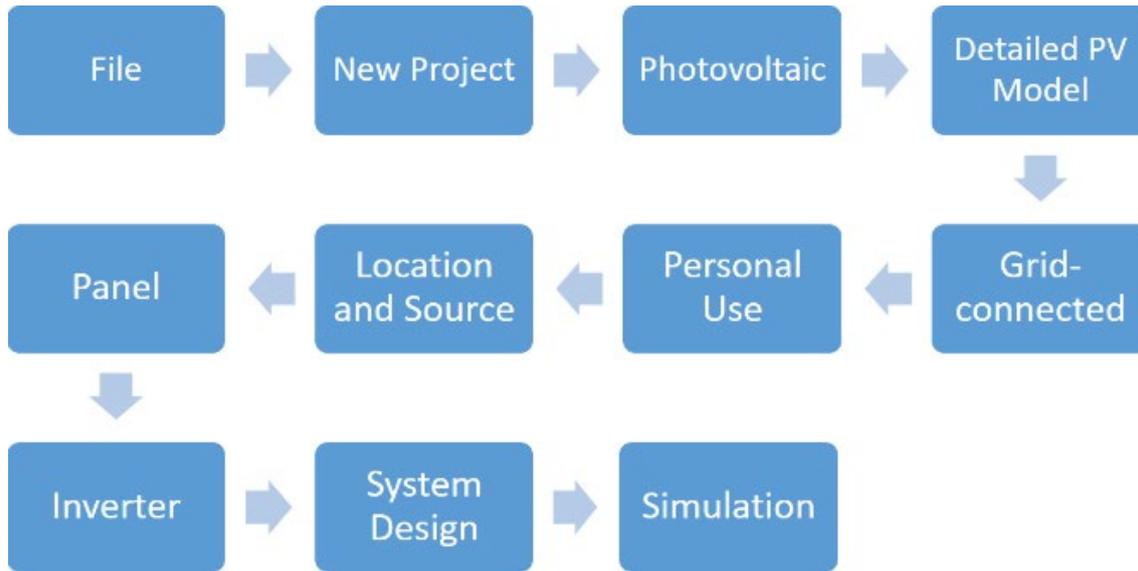
Figure 7. SAM software process flow chart.

2.4. Statistical Analysis

As a result of the simulation studies, one-year data was taken, and these data were compared with the real data and with each other on a monthly and annual basis. Several comparison parameters are used to facilitate the calculation of the deviation between each software and to obtain a reliable comparison. Using Equation 1, monthly and annual deviation rates were calculated. In addition to the annual deviation between the software, the RMSD (Root Mean Square Error) given in equation 2 and the MAD (mean absolute deviation) analysis methods given in equation 3 were also used.

$$\% \, DEVIATION = \frac{D_g - D_s}{D_g} \times 100 \qquad (1)$$

In Equation 1, D_g represents the actual value for the corresponding month. The D_s value represents the value of the same month for one of the simulation programs used.

$$RMSD = \sqrt{\frac{1}{n} \sum_{t=1} (G_t - S_t)} \qquad (2)$$

$$MAD = \frac{1}{n} \sum_{t=1} |G_t - S_t| \qquad (3)$$

In Equations 2 and 3, the "n" value represents the total number of months in a year, and "G_t" and "S_t" represent the actual production value of the month for which the calculation is made and the value belonging to the simulation, respectively. In this study, the most commonly used analysis methods in the literature were preferred.

3. RESEARCH FINDINGS AND DISCUSSION

The monthly and annual electricity production values obtained from the simulations using the PVsyst and SAM program were compared with the actual values taken from the power plant on a monthly and annual basis. The comparison of PVsyst, SAM, and power plant electricity generation data is presented graphically in Figure 8. It has been calculated that October is the month in which the PVsyst data and the power plant data are closest to each other, and there is an electricity generation difference of approximately 73 kWh between the two data. The month

68

in which the largest difference between the two data was observed was June. This month's difference between the two data was calculated as 3630 kWh. It was calculated that the plant data is closest to each other with the generation data obtained from the SAM software and that there is an electricity generation value difference of approximately 947 kWh between the two data. It was calculated that the most significant difference between the data occurred in June, and the difference between the two data in this month was 4530 kWh. When examined in general, it has been calculated that the electricity generation values obtained from the PVsyst and SAM software in April are very close to each other. There is an electricity generation difference of 79 kWh. In July and November, it was calculated that the electricity generation difference between the software was the highest, and this difference was obtained as 1180 kWh.
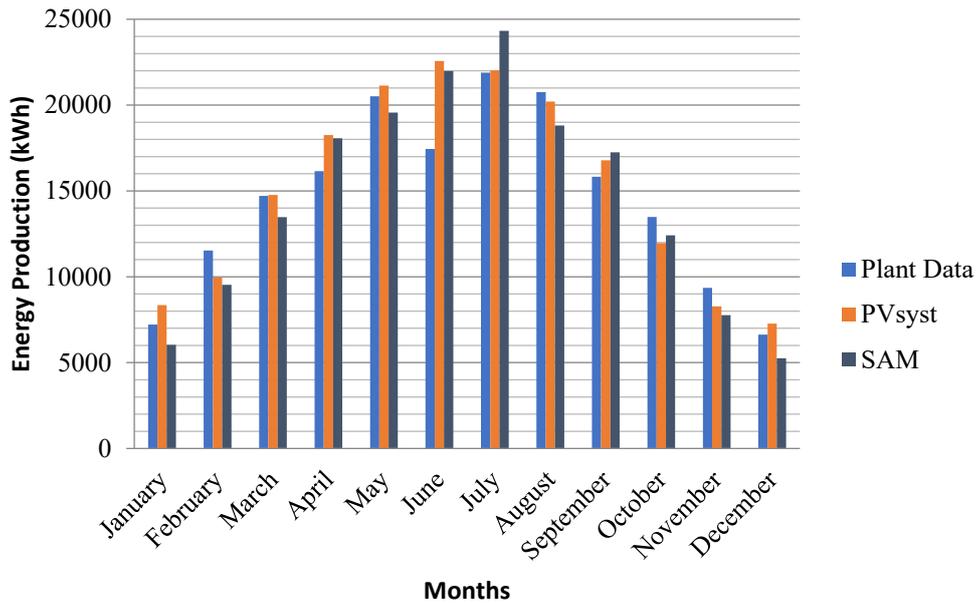
Figure 8. Monthly PVsyst-SAM and power plant data graph

The annual total electricity production values of the software and the total annual electricity production of the plant are presented in Figure 9. The annual total electricity production of the power plant was 175515 kWh. As a result of the simulation made with the SAM software, the electricity production was 174481 kWh, and as a result of the PVsyst simulation, the electricity production was 177750 kWh.
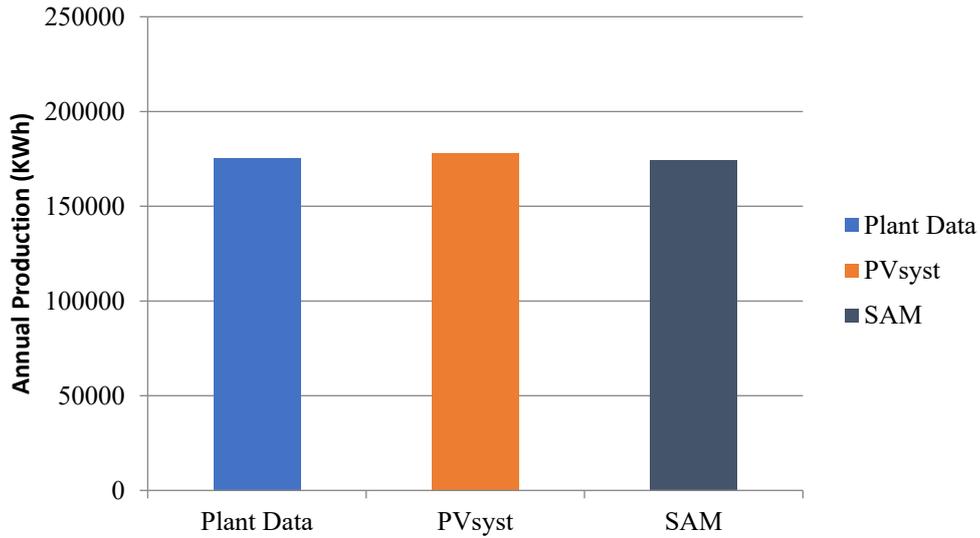
Figure 9. Annual production values of PVsyst, SAM, and plant data.

When the data obtained from the PVsyst software are evaluated, the monthly deviation rates from the plant values are given in Figure 10. When the rates are evaluated, the deviation rates are approximately 4% in January, March, and November, 6% in May, July, and December, 9% in February, 11% in August and September, 12% in April, 21% in June and 0.5% for October.
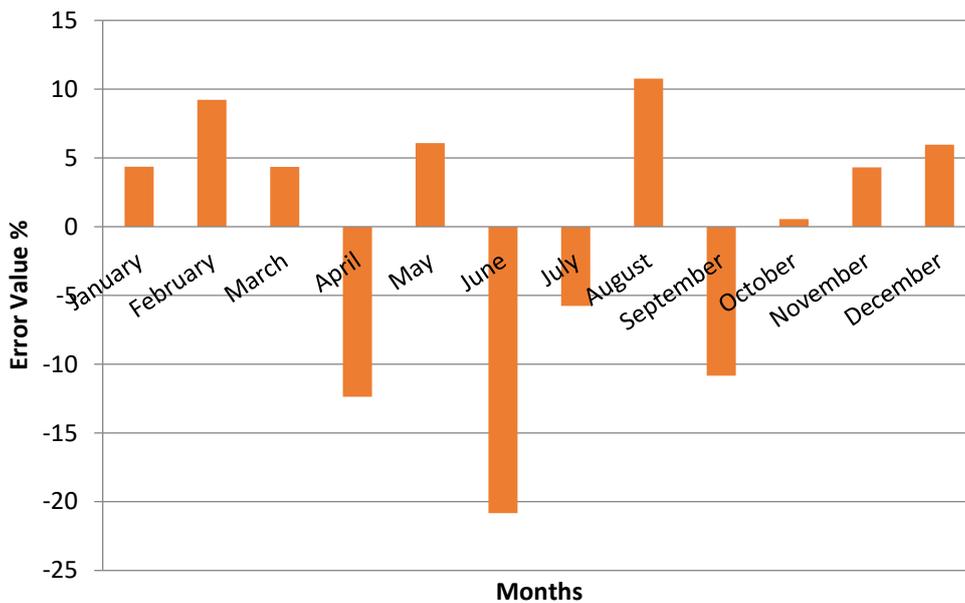
Figure 10. Monthly deviation rate of PVsyst software according to plant values.

When the data obtained from SAM is evaluated, monthly deviation rates from the central values are given in figure 11. When the rates are evaluated, the deviation rates are approximately 4% in May, 8% in March and October, 9% in August and September, 11.5% in April and July, 16.5% in January and November, 17.5% in February, 21% for December and 26% for June.
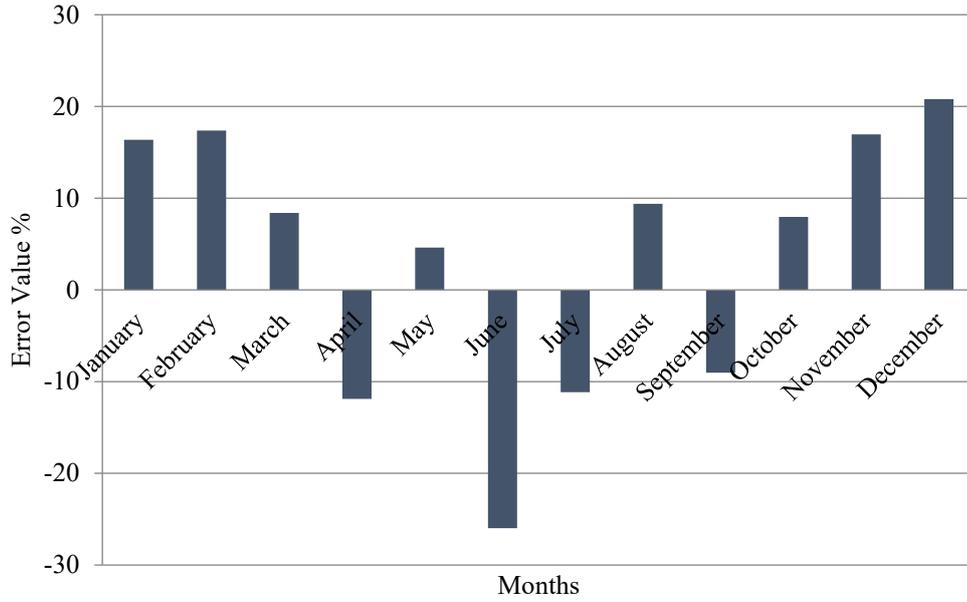
Figure 11. Monthly deviation rate of SAM software according to central values.

The loss diagram of the simulation performed in the PVsyst software is presented in Figure 12. Here, it is seen that the losses occur primarily at the nominal string energy and the total loss rate is approximately 20%. When the losses are subtracted, it is calculated that the net energy value produced is approximately 177.7 MWh.
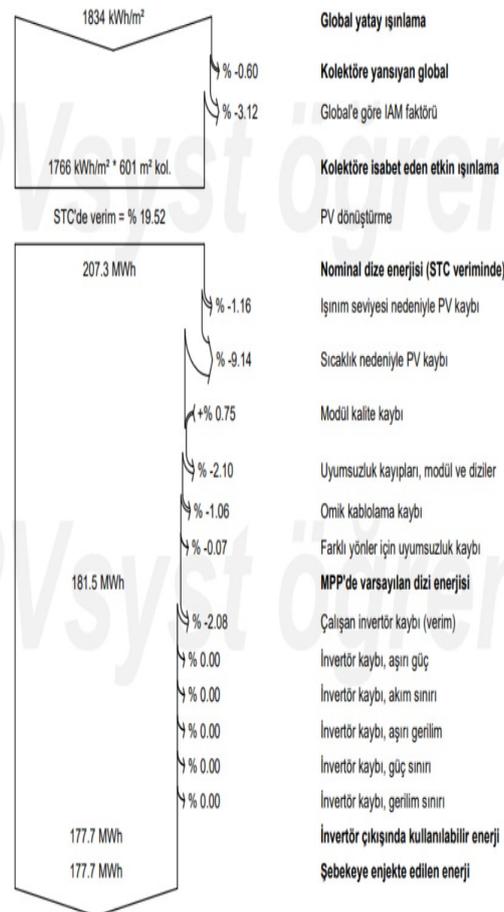
Figure 12. Loss diagram for PVsyst software

The loss diagram of the simulation performed in the SAM software is presented in Figure 13. It is seen that the total loss rate is approximately 15%, the electrical energy value given to the grid is calculated as 174.5 MWh and there are losses especially in the nominal radiation value coming to the panel surface.
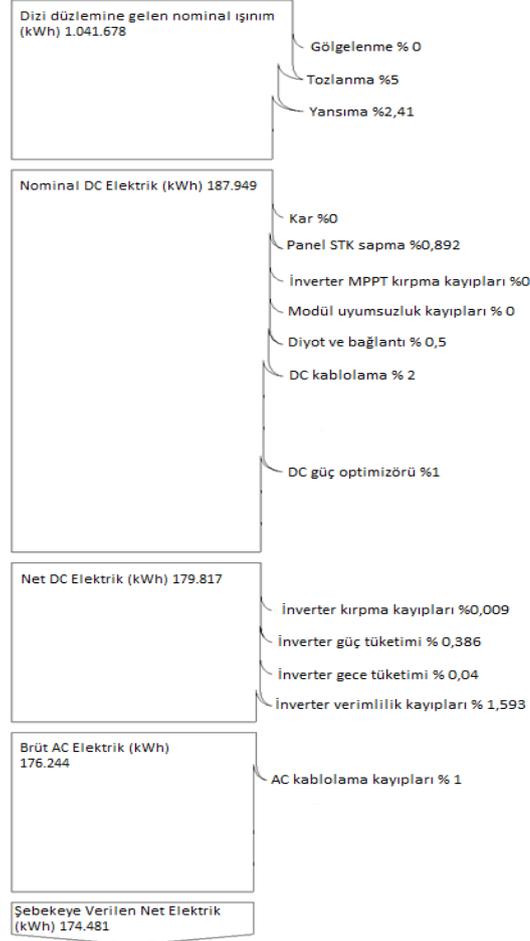
Figure 13. Loss diagram for SAM software

Figure 14 shows the data of the RMSD analysis method of the PVsyst and SAM. Here, it is seen from the plant data that the error values are lower for the SAM in April, May, and August, and the PVsyst has fewer error values in all other months. The annual deviation value was calculated as 298.69 for SAM and 644.94 for PVsyst.
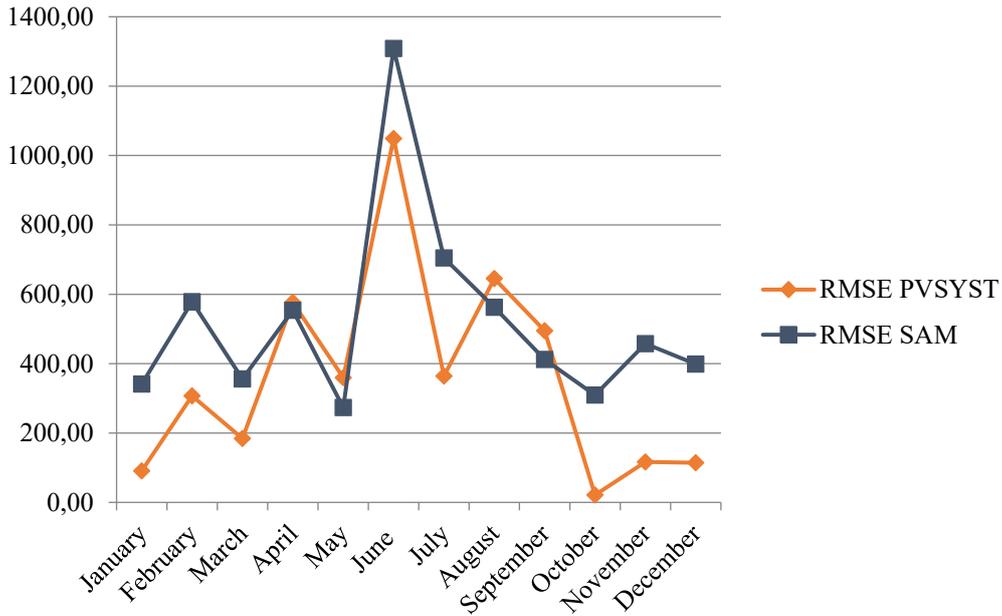
Figure 14. RSME results against actual production values for PVsyst and SAM simulations.

Figure 15 shows the data of the MAD analysis method of SAM and PVsyst. Here, it is seen that the deviation values from the plant data are lower for the SAM software in April, May, August, and September, and the PVsyst has fewer deviation values in all other months. The annual deviation value was calculated as 86.23 for SAM and 186.18 for PVsyst.
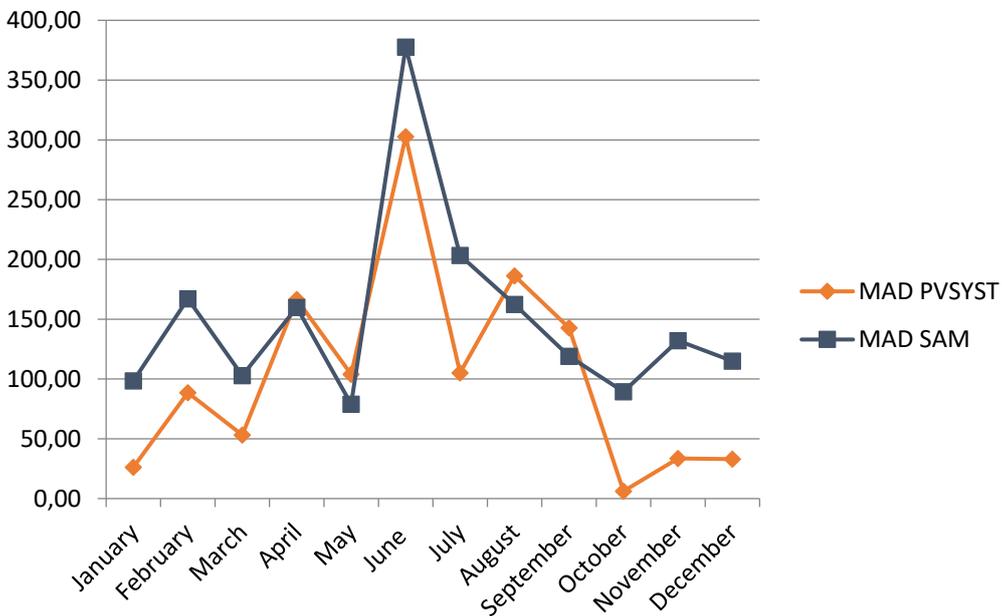
Figure 15. OMS(MAD) results against actual production values for PVsyst and SAM simulations

4. CONCLUSIONS AND RECOMMENDATIONS

In recent years, there has been a great increase in energy demand, and the incapacity to respond to this surge in demand has caused a large supply deficit. Thus, there has been a significant increase in energy prices globally. At this point, foreign energy-dependent countries such as Turkey are more affected by energy price hikes. This increase becomes much more noticeable with the fluctuations in foreign exchange rates. In terms of climate change and the use of domestic resources, the trend towards electricity generation has gained momentum in recent years, especially by the discovery of renewable energy sources in our country. Solar energy, one of the renewable energy sources, is more favored in terms of investment, especially since its maintenance costs are not high and the initial investment costs are low compared to other renewable energy systems. It is very important to estimate the electricity production values in solar power plants since the return rates of the investments are a very important part of the investments made. In this study, SAM and PVsyst, which are software with a very common usage area in academia and commercial, were used especially in simulations of electricity generation in solar power plants. At the point of electricity generation from solar energy of these two software, error and deviation rates were calculated by using statistical analysis methods. Thus, if the related climate data package is used, a prediction about electricity production estimation for the investments to be made at the specified location and nearby installed powers is provided. Which one of the two software could have the lower error and deviation rates from the actual production on an annual or monthly basis was determined as they were compared with each other. As a result of the comparison, it was calculated that the deviation rate of the SAM software data is 0.59%, and the deviation rate of the PVsyst software data is 1.27% annually. When the analysis using the RMSD method was examined, it was seen that the annual error value was 298.69 for the SAM software and 644.94 for the PVsyst software, and the SAM software reached higher error values in all months except 3 months. In the MAD analysis, it was determined that the annual deviation values were 86.23 for the SAM software and 186.18 for the PVsyst software, and the deviation value of the SAM software was lower in only 4 months of the year. Evaluating the deviation rates on an annual basis and using the specified climate data showed that the deviation and error values of the SAM software were lower on an annual basis compared to all the analysis methods given in the study. When evaluated monthly, it was determined that the deviation and error rates of the electricity generation data of the PVsyst software were lower than all analysis methods. In addition, when losses were evaluated, it was determined that the loss rates for the two software were different. In light of all these data and the results that will be taken into account during the simulations of the power plants to be established, it is recommended to use the SAM software in annual evaluations since it gives results closer to the real electricity production when evaluated on an annual basis, and PVsyst software in monthly evaluations, since it gives more accurate results monthly. The location of the region which could produce the highest amount of electricity & the lowest return of investment periods for the power plant, which is planned due to the low deviation in the region, can now be calculated thanks to the study which was carried out with the software specified above. Similar simulations for solar power plants installed in other regions of our country can be carried out with the help of different software and by determining the deviation rates in the simulations, which gives more accurate results in which region can be determined.

5. ACKNOWLEDGEMENTS

Conflict of Interest

No conflict of interest was declared by the authors.

REFERENCES

[1]   IEA, International Energy Agency. (2021). "Renewable Electricity". https://www.iea.org/reports/renewables-2021/renewable-electricity. [Access Date: 04.03.2021].

[2]   EIGM, General Directorate of Energy Affairs. (2022). Turkish Electricity Investments January 2022 Summary Report. https://enerji.gov.tr/eigm-raporlari [Access Date: 20.02.2022].

[3]   Silva, J. L. D. S., Costa, T. S., Melo, K. B., Sako, E. Y., Moreira H. S., Villalva, M. G. (2020). A Comparative Performance of PV Power Simulation Software with an Installed PV Plant. IEEE International Conference on Industrial Technology (ICIT).

[4]   Gurupira T., Rix, A. J., (2017). PV Simulation Software Comparisons: PVsyst, NREL SAM and PVlib. Southern African Universities Power Engineering Conference (SAUPEC).

[5]   Alnoosani, A., Oreijah, M., Alhazmi, M. W., Samkari, Y. (2019). Design of 100MW Solar PV on-Grid Connected Power Plant Using (PVsyst) in Umm Al-Qura University. International Journal of Science and Research, 8, 356-363.

[6]   Matchanov, N. A., Seok, K. O., Mirzaev, A. A., Malikov M. A., Saidov, D. S. (2020). Study of Energy Yield on Grid Connected Micro-Inverter Type 2.24 kW PV System Using PVsyst Simulation Software. Applied Solar Energy, 56, 263-269.

[7]   Darwish, M. A. A. (2021). Design of a photovoltaic system using SAM and ETAP software. 2021 International Conference on Green Energy, Computing and Sustainable Technology (GECOST).

[8]   Kumar, R., Rajoria, C. S., Sharma A., Suhag, S. (2021). Design and simulation of standalone solar PV system using PVsyst Software: A case study. Materials Today: Proceedings, 46, 5322-5328.

[9]   Dabbousa, T. A., Al-Reqeb, I., Mansour S., Zainuri, M. A. A. M. (2021). The Effect of Tilting a PV Array by Monthly or Seasonal Optimal Tilt Angles on Energy Yield of a Solar PV System. International Conference on Electric Power Engineering.

[10]   Baqir, M., Channi, H. K. (2022). Analysis and design of solar PV system using Pvsyst software. Materials Today: Procedings, 48, 1332-1338.

[11]   Rout, K. C., Kulkarni, P. S. (2021). Design and Analysis of Grid-Tied Rooftop Solar PV System at Bhubaneswar, Odisha Using SAM. International Conference on Intelligent Technologies.

[12]   Doğan Y., Korkmaz, M. (2021). Application And Economic Contribution Of The Solar Energy System In Agricultural Plants: Using PVsyst Software. Engineering Sciences, 16, 89-96.

[13]   Muralidhar, K., Rajasekar, N. (2021). Soiling and Shading Analysis of Hybrid PV System for Rural Application using PVsyst Software. 2021 Innovations in Power and Advanced Computing Technologies (i-PACT).

[14]   MGM, Republic of Turkey General Directorate of Meteorology. (2022). Climate Data.

https://www.mgm.gov.tr/iklim/iklim-siniflandirmalari [Access Date: 24.03.2022].

[15]   Republic of Turkey Ministry of Energy and Natural Resources General Directorate of Energy Affairs. (2020). Turkey Solar Energy Potential Antalya Data. https://gepa.enerji.gov.tr/MyCalculator/pages/7.aspx [Access Date: 24.03.2020].

[16]   PVsyst. (2022). Programme Interface. https://www.pvsyst.com/. [Access Date: 31.03.2022].

[17]   SAM, System Advisor Model. (2022). Programme Interface. https://sam.nrel.gov/. [Access Date: 31.03.2022].

Research Article

BROAD PHASE RESPONSE UNIT CELL AND HIGH GAIN REFLECARRAY ANTENNA DESIGN WITH CIRCLE-MINKOWSKI STRUCTURES

Authors: Bülent Urul (iD)

International Journal of Engineering and Innovative Research

http://dergipark.gov.tr/ijeir

BROAD PHASE RESPONSE UNIT CELL AND HIGH GAIN REFLECARRAY ANTENNA DESIGN WITH CIRCLE-MINKOWSKI STRUCTURES

Bülent Urul[1]*

[1]Isparta Applied Sciences University, Vocational School of Technical Science, Electronics and Automation Department, Isparta, Turkey.

*Corresponding Author: bulenturul@isparta.edu.tr

ABSTRACT: In this study, it is aimed to increase the phase responses of the obtained unit cells by using the fractal structures nested together. Then, the effect of these obtained broad phase-response unit cells on the antenna gain is examined by using them as reflective elements on the reflect array antenna. For this purpose, 3 different structures are designed: the circle, the Minkowski used in the circle, and the unit cells obtained by rotating the Minkowski structure in the circle. The phase response of the first designed circle structure could not meet the phase requirement for a whole band, and a phase response of 280° is obtained. Then, in the second stage, the Minkowski structure is designed in the designed circle, and a phase response of 329° is obtained in this structure. Finally, a structure sufficient for the entire phase response is obtained by rotating the Minkowski structure in the circle between $0^o - 30^o$. A unit cell with a wide phase response and a 11.7 dBi horn antenna and reflect array antenna are designed. The gain of the designed reflect array antenna has increased by 91% compared to the horn antenna and has been obtained as 22.4 dBi. With this result, it has been revealed that the phase response can be increased by using fractal structures together and especially by rotating the structures, and with this method, high-gain reflect array antennas with broadband phase response can be designed.

Keywords: Fractal structures, Reflect array antenna, Antenna gain.

1. INTRODUCTION

Reflect array antennas (RAA) are antenna structures that significantly demonstrate effectiveness in communication technologies, wireless communication systems and satellite communications. These structures basically consist of a horn antenna as a feed antenna and multiple reflective microstrip structures placed on a flat ground. As it is known, microstrip antennas are highly preferred by engineers and researchers due to their low cost, easy production, thin and planar production capabilities, and so they are the subject of many studies[1-3]. Likewise, horn antennas are antennas with high directivity and wide bandwidth. RAA which can normally be produced as parabolic, can be produced in a thin planar way by combining these superior properties of horn and microstrip antennas.

Fractal structures such as Penta, Koch-triangle, and Minkowski are frequently used as reflective unit cells used in RAA. Fractal geometries are characterized by the use of the same geometry in a certain ratio of small and large versions. That is, a particular shape is scaled and repeated several times to create the fractal structure used. When creating fractal structures, the fractal

shape is derived in an iterative procedure based on the scaling factor of an initial shape, the fractal generator, the size of the shape to scale, and the number of iterations. The application of fractal geometries to conventional antennas increases the antenna performance, thus reducing the overall size of the structure used [4-6]. Because of these properties of fractal structures, it is often preferred in the design of reflective array antennas and phased array antennas.

However, bandwidth limitation is a major problem in design of RAA, which is due to the narrow bandwidth of the radiating elements themselves. Various methods have been suggested in the literature to increase the bandwidth of the radiating elements, such as using patch elements of different structure. Single-layer wideband reflect arrays have been studied by using multi-resonant radiating elements. Efforts have also been made to improve bandwidth using single-layer broadband reflector arrays, multi-resonant radiation elements, or using sub-wavelength elements. With these applications, the bandwidth can be increased even in single-layer structures [7-13].

The working principle of RAAs is to reflect the incoming wave from the surface of the reflective array elements and direct it to a desired point. Sometimes the source is placed in the center directly opposite the reflective antenna, and sometimes it can be placed as an offset. The biggest advantage of reflective array antennas over normal reflective antennas is that they can be placed on a flat surface. Therefore, it has the advantage of easy production [14,15]. However, in order to reflect the incoming beam to the desired point, it must first be determined how much reflection phase is required at which point on the antenna. The patch reflective elements then need to be placed on the planar antenna surface. By changing the values of each element placed on the surface, such as size, shape, angle of rotate, the reflection phase values required by each point on the antenna are obtained. This process is called phase compensation process[16,17].

In this article, first a circular reflector is designed as a reflector array element, and then the Circle-Minkowski shape obtained by removing the Minkowski shape, which is a fractal structure, from the circle by etching is designed. The Minkowski fractal reflective array cell is used by many researchers in their work. While the patch size is sometimes properly kept constant during the design phase, the reflection phase control is accomplished by varying the scaling factor n. In our study, the phase compensation of the Minkowski cell was achieved by changing the scaling ratio n and accordingly the patch size t and the indentation value s. In addition, the effect of the circle used on the reflection phase was evaluated. As a result of all the operations, unit cell size values that can provide the phase requirements at all points of the RAA have been found. Finally, the RAA gain values obtained after appropriate phase compensation are obtained.

2. METHODOLOGY

2.1. Reflective unit cell designs

2.1.1. Circular unit cell design

In this part, 3 different designs are being made with 11GHz center frequency. The first design is only in the form of a circle, as seen in Figure 1. All studies are designed and simulated with the help of CST electromagnetic simulation program. For the simulation setup in the simulation program, open (add space) is selected for all axes as boundary conditions. In addition, the number of cells for each wavelength is 10, the accuracy is -60 dB.
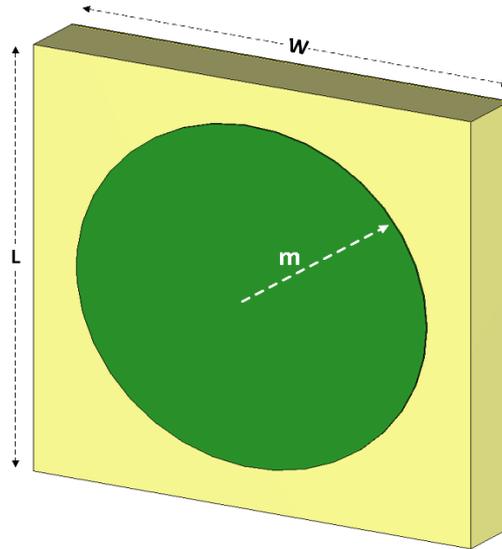
Figure 1. Circle reflective unit cell

Here, Taconic RF-35 (lossy) substrate is preferred as substrate. The loss tangent of the substrate is 0.0018 for the 11 GHz frequency and its electrical permeability is 3. In order to maximize reflection, the ground layer is covered with copper. The patch used on the substrate is preferred as copper. The radius of the circle structure used varies in the range of 2-5 mm. Circle unit cell parameters are given in Table 1.

Table 1. Circle unit cell design parameters

Parameters	Unit (mm)
m	Between 2-4.8
Substrate length (L)	10
Substrate width (W)	12
Substrate thickness	1.5
Copper thickness	0,035

After the design process, the circular reflective unit cell is simulated by the electromagnetic simulation program and the phase correspondence values according to the circle radius are obtained as shown in Figure 2.
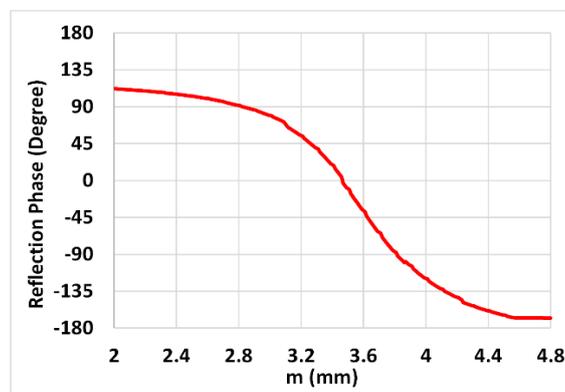
Figure 2. Phase response plot corresponding to m for a circle reflective unit cell

When the graph in Figure 2 is examined, it is seen that the reflection phase angle values corresponding to the m value vary between 112° and -168° and a total phase response of 280° can be obtained.

2.1.2. Circle-Minkowski unit cell design (Without rotation)

In the second reflective unit cell design, as seen in Figure 3, the Minkowski structure is extracted from the circle shape by etching.
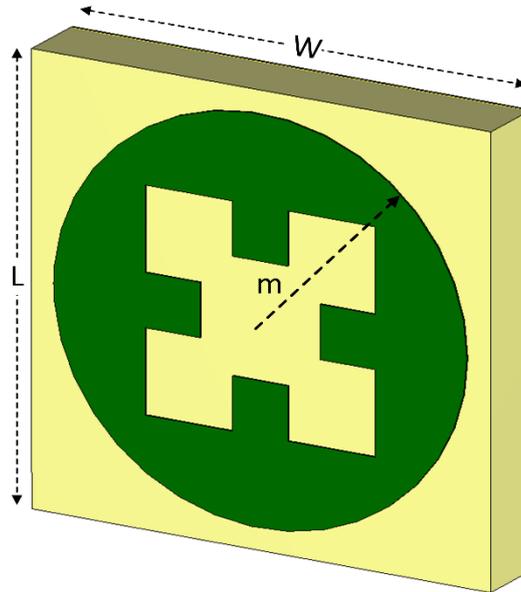
Figure 3. Unit cell with Minkowski structure etched from the circle

In Figure 3, the unit cell structure with the Minkowski structure etched from the circle is seen. In this design, the change of the reflection phase angle is examined by keeping the basic parameters constant and changing the parameters of the circle and Minkowski structures.

The shape parameters of the Minkowski structure are shown in Figure 4. There are 3 different cases for m, t and s values. Two of these parameters should be kept constant, one should be changed, 3 different simulation processes should be performed and phase responses should be evaluated. Accordingly, firstly, the unit cell is simulated by keeping the shape parameters of the Minkowski structure, t and s constant, and changing the circle radius (m). But here, in order that the radius of the circle is not smaller than the Minkowski shape, the dimensions of the Minkowski structure should be as small as possible and the chosen circle radius should be chosen in accordance with the Minkowski dimensions. Accordingly, the relation given in Equation 1 between the indentation s and the width t, used on the Minkowski structure, is taken into account. The value of n is preferred in the range of 0 to 1. Accordingly, t = 2 mm in Figures 3 and 4 is kept constant at s = 0.53mm (n=0.8) and the graph in Figure 5 is obtained by changing the circle radius between 2-4.8mm.

$$n = \frac{s}{t/3} \qquad 0 \leq n \leq 1 \tag{1}$$
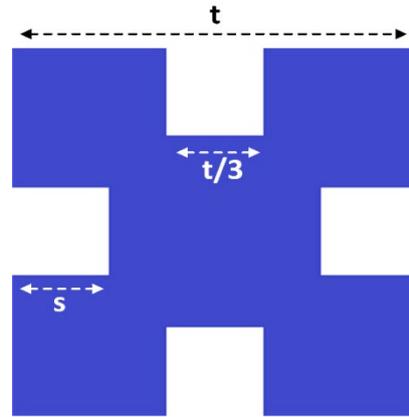
Figure 4. Minkowski structure
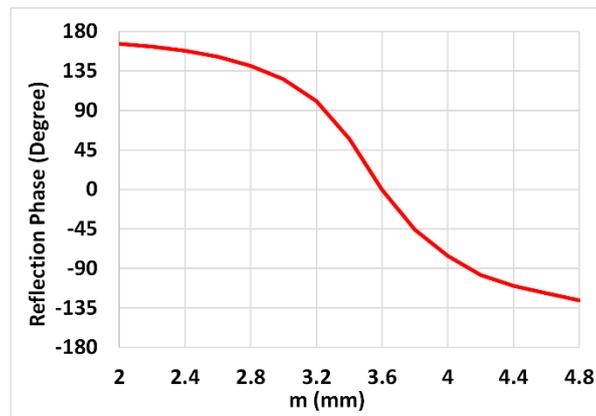
Figure 5. Phase response plot corresponding to m value for Circle-Minkowski reflective unit cell (m=2-4.8 mm, t=2 mm, s=0.53mm)

When Figure 5 is examined, when the circle radius m value increases for the Circle-Minkowski structure, the reflection phase value decreases, and on the other hand, a phase response of 294° between $+126^o$ and -168° is obtained for all angle values. appears to be unavailable.

In the second case, the effect of changing the t minkowski width on the reflection phase value is examined by keeping the m value, which is the circle radius, and the s minkowski indentation value constant. Accordingly, the unit cell is simulated according to the change of t value by keeping it constant at m = 4.5 mm and s=0.53 mm (n = 0.8 mm) and Figure 6 is obtained.
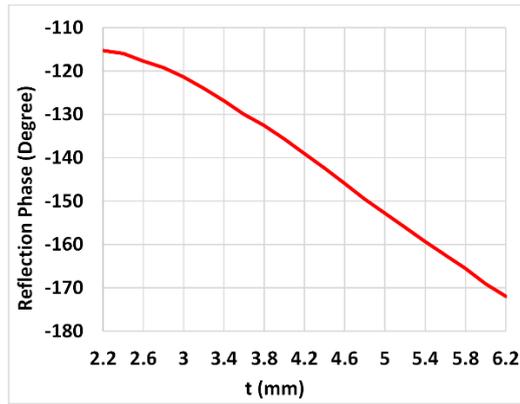
Figure 6. Phase response plot corresponding to the m value for the Circle-Minkowski reflective unit cell (m=4.5 mm, t=2.2-6.2 mm, s=0.53 mm)

When Figure 6 is examined, it can be seen from the graph that a phase equivalent can be obtained between about -115° and -172°, and the reflection phase value decreases as the t value increases.

In the third case, the effect of changing the s value, which is the indentation size, on the phase response is examined by keeping the m and t values constant. The unit cell is simulated by keeping m = 4.5 mm and t = 3 mm constant and changing the s value in the range of 0.05-0.85 mm. Accordingly, the graph in Figure 7 is obtained.
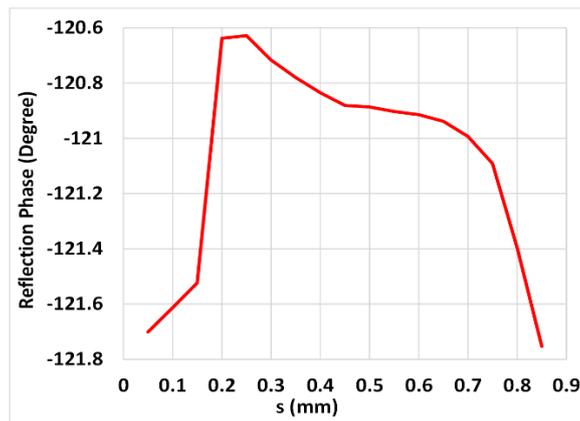
Figure 7. Phase response plot corresponding to m value for Circle-Minkowski reflective unit cell (m=4.5 mm, t=2-6.2 mm, s=0.53mm)

When Figure 7 is examined, it is seen that there are very small irregular changes in the phase value, and the phase angle varies between $-120,62^o$ and $-121,7^o$. Accordingly, it can be said that the s indentation value has a very small effect on the phase angle. According to all these data, the common usage and changes of m, t and s values and the unit cell given in Figure 3 are simulated according to the simulation parameters given in Table 2.

Table 2. Circle-Minkowski structure design parameters

Parameters (mm)		
m	**t**	**s**
4.8-4.5	6.2-2.0	0.05-0.85
4.4-4.0	5.5-2.0	0.05-0.85
3.9-3.2	4.4-2.0	0.05-0.85
3.1-2.3	3.2-2.0	0.05-0.85

While preparing Table 2, it should be taken into account that the value of m cannot be less than the value of t. The simulation process was performed according to these parameters and Figure 8 is obtained. In addition, since the phase response will depend on the m, t and s values at the same time, Figure 8 is given as the phase response graph corresponding to the simulation number.
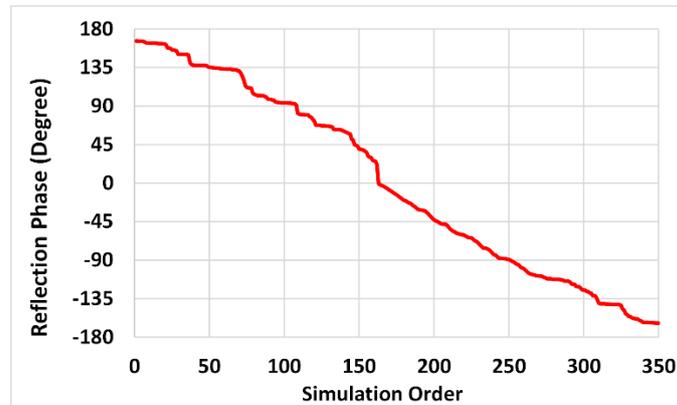
Figure 8. Phase response plot for Circle-Minkowski reflective unit cell

When Figure 8 is examined, it is seen that the phase response varies between $+166^o$ and -163° and there is a phase gap of 31° where no phase response can be obtained. Therefore, this means that there are points on the substrate where phase response cannot be obtained while designing the reflective array.

2.1.3. Circle-Minkowski unit cell design (With rotation)

The third step in the design of the reflective unit cell is to simulate the circle-Minkowski structure by rotating it between 0°-30° as seen in Figure 9. The simulation parameters are the same as in the previous step and the simulation process was performed by only rotating.
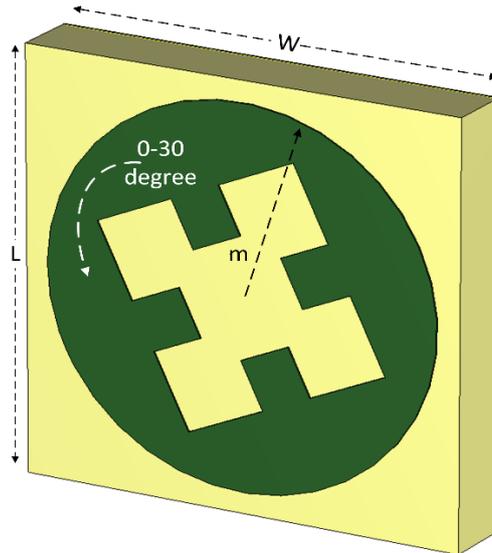
Figure 9. Circle-Minkowski reflective unit cell (With rotation)

A total of 3500 simulations were performed for the parameters used in Table 2 and for 10 angle values between 0°-30° and the reflection phase graph corresponding to these parameters is given in Figure 10. As can be seen in Figure 10, the phase response rotation of the unit cell spreads over a wider range, ranging from $+180^o$ to -180°. This ensures that the phase response can be obtained for each point on the antenna while designing the reflective array antenna and the corresponding unit cells can be placed at all points.

Figure 10. Phase response plot for Circle-Minkowski reflective unit cell (With Rotation)

2.2. Reflect array antenna design

RAAs are generally designed in 3 different structures as circle, square and rectangular incoming plane waves. However, the working process of all of them is based on the phase delay principle after the wave coming to the antenna surface illuminated by a source placed in the center or offset, after it is reflected again. The top and side view structure of the RAA is given in Figure 11.
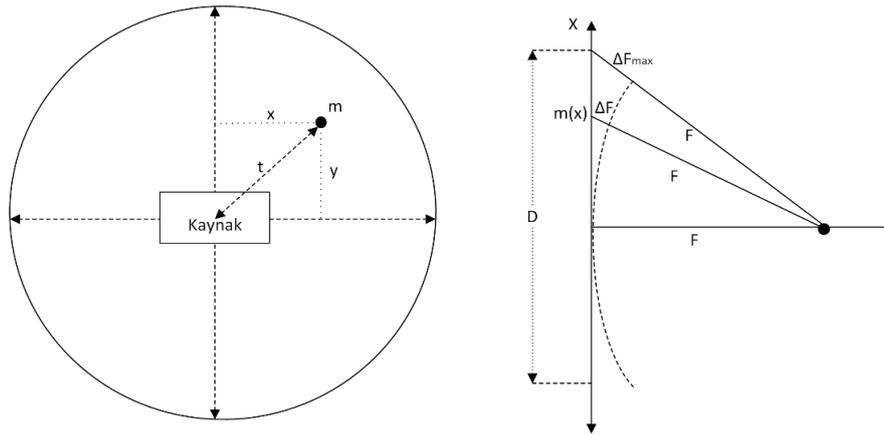
Figure 11. Top and side view for reflective array antenna (with Calculation parameters)

In the reflective array antenna, the basic structure of which is given in Figure 11, the D distance is the diameter of the antenna, the F distance is the distance between the source and the antenna, the ΔF distance is the path length that must be compensated by the phase delay for the reflective element at any point, and the distance ΔF_{max} also represents the maximum amount of path that needs to be compensated at the corner of the antenna. The m in Figure 10 indicates the coordinate of the unit cell placed on the antenna and using Equation 2, the distance of the unit cell to the origin point is calculated.

$$t = \sqrt{x^2 + y^2} \tag{2}$$

The distance ΔF, which represents the amount of path to be compensated at the point where the unit cell is located, can be calculated using Equation 3. Here, the ΔF path difference is calculated by subtracting the distance of the unit cell from the source connected to F and t, from the source to the origin point.

$$\Delta F = \sqrt{F^2 + t^2} - F \tag{3}$$

The required phase delay amount (φ) placed at any m point of the antenna can be calculated using Equation 4.

$$\varphi = -\beta(\Delta Fmax - \Delta F) \tag{4}$$

β, used in Equation 4, represents the path constant of the medium and is expressed by $\beta = -2\pi\frac{f}{c}$. Therefore, Equation 4 can also be expressed as Equation 5. Here, f represents the frequency and c represents the speed of light.

$$\varphi = -2\pi\frac{f}{c}(\Delta Fmax - \Delta F) \tag{5}$$

Using these equations and antenna structure, the phase delay requirement at each point on the RAA is calculated. Then, using the simulation values in Section 2.1.1-2, the unit cell structures that provide the phase requirement of each point on the antenna are placed on the antenna. After the correct sized unit cell structures are placed on the antenna, a horn antenna with a center frequency of 11 GHz is placed on the RAA as shown in Figure 12. In addition, the shape and dimensions of the horn antenna used are given in Figure 13.
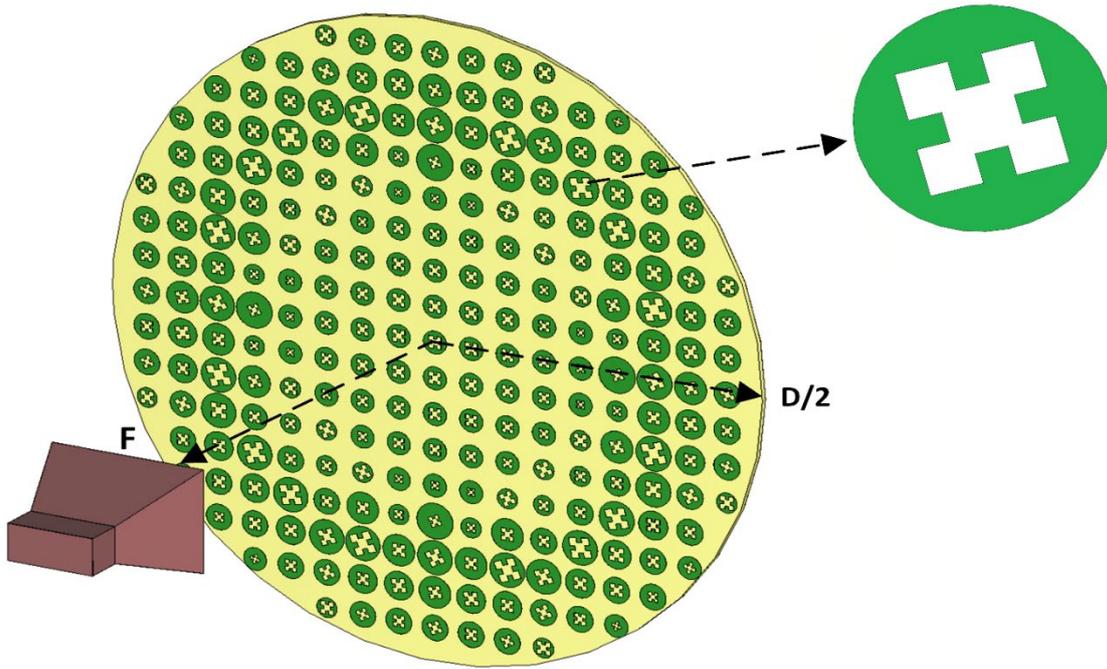
Figure 12. Reflective array antenna designed with Circle-Minkowski unit cells
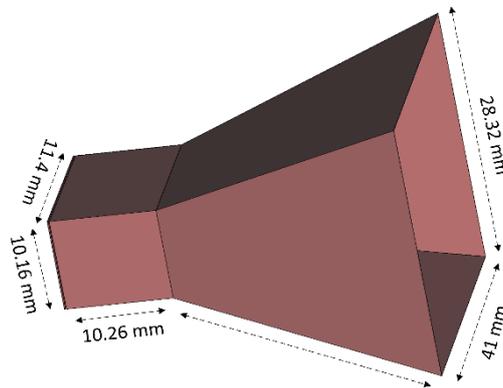
Figure 13. Horn antenna shape and dimensions

The phase response of all points on the RAA is provided with the unit cell obtained using the parameters and rotation angle of the Circle-Minkowski structure in Table 2, and accordingly, unit cells can be placed at all points on the RAA. After completing the design with RAA and horn antenna, the antenna is simulated with the help of electromagnetic simulation program. The gain of the horn antenna used here is 11.7 dBi. As a result of the simulated process, the gain graph shown in Figure 14 is obtained.
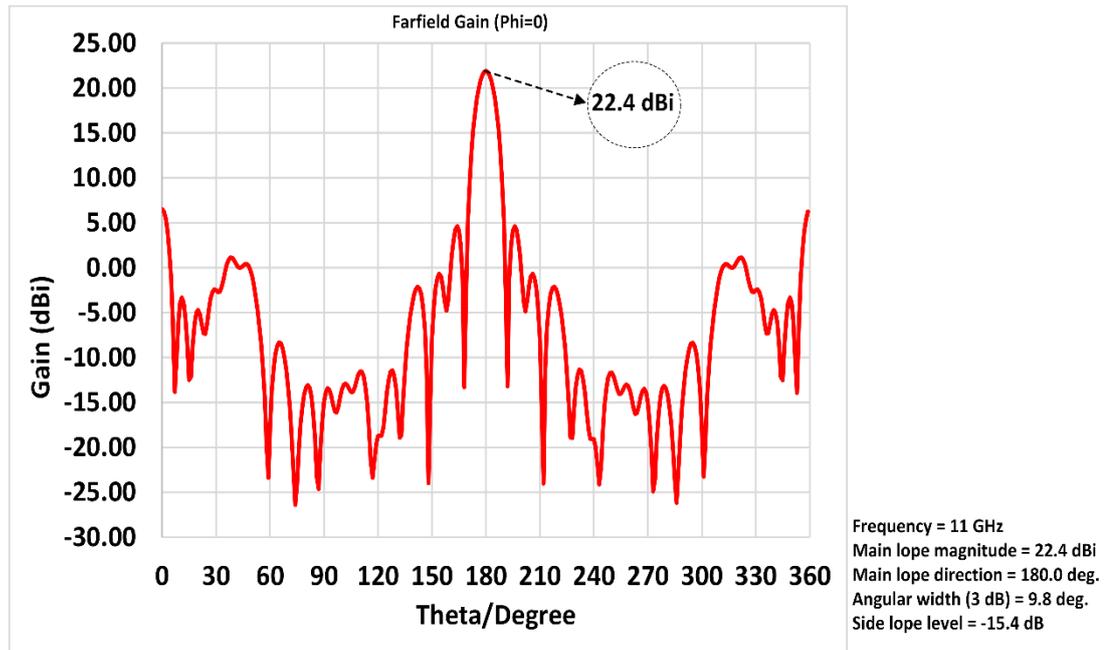
Figure 14. Gain graph of RAA

Figure 14 shows the cartesian gain graph. When the graphs are examined, it is seen that the maximum gain is 22.4 dBi and there is a good focus on the horn antenna.

3. RESULTS AND DISCUSSION

In this study, 3 different unit cell designs were made to be used on the reflective array antenna. First, the structure in Figure 1 was designed and simulated as a unit cell, and the reflection phase response was obtained depending on the circle diameter. According to the simulation results, the phase response of 280° was taken as seen in Figure 2. This means that phase response cannot be obtained throughout the entire band, and reflective unit cells cannot be placed at some points on the RAA to be formed depending on this situation. For this reason, the structure created by etching the Minkowski structure from the circle seen in Figure 3 was designed. While designing the Circle-Minkowski structure, there were three cases where two of the parameters m, t and s were kept constant and one of them was changed. For these three cases, 350 simulations were made using the parameter ranges given in Table 2 and a phase response of 329° was obtained. In the last step, the parameters of the circle-minkowski structure and the rotation of this structure for 10 angle values between 0°-30° were simulated and 3500 simulation processes were performed. As a result of the simulation, a phase response of 360° was obtained.

After the unit cell design, whose phase response can be obtained throughout the entire band, the antenna structure seen in Figure 11, created by placing a reflective unit cell at each point in the RAA formation, was simulated and the antenna gain at 11 GHz was obtained as 22.4 dBi. In addition, broadband antenna gain is given in Figure 15.
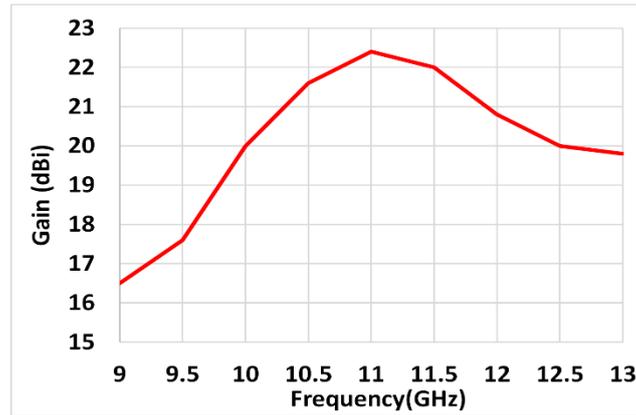
Figure 15. Wideband RAA gain graph

When Figure 15 is examined, it is seen that the antenna gain is 16.5 dBi for 9 GHz, 20 dBi for 10 GHz, 22.4 dBi for 11 GHz, 20.8 dBi for 12 GHz and 19.8 dBi for 13 GHz. Accordingly, it is seen that the antenna gain at 11 GHz is higher than the other frequencies.

4. CONCLUSIONS

In this study, it was first aimed to design a reflective unit cell with a wide phase response range. For this, a three-stage method was followed. Firstly, the reflective unit cell was simulated using a circular structure and the phase response of 280° was obtained as a result of the simulation. Then, in Stage 2, a new reflective unit cell was designed and simulated by etching the Minkowski structure from the circle structure. As a result of the simulation process according to the design parameters of the structure, 329° phase response was obtained. However, since the phase response could not be obtained for a full band, the last stage was started. At this stage, the Minkowski structure etched from the circle was rotated and simulated again, and a phase response of 360° was obtained. This allows adding a reflective unit cell to all points on the reflector array antenna, since phase response can be obtained over a full band. The RAA formed with these unit cells is shown in Figure 12. As a result of the simulation of the RAA, a gain of 22.4 dBi was obtained. Considering that the gain of the horn antenna is 11.7 dBi, a gain of 91% has been achieved compared to the gain of the horn antenna. According to these results, it has been revealed that a RAA design with wide phase range and high gain can be made by using the Circle-Minkowski structure by rotating effect.

REFERENCES

1. Genç, A.(2019). Gain Increase of Horn Antenna with Waveguide Feeding Network by using 3D Printing Technology. *Bayburt Üniversitesi Fen Bilimleri Dergisi*, Cilt 2, Sayı 1, Sayfa 17-25.

2. Genç, A., Başyiğit, İ. B., Çolak B., Helhel, S.(2018). Investigation of the characteristics of low-cost and lightweight horn array antennas with novel monolithic waveguide feeding networks, *AEU - International Journal of Electronics and Communications,* vol. 89, issue 1, pp 15-23.

3. Tütüncü, B., Urul, B. (2019). LHM superstrate for high directivity microstrip antenna", *Celal Bayar University Journal of Science*, vol. 15, issue 1, pp 71-74.

4. Gianvittorio, J.P., Rahmat-Samii, Y. (2002). Fractal antennas: a novel antenna miniaturization technique, and applications. *IEEE Antennas and Propagation Magazine*, vol. 44,no. 1, pp. 20–36.

5. Werner, D.H., Ganguly, S. (2003). An overview of fractal antenna engineering research. *IEEE Antennas and Propagation Magazine*, vol. 45, no. 1, pp. 38–57.

6. Costanzo, S., Venneri, F., Di Massa, G., Borgia, A., Costanzo, A., Raffo, A. (2016). Fractal reflectarray antennas: state of art and new opportunities. *Hindawi Publ.Corp.Int.J.of Antennas and Propagation*, vol. 2016, Art. ID 7165143, pp 17 http://dx.doi.org/10.1155/2016/7165143

7. Venneri, F., Costanzo, S., Di Massa, G., Amendola, G. (2008). Aperturecoupled reflectarrays with enhanced bandwidth features. *J. Electromagn. Waves Appl.*, vol. 22, pp. 1527–1537.

8. Al-Saedi, H., Abdel-Wahab, W.M., Raeis-Zadeh, S.M., Gigoyan, S., Safavi-Naeini, S. (2018). An Ultra-Wideband Modified Aperture-Coupled Millimeter-Wave Reflectarray Antenna. *IEEE International Symposium on Antennas and Propagation & USNC/URSI National Radio Science Meeting*, Boston, MA, USA, pp. 1423–1424, Jul.

9. Chaharmir, M.R., Shaker, J., Gagnon, N., Lee, D. (2010). Design of broadband, single layer dual-band large reflectarray using multi open loop elements. *IEEE Trans. Antennas Propagat.*, vol. 58, no. 9, pp. 2875–2883, Jun.

10. Li, L., Chen, Q., Yuan, Q., Sawaya, K., Maruyama T. (2009). Novel broadband planar reflectarray with parasitic dipoles for wireless communication applications. *IEEE Antennas Wireless Propag. Lett.*, vol. 8, pp. 881–885, Jul.

11. Yoon, J.H., Yoon, Y.J., Lee, W.S., So, J.H. (2015). Broadband microstrip reflectarray with five parallel dipole elements. *IEEE Antennas Wireless Propag. Lett.*, vol. 14, pp. 1109–1112, Jan.

12. Pozar, D.M. (2007). Wideband reflectarrays using artificial impedance surfaces. *Electron. Lett.*, vol. 43, no. 3, pp. 148–149, Feb.

13. Qin, P.Y., Guo, Y.J., Weily, A.R. (2016). Broadband reflectarray antenna using subwavelength elements based on double square meander-line rings. *IEEE Trans. Antennas Propag.*, vol. 64, no. 1, pp. 378–383.

14. Zubir, F., Rahim, M.K.A., Ayop, O., Wahid , A., Majid, H. A. (2010). Design and analysis of microstrip reflectarray antenna with minkowski shape radiating element. *Progress in Electromagnetics Research B*, vol. 24, pp 317–331.

15. Huang, J., Pogorzelski, R.J. (1998). A ka-band microstrip reflectarray with elements having variable rotation angles. *IEEE Transactions on Antennas and Propa.*, vol. 46, Issue 5, pp 650–656.

16. Lingasamy, V., Selvan, K.T. (2019). A comparison of planar convex dielectric lens loaded flat reflector with parabolic reflector and reflectarray. *Micr. and Optical Tech.Letters*, vol. 61 Issue 11, pp 2500-2505.

17. Keyghobad, K., Homayoon O. (2007). Phase Response of Microstrip Reflectarray Elements by FDTD Analysis. *Workshop on Computational Electromagnetics in Time-Domain, IEEE*, pp 1-3.